NASA CONTRACTOR REPORT

NASA CR-4

NASA CR-459

A STUDY OF FINNED TUBE GAS-TO-LIQUID HEAT EXCHANGERS FOR BRAYTON CYCLES IN SPACE

by S. V. Manson

NATIONAL AERONAUTICS AND SPACE ADMINISTRATION • WASHINGTON, D. C. • APRIL 1966

ERRATA

NASA Contractor Report CR-459

A STUDY OF FINNED TUBE GAS-TO-LIQUID HEAT

EXCHANGERS FOR BRAYTON CYCLES IN SPACE

by

S. V. Manson

May 24, 1966

The attached page of Contents replaces page vii.

Page 70: In sketch shown, above the words "Straight Tube," draw a straight line.

Page 74: Add an equal sign (=) in second equation directly below and in the same position as the above equation.

A STUDY OF FINNED TUBE GAS-TO-LIQUID HEAT EXCHANGERS

FOR BRAYTON CYCLES IN SPACE

By S. V. Manson

FOREWORD

iii

ABSTRACT

A study of gas-to-liquid heat exchangers is made for Brayton cycle powerplants in space. The function of the studied heat exchangers is to enable the cycle working gas to transfer the waste heat of the cycle to a liquid coolant. In the heat exchanger configuration considered, hot argon and hot neon flow across banks of externally finned tubes and transfer cycle waste heat to liquid NaK, lithium and water flowing inside the tubes. Heat exchangers are calculated for cycle power levels of 10 to 1000 KW_e . At high performance operating conditions, the heat exchangers are computed to have specific weights of about 1 lb/KW_e in a 1000 KW system, about 1.5 lb/KW_e in 500 and 100 KW systems, and about 3.5 to 5.5 lb/KW_e in a 10 KW system.

Contents

SUMMARY

Gas-to-liquid heat exchangers are discussed in relation to Brayton
cycle powerplants for space applications. It is indicated that for
missions in space, the reliability of a heat exchanger is as
important as its weight. In order to satisfy the reliability and
weight requirements, a heat exchanger geometry that employs
externally finned tubes is selected. In the selected geometry, the
gas flows across the finned tubes and the liquid flows inside the
tubes. A multipass cross-counterflow arrangement of the fluid flow
paths is postulated.

Sizes and weights are computed for finned tube gas-to-liquid heat
exchangers that operate with argon and neon as primary fluids and
with NaK, lithium and water as coolants, in Brayton cycle systems
that are capable of generating 10 to 1000 kilowatts of electrical
power in space applications.

The effects of geometric, thermal, coolant and materials parameters
on the size and weight of finned tube gas-to-liquid heat exchangers
are discussed.

A criterion is presented for estimating suitable values of thermal
parameters in the systems under consideration. The criterion is
applied to the selection of potentially attractive combinations of
heat exchanger cooling effectiveness and gas stream-to-coolant
stream heat capacity ratio at each of four cycle power levels

considered. At the selected conditions, high performance heat exchangers are computed to have specific weights of about 1 lb/KW_e in a 1000 KW system, about 1.5 lb/KW_e in 500 and 100 KW systems, and about 3.5 to 5.5 lb/KW_e in a 10 KW system.

A method of calculating externally finned, multipass, cross-counterflow gas-to-liquid heat exchangers is indicated in an appendix. A variation of Jameson's method of correlating data on flow across banks of externally finned tubes is applied to 15 sets of experimental data and is indicated in a figure herein.

ILLUSTRATIVE HEAT EXCHANGER DATA

Cycle power levels, working fluids, thermal and pressure performances, tube and fin materials, and heat exchanger sizes and weights illustrative of the combinations considered in the present study are indicated on the following page.

Illustrative Heat Exchanger Data*

Power level (KW)	10	10	10	100	500	1000	1000
Gas	A	A	A	Ne	Ne	A	A
Coolant	NaK	NaK	H_2O	NaK	NaK	NaK	Li
Cooling effectiveness	.95	.95	.95	.95	.95	.95	.95
$(\dot{m}c_p)_{gas}/(\dot{m}c_p)_{coolant}$	1.0	1.0	1.0	.95	.95	.95	.95
Coolant $\triangle p$ (psi)	10	10	10	30	30	30	30
Tube o.d. (inch)	1/8	1/8	1/8	3/16	3/16	3/16	3/16
Tube metal	Al	Steel	Steel	Steel	Steel	Steel	Cb-1%Zr
Fin metal	Al	Al	Al	Al	Al	Cu	Cu
Wet weight, excl. shell, (lb)	32.6	51.3	54.3	132	660	1155	860
Core volume (ft^3)	.78	.78	.88	1.6	8.1	8.3	7.2
No. of tubes	295	295	100	540	2700	3030	1270
Specific wt., excl. shell, (lb/KW)	3.3	5.1	5.4	1.3	1.3	1.2	.86
Core specific vol., (ft^3/KW)	.078	.078	.088	.016	.016	.0083	.0072

-----

* In every case, the number of coolant passes in cross-counterflow is 8, the tube (i.d./o.d.) is 0.85, the number of fins per inch is 30, the fin thickness is .005 inch and the fin (o.d./i.d.) is 2.0.

INTRODUCTION

In Brayton cycle powerplants that generate electrical power in space, the weight of the waste heat radiator may contribute as much as 50 percent of the total weight of the system (References 1, 2). Methods of reducing the radiator weight therefore require study.

One possible approach to reducing the weight of Brayton cycle radiators is to use a high performance liquid, instead of the primary cycle gas, as the radiator working fluid. Use of a high performance liquid has major advantages: (1) The convective heat transfer process in the radiator channels is improved. (2) Relatively small diameter radiator tubes and small diameter headers can be used without excessive pressure drop or pumping power. Both of the cited factors can lead to significant reductions in meteoroid armor weight.

If a liquid is to replace the cycle gas as the radiator working fluid, provision must be made to transfer the waste heat of the cycle from the primary gas to the liquid. To implement this exchange of heat, an auxiliary heat exchanger must be employed. Figure 1 indicates the manner in which the heat exchanger is introduced into the cycle.

The auxiliary heat exchanger in which the waste heat of the cycle is transferred from the primary gas to an auxiliary liquid is the subject of discussion in the present report. The selection of a

suitable geometry for the gas-to-liquid heat exchanger, and the
calculation of its sizes and weights at a variety of cycle
operating conditions, are objectives of the present study. The
explicit purposes of the study are as follows:

(1) to indicate a gas-to-liquid heat exchanger geometry
that can offer both low weight and high reliability;

(2) to perform parametric studies of this heat exchanger
geometry at operating conditions of interest in four possible
Brayton cycles in space.

Toward meeting the first of the stated purposes, an externally
finned tubular heat exchanger element is chosen in this study, as
suggested in figure 2. The upper half of figure 2 shows a
cylindrical tube with circular fins bonded to its outer surface.
Liquid is assumed to flow inside the tube, the interior surface
of which is unfinned. The lower half of figure 2 shows tubes of
this sort arranged in a staggered array. The cycle gas flows
across the staggered tubes and transfers its heat to the fins
and to the tube outer surfaces. This heat is then transferred
by the tube walls to the liquid that flows in the tube interiors.
The flow path of the liquid is shown in figure 3. This figure
shows that the coolant flow is perpendicular to that of the cycle
gas in any one pass, but that by performing successive passes the
coolant ultimately moves in counterflow to the gas. The cross-
counterflow arrangement depicted in figure 3 is a standard one
and is well known. It permits an approach to thermal counterflow
with a circuit that employs local crossflow of the heat exchanging
fluids.

Toward meeting the second of the above-stated purposes, the following geometric, material, thermal and coolant parameters are explored: tube diameter, fin diameter, fin thickness, number of fins per inch of tube length; tube material, fin material, coolant composition; heat exchanger cooling effectiveness, gas-to-coolant $(\dot{m}c_p)$-ratio, number of coolant passes in cross-counterflow (figure 3) and coolant pressure drop. Details of the parametric variations are as follows:

Tube outside diameter (inch)	0.125 to 0.250
Fin-to-tube diameter ratio	1.4 to 2.5
Fin thickness (inch)	.005, .010
Fins per inch	10 to 40
Tube materials	Al, Steel, Cb-Zr
Fin materials	Al, Cu
Coolants	NaK, Li, H_2O
$(\dot{m}c_p)_{gas}/(\dot{m}c_p)_{coolant}$	.90, .95, 1.0
Cooling effectiveness	.90, .925, .95
Number of coolant passes (fig. 3)	6, 8
Coolant pressure drop (psi)	5 to 100

The cycle power levels at which the studies were made were 10, 100, 500 and 1000 KW_e . In the 10 and 1000 KW cycles the working gas was argon; in the 100 and 500 KW cycles the working gas was neon.

For the calculations, use was made of the equations of resistance to fluid flow and heat transfer, which require a knowledge of friction

factors and heat transfer coefficients. In order to obtain working curves for the friction factors and heat transfer coefficients of the gas, 15 sets of data on friction and heat transfer in flow across finned tubes of the sort shown in figure 2 were correlated. For the liquid coolants, flow resistance and heat transfer were computed with relations presented in References 3 and 4.

The calculations yielded the axial, transverse and no-flow dimensions of the gas cooler (exclusive of the enclosing shell); the number of tubes and their length; and the weights of the tubes, fins, liquid and return bends. No attempt was made to determine the size or weight of the enclosing shell, as the detailed stress analyses required for lightweight shell design were outside the scope of the present study.

The numerical results that appear herein are viewed as possible starting values in the event that detailed design studies are ultimately undertaken. The parametric nature of the present calculations discloses the parameters and the directions in which changes might desirably be made in optimizing a design at one or more of the power levels studied.

OBJECTIVES

The two purposes of the present study are (1) to indicate a basic
heat exchanger geometry that has the potential to be both lightweight
and reliable, and (2) to generate parametric data on gas coolers
that use the basic heat exchanger geometry to meet the following
operating specifications:

Table 1. Gas Cooler Operating Conditions

Cycle electrical output (KW)	10	100	500	1000
Gas	Argon	Neon	Neon	Argon
Gas $\dot{m}c_p$ (Btu/sec ^OR)	.0758	.94	4.7	5.42
Gas inlet temp. (^OR)	915	1193	1193	1584
Gas outlet temp. (^OR)	536	690	690	975
Gas inlet pressure (psia)	6.57	54.5	54.5	213
Gas outlet pressure (psia)	6.00	50.0	50.0	200
Gas pressure drop (psi)	0.57	4.5	4.5	13

In order to cool the gases between the temperature limits shown
in Table 1, NaK, lithium and other suitable coolants are to be
considered.

SELECTION OF BASIC HEAT EXCHANGER GEOMETRY

Reliability and Weight

In selecting a basic heat exchanger geometry for power systems in space, the requirement of high reliability must be given the same importance as the requirement of low weight and volume. Reference 5 asserts that "Electric power systems for space applications have many unique and restrictive requirements imposed upon their design. Chief among these is the requirement for extreme reliability for long periods of unattended operation."

The factors that affect heat exchanger reliability may vary from one system to another. In the gas coolers of the present study such factors include thermal stress, thermal strain cycling, stresses arising from local pressure differences between the heat exchanging fluids, formation of deposits on the walls and non-uniform distribution of the fluids. These factors are examined briefly in the following paragraphs.

Thermal stress is a potential factor in reliability because, as shown by Table I, the temperature of the gas will change by substantial amounts in the gas coolers, the temperature drop ranging from about $380^{\circ}R$ in the 10 KW system to about $610^{\circ}R$ in the 1000 KW system. At the high cooling effectivenesses to which the gas coolers will be designed, the liquid and wall temperatures will also change by several hundred degrees from inlet to exit stations. The thermal expansions of the various metal regions will therefore

differ non-negligibly from one another, and unless there is freedom for differential thermal growth, thermal stress will result.

Thermal strain cycling is a potential factor in reliability because the power level may not remain steady, either because of a planned schedule of power change or because of unforeseen developments during long periods of unattended operation in space.

In discussing the experience gained from a high performance heat exchanger development program at the Oak Ridge National Laboratory, Reference 6 asserts that "It was found that thermal stresses imposed the most important single set of fundamental limitations on the heat exchanger design, and that thermal strain cycling associated with changes from low to high power was the most important failure mechanism." This assertion, taken together with the comments in the preceding two paragraphs, makes clear that the basic geometry of the gas coolers must be selected so as to minimize the occurrence of thermal stress and insure low vulnerability to thermal strain cycling.

Mechanical stresses originating from local pressure differences between the heat exchanging fluids are potential factors in gas cooler reliability because of the fluid pressure changes that will occur along the gas cooler channels. Even in the case of the 10 KW system, in which the pressure change of the gas is small (Table I), the liquid pressure drop may be substantial. Liquid pressure drops in the range 20 to 30 psi might readily be required in order to achieve uniform coolant distribution, adeouate heat

transfer coefficients, reasonable header weights and non-cavitating and efficient pump operation, particularly where liquid metals are concerned. Depending on the pressure levels and pressure drops of the gas and coolant, substantial pressure differences could exist between the fluids at the inlet or exit stations of the gas coolers; reversals in the algebraic sign of the pressure difference might also occur at intermediate points along the channel lengths. For these reasons the basic gas cooler geometry should be one that has inherently good structural characteristics under differential pressure loads.

Deposit formation on the walls of the gas cooler channels is also a potential factor in reliability, particularly if liquid metals are used. In the presence of substantial temperature changes along the channel walls, transfer of wall material from hot to cooler regions may be caused by the liquid metals. In the cases of molten lithium and NaK, oxide formation and deposition on the walls may also occur. Accretions of transferred mass and of oxides would affect the flow distribution and pressure drop of the liquid, as well as the resistance to the flow of heat. To minimize plugging, flow distortion and excessive pressure drop, the liquid channels must have adequate dimensions transverse to the direction of fluid flow, without involving excessive volume or weight of the liquid.

Fluid flow distribution is also a factor in reliability because unless the gas and coolant are both properly distributed, the

performance of the gas cooler, and ultimately of the system, will differ from the intended performance. For this reason the basic geometry must be chosen so as to minimize maldistribution of the gas or liquid.

In addition to satisfying the foregoing reliability requirements, the gas cooler geometry must be capable of being light in weight. Thus, the geometry must provide high gas side heat transfer coefficients, lend itself readily to the use of a large amount of fin surface on the gas side of the walls, and be structural when thin gage materials are used without weight-augmenting support members.

On the basis of the foregoing considerations, externally finned tubes of the type shown in figure 2 were selected as the basic elements of the gas cooler, and a staggered array of the tubes, as suggested in figure 2, was postulated. In this arrangement the gas flows across the tubes and the liquid flows in the tube interiors. The liquid moves in cross-counterflow to the gas, as suggested in figure 3. Heat is convected by the gas to the fins and to the tube outer surfaces; the heat is then conducted across the tube walls and is transferred by convection to the liquid that sweeps the tube inner surfaces.

From the viewpoints of thermal stress and thermal strain cycling, the geometries shown in figures 2 and 3 are believed to be satisfactory because each tube and each fin has considerable freedom to adjust to its own thermal growth requirements. Inasmuch as disk fins rather than plate fins are employed, the fins do not

tie the tubes together; hence the tubes can perform differential transverse motions. Such motions might be required to allow individual tubes to adjust to differential thermal growths of the end supports. Similarly, the fact that the fins do not tie the tubes together facilitates differential growths of the tube lengths. Stress from unequal tube length expansions is further avoided by virtue of the multi-pass nature of the liquid circuit and by the use of U-bends to join the tubes of successive passes. The multi-pass factor insures that temperature differences between tubes having common supports will not be large; and, at moderate temperature inequalities, U-bends can be properly shaped to accommodate the unequal growths.

The described freedom for differential thermal expansions of the individual tubes and fins reduces the probability of structural failures and of fluid leakage at welded or brazed junctions. In addition, the external locations of the fin-to-tube and tube-to-U-bend junctions permit the use of standard methods of inspection, and thereby facilitate quality control during fabrication and assembly.

From the viewpoint of structural soundness under differential pressure loads, tubes are well known to be satisfactory. With regard to such loads, it is noteworthy that the structural soundness of the finned tubes of figure 2 is not impaired by imperfect bonding between fin and tube, as the function of the fins is entirely thermal and not structural.

13

Tubes are also able to satisfy well the requirement of adequate channel dimensions transverse to the direction of liquid flow without involving large volumes of the liquid. In comparing tubular and parallel plate channels from this viewpoint it is found that, for equal wall perimeters and equal liquid cross sectional areas in the two geometries, the diameter of a tube is twice as large as the spacing between parallel plates.

From the viewpoint of uniform distributions of the liquid and gas, the geometries of figures 3 and 2 are believed to be suitable for the following reasons:

The multi-pass arrangement of the liquid circuit results in large values of channel length-to-diameter ratio and substantial pressure drops at moderate liquid velocities. Because of the substantial flow resistance of the channels, liquid in the header plenum tends to distribute itself uniformly at the entrance to the tubes. Thereafter, the guidance provided by the U-bends prevents either "piled up" or "dead water" regions at stations where the liquid reverses its flow direction, so that uniform distribution con-tinues all along the liquid path.

In the case of the gas, the near-counterflow temperature pattern achieved with a multi-pass liquid circuit precludes substantial density variations from one gas filament to the next; hence, gas maldistribution due to density variations may be expected to be non-serious. In addition, because the friction factors are high

14

in flow across finned tubes, it is necessary to use moderate gas velocities in order to maintain reasonable pressure drops. Accordingly, fairly small deviations in local velocity result in relatively large deviations in dynamic head and in local resistance to flow. If the design pressure drop is a significant fraction of the entrance pressure, the relatively large response of local flow resistance to non-uniformities in velocity would tend to keep the gas distribution nearly uniform.

The finned tube configurations in figures 2 and 3 are also satisfactory from the viewpoint of high performance heat transfer, with attendant low weight and volume; for,

(1) High heat transfer coefficients are obtained with the types of boundary layer structure that occur during flow across tubes and along discontinuous fins.

(2) A large amount of thin fin surface can be bonded with good quality control to the outer surface of a tube.

(3) The use of a multi-pass liquid circuit permits a close thermal approach to pure counterflow and makes possible the attainment of high heat exchanger effectivenesses with reasonable weight.

Geometric and Materials Parameters

The geometric variables that require exploration in the finned tube configuration may be inferred from figures 2 and 3. The variables are: the tube outside diameter, the ratio of tube i.d. to tube o.d. (which, together with the tube outer diameter, measures the tube

inside diameter and wall thickness), the ratio of fin o.d. to fin i.d., the fin thickness, the number of fins per inch, and the axial and transverse spacings of the tubes.

Each of the foregoing variables can have large effects on the size, weight or reliability of the heat exchanger. In the present study the effects of four of the variables will be discussed on the basis of numerical data. These variables will be the tube diameter, the ratio of fin o.d. to fin i.d., the fin thickness and the number of fins per inch. The remaining three variables-- the ratio of tube i.d. to tube o.d., and the axial and transverse spacings of the tubes -- will be discussed qualitatively.

A parameter whose significance is both geometric and thermal is the number of liquid passes in cross-counterflow (figure 3). For the high cooling effectivenesses of interest in the present study, the number of liquid passes is a very important parameter. Unless a sufficient number of passes is used, the fluid temperature fields may make it impossible to attain a desired cooling effectiveness even if high heat transfer coefficients and a large amount of heat transfer surface are made available (Ref. 7). Through its effect on the fluid temperature patterns, the number of liquid passes has a direct effect on the heat exchanger size and weight. In addition, the number of passes affects the weight of the return bends and their contained liquid, and affects also the length and number of tubes, as well as the no-flow dimension of the heat exchanger face (figure 3). Numerical results will be presented for 6- and 8-pass arrangements,

16

which are adequate and not far from optimum for the gas coolers of the present study.

The materials of which the fins and tubes are composed, as well as the composition of the coolant, are additional important gas cooler parameters. Table I shows that the temperature level of the gas changes sufficiently from one cycle to another so that changes in tube, fin and coolant composition are possible and desirable in going from one cycle to the next. Lightweight aluminum tubes and fins, and water as coolant, are of interest at the temperatures involved in the gas cooler of the 10 KW system; heavier, higher temperature tube materials, copper fins, and a liquid metal coolant may be required in the gas cooler of the 1000 KW system. The choice of materials for the tubes, fins and coolant will affect significantly the weight, size, shape and reliability of the gas coolers.

OUTLINE OF CALCULATION PROCEDURE

Heat exchangers are governed by the laws of conservation of momentum, energy and mass. Momentum conservation is expressed by pressure drop equations; energy conservation by heat balance equations or by equivalent thermal resistance equations; and mass conservation by continuity equations. The main sequence in which such relations are used in the present study is as follows:

Gas pressure drop: The pressure drop requirement of the gas (Table 1) is satisfied first. This step yields the following

17

information:

(a) Gas flow area and gas face area

(b) Number of banks of tubes

(c) Total heat transfer surface in gas channel, total heat transfer surface in coolant channel, and total tube wall area across which heat flows by conduction

(d) Heat transfer coefficient of the gas

(e) Thermal resistance of the gas

(f) Thermal resistance of the tube walls

Liquid thermal resistance: The required thermal resistance of the liquid is then found from the following equation,

(Required thermal resistance of liquid coolant) =

$$\frac{1}{UA} - (\text{gas thermal resistance} + \text{wall thermal resistance})$$

in which $1/UA$ is the pre-calculated total thermal resistance associated with a desired combination of cooling effectiveness and gas-to-coolant $(\dot{m}c_p)$-ratio. The liquid thermal resistance, together with the known heat transfer surface in the coolant channel (item (c) above), determines the required heat transfer coefficient of the coolant. The associated coolant velocity is then determined from the formula for the coolant heat transfer coefficient.

Liquid continuity equation: The coolant flow area required to yield the known coolant velocity (see last sentence of preceding

paragraph) is then computed with the one-dimensional liquid continuity equation. This yields the number of tubes per pass, the no-flow dimension of the gas cooler and, in conjunction with the known gas face area (item (a) under Gas Pressure Drop), yields the length of the tubes.

The coolant pressure drop, the total number of tubes and the heat exchanger weight are then calculated with the information available from the foregoing steps.

The foregoing represents the main thread of the calculation sequence, and may help to make clear the ways in which the various items defined in Appendix A and discussed in detail in Appendix B fit into the total computational procedure.

RESULTS AND DISCUSSION

The discussion of numerical results is divided into sections as follows:

Under the two headings, "Effects of Geometric Parameters" and "Effects of Thermal, Coolant and Materials Parameters", significant design variables are identified and are discussed in terms of their effects on heat exchanger weight, volume, component dimensions and number of tubes. Conclusions thought to be useful for design in the present application are formulated. After the discussion of each parameter, the value (or range of values) assigned to that parameter in the present study is indicated.

Under the heading "Parametric Data", the results of systematic
calculations of heat exchanger sizes and weights are presented
for the four Brayton cycle power levels identified in Table 1.

Under the heading "Liquid Temperatures And Radiating Potentials",
the coolant temperatures at entrance to and exit from the heat
exchangers of item 2 above are indicated and are discussed in
relation to the radiating potential of the space radiator.
Illustrative heat exchanger data are then tabulated at operating
conditions for which the radiating potentials appear attractive.

Effects of Geometric Parameters

Geometric parameters can produce large effects on the weight and
other characteristics of externally finned tubular heat exchangers.
The following seven parameters are of interest (see figure 2): the
number of fins per inch, fin diameter ratio (o.d./i.d.), fin
thickness, tube diameter, tube diameter ratio (i.d./o.d.), tube
spacing perpendicular to, and tube spacing parallel to, the gas
flow direction.* In the following paragraphs the effects of the
first four of the seven parameters are discussed in terms of
computed heat exchanger weights, dimensions and numbers of tubes.

----

* The number of coolant passes, which is both geometric and thermal
in nature, is also of interest. This parameter will be discussed
under the heading "Effects of Thermal, Materials and Coolant
Parameters".

The effects of tube diameter ratio and of tube spacings are
discussed in other terms that convey information concerning the
numerical results presented herein and that are thought to be
useful for purposes of design.

Effect of number of fins per inch: The addition of fins on the
external surfaces of the tubes can greatly augment the heat
transfer surfaces available to the gas, with substantial attendant
benefits. The effects of increases in the number of fins per
linear inch of tube length are shown in figure 4.

Figure 4 presents properties of heat exchangers computed for the
1000 KW cycle defined in Table I. The values in figure 4 are
based on the following assumptions (see also Table I): Copper
fins of .005 inch thickness on steel tubes of 3/16 inch o.d.,
fin o.d.-to-i.d. ratio equal to 1.8; argon gas, NaK coolant,
a NaK pressure drop of 30 psi in 8-pass cross-counterflow,
$(mc_p)_{gas}/(mc_p)_{coolant}$ and heat exchanger cooling effectiveness
both equal to 0.90.

Illustrative values from figure 4 are shown in Table 2. Figure 4
and Table 2 show that an increase in the number of fins per inch
from 10 to 30 produces marked (50 percent or larger) decreases in
the weight, volume, tube length and axial length, and a worth-
while decrease in the number of tubes of the heat exchanger core.
As the number of fins per inch increases from 10 to 30, the
frontal area increases by less than 2 percent. The no-flow
dimension is the only property that increases substantially

Table 2. Effect of Number of Fins per Inch

No. of fins per inch	10	30	40
Wt. of wet core plus return bends (lb)	692	387	342
Core volume (ft^3)	5.78	2.69	2.18
Core frontal area (ft^2)	2.64	2.69	2.73
Tube length (ft)	2.75	1.63	1.38
No-flow length (ft)	0.96	1.65	1.98
Axial length (ft)	2.19	0.998	0.799
No. of tubes	2900	2305	2160

(by a factor of about 1.7), and in this instance an increase is desirable until the no-flow length and the tube length are equal or nearly equal to each other. For the heat exchangers of figure 4 and Table 2, equality between the tube length and no-flow length occurs at about 30 fins per inch.

Figure 4 shows that as the number of fins per inch increases from 30 to 40, all heat exchanger properties continue to vary in the directions already noted, but the rates of change are smaller than when the number of fins per inch increases from 10 to 20, or from 20 to 30. Notwithstanding the decreased rates of change, the values in figure 4 and in Table 2 show that the additional benefits from increasing the number of fins per inch from 30 to 40 are not negligible; the core volume, in particular, decreases about 19 percent as the number of fins per inch increases from 30 to 40.

The foregoing values show that in the present application, a large number of fins per inch is very beneficial. Unless adverse heat transfer and friction coefficient variations arise to nullify the gains from increases in the number of fins per inch, or unless fabrication problems become prohibitive, 40 fins per inch could be justified from the viewpoint of core volume, and at least 30 fins per inch could be justified from the viewpoints of core weight, core component dimensions and number of tubes at the conditions underlying figure 4.

In the bulk of the calculations of the present study, the number of fins per inch was set at 30.

Effect of fin diameter ratio (o.d./i.d.): For prescribed tube outside diameter, the ratio of fin o.d. to fin i.d. defines the amount of exposed surface per fin and provides information on two of the factors (fin height and fin diameter ratio) that control the value of the fin effectiveness (Ref. 8). A rational selection of the fin diameter ratio is very desirable.

Figure 5 presents the effects of fin diameter ratio on heat exchanger weight and volume, frontal area, component dimensions and number of tubes. The values in figure 5 are for heat exchangers of the 1000 KW cycle defined in Table I, with the following additional specifications: Copper fins of .005 inch thickness, 30 fins per inch on steel tubes of 3/16 inch o.d.; argon gas, NaK coolant, a NaK pressure drop of 30 psi in 8-pass cross-counterflow, $(\dot{m}c_p)_{gas}/(\dot{m}c_p)_{coolant}$ and heat exchanger

cooling effectiveness both equal to 0.90.

Figure 5 shows that as the ratio of fin o.d.-to-fin i.d. increases from a sufficiently low starting value, the following effects occur: The weight goes through a minimum; the volume increases steadily; the frontal area and the tube length both decrease; the axial length increases. Careful examination of figure 5 discloses that the no-flow dimension goes through a very shallow minimum (see Table 3, below) and then increases very slowly, the net change being small throughout the whole range of fin o.d.-to-i.d. ratios in the figure. Figure 5 also shows that as the ratio of fin o.d.-to-i.d. increases, the number of tubes decreases steadily.

Values illustrating the changes described in the preceding paragraph are shown in Table 3.

Table 3. Effect of Fin Diameter Ratio (o.d./i.d.)

Ratio of fin o.d. to fin i.d.	1.4	1.8	2.0
Wt. of wet core plus return bends (lb)	539	387	409
Core volume (ft^3)	2.58	2.69	2.97
Core frontal area (ft^2)	3.84	2.69	2.52
Tube length (ft)	2.26	1.63	1.48
No-flow length (ft)	1.70	1.65	1.70
Axial length (ft)	0.672	0.998	1.18
No. of tubes	2655	2305	2285

As stated above, there exists a fin diameter ratio at which the core weight is a minimum. For the conditions underlying figure 5 and Table 3, the fin o.d.-to-i.d. ratio at which the minimum weight occurs is 1.8. Figure 5 shows no significant incentive to operate at a fin diameter ratio even moderately lower than 1.8; figure 5 and Table 3 do, however, show substantial penalties if a diameter ratio significantly lower than 1.8 is used. For example, if an o.d.-to-i.d. ratio of 1.4 were used, there would be a weight penalty of nearly 40 percent and a frontal area penalty exceeding 40 percent, as well as significant increases in the tube length and number of tubes, in comparison with the values at a fin diameter ratio of 1.8.

On the other hand, figure 5 and Table 3 show that fin o.d.-to-i.d. ratios somewhat higher than the weight-optimum value can be used to obtain slight reductions in frontal area, tube length and number of tubes, with only moderate penalties in core weight and volume.

The value of fin o.d.-to-i.d. ratio at which the lowest heat exchanger weight occurs is not a universal constant. It changes with the material and thickness of the fin, with the diameter of the tube, and with operating conditions in both gas and coolant channels. A determination of the optimum fin diameter ratio at each new combination of working conditions is normally desirable.

In the present study the fin o.d.-to-i.d. ratio was kept constant at 2.0 in the bulk of the calculations. This value, which is moderately higher than the optimum one at the conditions underlying figure 5, was chosen to allow for potentially significant decreases in gas heat transfer coefficient at operating conditions less favorable than those of figure 5, and to facilitate fabrication of return bends in the event that close-return radii acquired interest at any station in the heat exchanger. As previously indicated, the use of fin diameter ratios moderately higher than the weight-minimum value involves modest penalties in core weight and volume and leads to small decreases in heat exchanger frontal area, tube length and number of tubes.

Effect of fin thickness: From the viewpoint of fabrication and handling, as well as from the viewpoint of the fin's ability to conduct heat, an increase in fin thickness is of interest. The fin thickness underlying figures 4 and 5 and Tables 2 and 3 is .005 inch. The effects of increasing the fin thickness from .005 to .010 inch at operating conditions of interest in the present study are shown in Table 4.

The heat exchangers in Table 4 are for the 1000 KW cycle identified in Table 1, with the following additional specifications: Copper fins, 30 fins per inch, fin o.d.-to-i.d. ratio equal to 2.0, on steel tubes of 3/16 inch o.d.; argon gas, NaK coolant, a NaK pressure drop of 30 psi in 8-pass cross-counterflow, and a ratio of gas-to-coolant heat capacity rates equal to 0.90.

For Table 4 the heat exchanger cooling effectiveness is 0.925.

Table 4. Effect of Fin Thickness

Fin thickness (inch)	.005	.010
Wt. of wet core plus return bends (lb)	545	711
Core volume (ft^3)	3.88	3.10
Core frontal area (ft^2)	2.77	2.65
Tube length (ft)	1.82	1.54
No-flow length (ft)	1.52	1.72
Axial length	1.40	1.17
No. of tubes	2450	2290

Table 4 shows that as the fin thickness is doubled from .005 to
.010, the weight of the core plus return bends increases by 30
percent. All other quantities in the table improve as the fin
thickness increases: Primarily because of the decrease in axial
dimension, the core volume decreases by 20 percent. In addition,
the tube length decreases by 15 percent, the number of tubes
decreases by 8 percent and the frontal area decreases by 4 percent.
The no-flow dimension increases, and the net effect of the simul-
taneous increase in no-flow length and decrease in tube length is
a slight improvement in aspect ratio of the gas channel cross
section.

Table 4 shows that if reductions in core volume and tube length,

and small reductions in the number of tubes, are more important than increases in weight, then increases in fin thickness are justified. If weight is the item of primary concern, then reductions in fin thickness are justified.*

In the majority of the calculations of the present study the fin thickness was set at .005 inch. In two families of heat exchangers for the 1000 KW cycle, results were generated at fin thicknesses of both .005 and .010 inch.

Effect of tube diameter: An increase in tube diameter results in a decrease in the required number of tubes, a decrease in the number of brazed or welded joints at which leakage might occur, and an increase in ease of fabrication. It is therefore of interest to determine the effects of increased tube diameter on heat exchanger size and weight. The effects of increasing tube diameter in the range between 0.15 and 0.25 inch are shown in figure 6.

The heat exchangers in figure 6 are for the 1000 KW cycle defined in Table I, with the following additional specifications: Steel

----

* Because the conducting efficiency of the fins decreases as the fin becomes thinner, the core weight does not decrease continually as the fin thickness decreases; the core weight reaches a minimum and then increases again. The fin thickness for minimum core weight depends on the fin material, tube diameter and other factors. In the heat exchangers of the present study the weight-optimum fin thickness is probably less than .005 inch.

tubes, copper fins, 30 fins per inch, fin o.d.-to-i.d. ratio
equal to 2.0, fin thickness .005 inch; argon gas, NaK coolant,
a NaK pressure drop of 30 psi in 8-pass cross-counterflow,
$(\dot{m}c_p)_{gas}/(\dot{m}c_p)_{coolant}$ equal to 0.90 and a heat exchanger cooling
effectiveness equal to 0.925. In all heat exchangers of figure
6, the tube i.d.-to-tube o.d. ratio is 0.85.

Figure 6 shows that increases in tube diameter result in undesir-
able increases in the weight, volume, tube length and axial
length of the heat exchanger core. The frontal area changes
slowly.* The no-flow length decreases substantially. One factor
that improves markedly is the number of tubes, which decreases
strongly as the tube diameter increases. Illustrative values
from figure 6 are shown in Table 5a.

Table 5a. Effect of Tube Diameter (1000 KW System)

Tube outside diameter (inch)	.150	.1875	.250
Wt. of wet core plus return bends (lb)	463	545	705
Core volume (ft^3)	3.21	3.88	5.00
Core frontal area (ft^2)	(2.70)*	(2.77)*	(2.81)*
Tube length (ft)	1.47	1.82	2.36
No-flow length (ft)	1.84	1.52	1.19
Axial length (ft)	1.19	1.40	1.78
Number of tubes	3910	2450	1345

----

* See text below for discussion of these values.

The tabulated values show that at the conditions underlying Table 5a, the 67 percent increase in tube diameter from 0.15 to 0.25 inch o.d. results in increases of 50 percent or more in the weight, volume, tube length and axial length of the heat exchanger core. The no-flow dimension decreases about 35 percent. The frontal area changes very little. Table 5a shows that as the tube o.d. increases from 0.15 to 0.25 inch, the single large improvement is the 66 percent reduction in the number of tubes.

In Table 5a the values listed for the core frontal areas are enclosed in parentheses to indicate that an uncertainty of several (perhaps 5 to 10) percent exists in these values. Underlying the data in Table 5a are the specifications that as the tube diameter increases, the fin o.d.-to-i.d. ratio and the number of fins per inch remain constant at the values 2.0 and 30, respectively. Under these conditions the surface per unit gas flow area increases as the tube diameter increases. The variation in frontal area then depends on the relative rates of change of the friction factor, the heat transfer coefficient and the effective heat transfer surface. Because the change in the frontal area is small (4% in Table 5a), small changes in the relative rates of variation of the indicated factors could reverse the direction of change of the frontal area. An example illustrating a reversal in the direction of frontal area variation is shown in Table 5b.

The heat exchangers in Table 5b are for the 10 KW system defined in Table 1, with the following additional specifications: Steel

tubes, tube i.d.-to-tube o.d. ratio equal to 0.85, aluminum
fins, 30 fins per inch, fin o.d.-to-i.d. ratio equal to 2.0,
fin thickness .005 inch; argon gas, NaK coolant, a NaK pressure
drop of 10 psi in 8-pass cross-counterflow, $(\dot{m}c_p)_{gas}/(\dot{m}c_p)_{coolant}$
equal to 1.0 and a heat exchanger cooling effectiveness equal to
0.95.

Table 5b. Effect of Tube Diameter (10 KW System)

Tube outside diameter (inch)	0.125	0.1875
Wt. of wet core plus return bends (lb)	51.3	66.4
Core volume (ft^3)	0.778	1.02
Core frontal area (ft^2)	(0.95)	(0.91)
Transverse dimension (ft)*	0.85	1.17
No flow dimension (ft)	1.11	0.78
Axial length (ft)	0.825	1.11
Number of tubes	295	125

Table 5b shows a change of about 4 percent in core frontal area
as the tube o.d. increases from 0.125 to 0.1875 inch. The
direction of the frontal area change in Table 5b, however, is
opposite that in Table 5a. While the smallness of the change
tends perhaps to make its direction unimportant, clarification
of the casue of the apparent reversal in the behavior of the

----

* With folded tubes. The transverse dimension is about 1/8th of the
  tube length.

frontal area appears desirable. Satisfactory resolution of this matter would require precise correlations of friction data and heat transfer data over the entire range of Reynolds numbers of interest, as well as additional calculations.

Table 5b shows the same kinds and magnitudes of effects of tube diameter as does Table 5a insofar as core weight, volume, component dimensions and number of tubes are concerned. Both parts of Table 5 show substantial incentives to use the smallest practical tube diameter. In discussing high performance gas-to-liquid heat exchangers built of tubes with plate-type outer fins, Reference 6 recommends that the smallest practical tube diameter be employed. In Reference 6 a tube of 1/8 inch o.d. is used.

In the bulk of the calculations of the present study a tube of 3/16 inch o.d. was used as a compromise among considerations of size and weight, number of tubes and plugging by mass deposits. In two families of heat exchangers for the 1000 KW cycle, results were generated at tube diameters of both 3/16 and 1/4 inch. If plugging and large numbers of tubes are shown to be non-serious factors in the present application, advantages in size and weight would result from the use of tubes of 1/8 inch o.d. or smaller.

Effect of tube diameter ratio (i.d./o.d.): For selected tube outside diameter, the tube diameter ratio (i.d./o.d.) measures both the thickness of the wall and the inside diameter of the tube.

From the viewpoint of minimizing tube wall weight, the tube wall
thickness should be as small as possible, consistent with limits
imposed by fabrication, strength and corrosion considerations.
Thus, for low tube wall weight, the i.d.-to-o.d. ratio of the
tube should be as close to 1.0 as practical. If the tube o.d.
is small, an i.d.-to-o.d. ratio close to 1.0 is also helpful in
keeping down the number of tubes required to maintain a reasonable
velocity of the in-tube fluid.

Items affected adversely as the tube i.d.-to-o.d. ratio increases
towards 1.0 are the volume and the weight of the in-tube fluid.
These factors are significant if the in-tube fluid is hazardous
or has high density.

In the present study the i.d.-to-o.d. ratio of the tubes was
maintained constant at 0.85. For the 3/16 and 1/4 inch o.d.
tubes considered in the study, a diameter ratio of 0.85 implies
tube wall thicknesses of .0141 and .0188 inch, and tube i.d.'s
of .159 and .213 inch, respectively. It is noteworthy that
these values may be conservative: If an i.d.-to-o.d. ratio of
0.89, (or tube wall thicknesses of .0103 and .0138 inch in the
3/16 and 1/4 inch diameter tubes, respectively), were permissible
in the present application, the number of tubes could be reduced
by 9 percent, and the weights of the cores-and-return bends by

15 percent, of the values cited herein. These percentage
reductions would apply equally to the 3/16 and 1/4 inch o.d.
tube assemblies.

The numerical values in the preceding paragraph and the foregoing
comments indicate that the tube diameter ratio is a significant
parameter. They also indicate that the heat exchanger weights
herein may be conservative. In a final design point study for
the present application, the tube i.d.-to-o.d. ratio should be
as close to 1.0 as possible, consistent with fabrication, strength
and corrosion limitations.

Effect of transverse and axial tube spacings: For fixed dimensions
of the tubes and fins, the tube spacings affect the volume and
weight of the heat exchanger core, and the size and weight of
the enclosing shell and support structure. In the present applica-
tion, small volumes and low weights are desired.

One measure of the potential compactness of a heat transfer
geometry is the number of square feet of heat transfer surface
contained per cubic ft of free space in the gas channel (Ref. 9).
For fixed dimensions of tubes and fins in the externally finned
tubular geometry, the heat transfer surface per unit gas volume
increases as the tubes move closer together. Barring overlap or
meshing of the fins of neighboring tubes, the maximum surface

34

per unit gas volume is obtained if the tubes are arranged on a triangular pitch (figure 2) and are so spaced that the fins of adjacent tubes just touch each other. Wider spacing of the tubes in directions either perpendicular or parallel to the direction of gas flow reduces the surface per unit volume and tends to make the heat exchanger less compact.

In the present study the tubes were assumed to be arranged in an equilateral triangular array in which the sides of the triangle were 1.01 times the o.d. of the fins (after allowance for fin thermal expansion). For the 3/16 inch o.d. tube, fin o.d.-to-i.d. ratio of 2.0 and 30 fins per inch at which the bulk of the calculations herein were performed, such a triangular tube array involves about 700 ft^2 of gas side heat transfer surface per cubic foot of free gas space. At 40 fins per inch, the specific surface increases to about 900 ft^2/ft^3. For transverse or axial tube spacings larger than those leading to nearly touching fins, the gas heat transfer surface per unit gas volume would be lower than 700 to 900 ft^2/ft^3, and the associated heat exchanger assemblies would probably be larger and heavier than those reported herein.

Thermal, Coolant and Materials Parameters

The following six parameters are discussed in the present section: the heat exchanger cooling effectiveness, $\eta_{cooling}$; the ratio of gas-to-coolant heat capacity rates, $(\dot{m}c_p)_{gas}/(\dot{m}c_p)_{coolant}$; the number of coolant passes in cross-counterflow; the coolant pressure drop; the coolant composition; and the materials of the tubes and fins. These parameters are discussed in terms of their effects on the heat exchanger weight, dimensions and number of tubes.

Effect of heat exchanger cooling effectiveness ($\eta_{cooling}$): In the present study an increase in the heat exchanger cooling effectiveness implies an increase in the temperature of the liquid at entrance to the heat exchanger; and this in turn implies an improvement in radiating ability at the low temperature end of the radiator. The effects of increases in $\eta_{cooling}$ on the heat exchanger size, weight and number of tubes are therefore of interest; such effects are shown in figure 7.

The values in figure 7 are for heat exchangers of the 1000 KW cycle defined in Table I, with the following additional specifications: Steel tubes of 3/16 inch o.d., tube i.d.-to-o.d. ratio equal to 0.85, copper fins of .005 inch thickness, 30 fins per inch, fin o.d.-to-i.d. ratio equal to 2.0; argon gas, NaK coolant, a NaK pressure drop of 30 psi in 8-pass cross-counterflow, with $(\dot{m}c_p)_{gas}/(\dot{m}c_p)_{coolant}$ equal to 0.90.

36

Figure 7 shows that as the heat exchanger cooling effectiveness increases, the only quantity that decreases is the no-flow dimension. All other quantities in figure 7 increase, and with increasing steepness, as the cooling effectiveness increases. Table 6 presents illustrative values from figure 7.

Table 6. Effect of Heat Exchanger Cooling Effectiveness ($\eta_{cooling}$)

$\eta_{cooling}$	0.90	0.925	0.950
Wt. of wet core plus return bends (lb)	409	545	832
Core volume (ft^3)	2.97	3.88	5.78
Core frontal area (ft^2)	2.52	2.77	3.16
Tube length (ft)	1.48	1.82	2.34
No-flow length (ft)	1.70	1.52	1.35
Axial length (ft)	1.18	1.40	1.83
Number of tubes	2285	2450	2830

Table 6 shows that when the cooling effectiveness is as high as 0.9, even small increases in the effectiveness involve large changes in the weight and size of the heat exchanger. An increase in $\eta_{cooling}$ from 0.90 to 0.95 essentially doubles the weight and volume of the heat exchanger; increases the tube length and axial dimension by more than 50 percent; and produces changes of more than 20 percent in frontal area, no-flow length and number of tubes of the heat exchanger assembly.

As stated above and indicated in figure 7, the values cited in the foregoing paragraph correspond to a gas-to-coolant $(\dot{m}c_p)$-ratio of 0.9. The increases in heat exchanger size and weight with increases in cooling effectiveness are larger than the above-cited values when the gas-to-coolant $(\dot{m}c_p)$-ratio exceeds 0.90.

Because of the rapid increase in weight and dimensions of the gas cooler with increases in $\eta_{cooling}$ in the range of interest, a final choice of cooling effectiveness might require a size and weight trade-off analysis between the gas cooler and the radiator or other component of the system. In the present study, heat exchangers with cooling effectivenesses of 0.90, 0.925 and 0.95 were computed for the 1000 KW cycle; heat exchangers with effectivenesses of 0.925 and 0.95 were computed for the 500 and 100 KW cycles; and heat exchangers with an effectiveness of 0.95 were computed for the 10 KW cycle, for both NaK and water as coolants.

Effect of gas-to-coolant $(\dot{m}c_p)$-ratio: For fixed gas conditions as in Table I, and for fixed cooling effectiveness, an increase in the ratio $(\dot{m}c_p)_{gas}/(\dot{m}c_p)_{coolant}$ implies an increase in the coolant temperature at exit from the heat exchanger; and this implies an increase in radiating ability at the hot end of the radiator. The effects of increases in the gas-to-coolant $\dot{m}c_p$-ratio are therefore of interest. Such effects are shown in figure 8.

The values in figure 8 are for heat exchangers of the 1000 KW cycle defined in Table 1, with the following additional specifications: Steel tubes of 3/16 inch o.d., tube i.d.-to-o.d. ratio equal to 0.85, copper fins of .005 inch thickness, 30 fins per inch, fin o.d.-to-i.d. ratio equal to 2.0; argon gas, NaK coolant, a NaK pressure drop of 30 psi in 8-pass cross-counterflow, and a cooling effectiveness equal to 0.90.

Figure 8 shows that as $(\dot{m}c_p)_{gas}/(\dot{m}c_p)_{coolant}$ increases, only the no-flow dimension decreases. The remaining size parameters and the weight increase. Illustrative values from figure 8 are shown in Table 7.

Table 7. Effect of $(\dot{m}c_p)_{gas}/(\dot{m}c_p)_{coolant}$

$(\dot{m}c_p)_{gas}/(\dot{m}c_p)_{coolant}$	.90	.95	1.0
Wt. of wet core plus return bends (lb)	409	508	633
Core volume (ft^3)	2.97	3.63	4.62
Core frontal area (ft^2)	2.52	2.71	2.94
Tube length (ft)	1.48	1.76	2.13
No-flow length (ft)	1.70	1.54	1.38
Axial length (ft)	1.18	1.34	1.57
Number of tubes	2285	2345	2440

The increments in the tabulated values are larger when the gas-to-coolant $(\dot{m}c_p)$-ratio increases from .95 to 1.0 than they are when the $(\dot{m}c_p)$-ratio increases from .90 to .95. Thus, even in 8-pass flow at a cooling effectiveness as non-extreme as .90, the dependence of the heat exchanger properties on $(\dot{m}c_p)_{gas}/(\dot{m}c_p)_{coolant}$ is non-linear.*

----
* The no-flow dimension is an exception in Table 7; the no-flow length decreases linearly as the $(\dot{m}c_p)$- ratio increases from .90 to 1.0.

Table 7 shows that for the relatively non-severe requirement of 0.90 cooling effectiveness in 8-pass cross-counterflow, an increase in $(\dot{m}c_p)_{gas}/(\dot{m}c_p)_{coolant}$ from 0.90 to 1.0 incurs more than 50 percent increases in the weight and volume of the tube assembly. The tube length increases more than 40 percent and the dimension in the axial (gas flow) direction increases more than 30 percent. Because the no-flow dimension decreases, the increase in frontal area is moderate (about 17 percent) even though the tube length increases more than 40 percent. The number of tubes does not increase very much (somewhat less than 7 percent) as the gas-to-coolant $(\dot{m}c_p)$-ratio increases from 0.90 to 1.0.

The values enumerated in the preceding paragraph apply when the cooling effectiveness is 0.90. At higher values of the cooling effectiveness, the effects of increases in the gas-to-coolant $(\dot{m}c_p)$-ratio are substantially larger than those indicated above, as will be seen from the later-presented results of the parametric calculations.

Because of the substantial increases in size and weight of the gas cooler with increases in $(\dot{m}c_p)_{gas}/(\dot{m}c_p)_{coolant}$ in the range of interest, choice of a final value of this ratio might require a size and weight trade-off between the gas-cooler and radiator or other component of the system. In the present study, gas-to-coolant (mc_p)-ratios of 0.90, 0.95 and 1.00 were evaluated at

every set of operating conditions explored.

Effect of number of coolant passes in cross-counterflow: As the number of coolant passes in figure 3 increases, the temperature pattern in the heat exchanger approaches more closely the temperature pattern that exists in pure counterflow. Accordingly, the overall specific conductance, $UA/(\dot{m}c_p)_{gas}$, required to attain a pre-assigned cooling effectiveness decreases, and the size and the weight of the active heat exchanger core decrease. Importantly, cooling effectivenesses that might otherwise not be feasible become attainable. The effects of increases in the number of coolant passes on other exchanger characteristics are therefore of interest. A list of such effects is presented in Table 8.

The values in Table 8 are for heat exchangers of the 1000 KW system defined in Table I, with the following additional specifications: Steel tubes of 3/16 inch o.d., tube i.d.-to-o.d. ratio equal to 0.85, copper fins of .005 inch thickness, 30 fins per inch, fin o.d.-to-i.d. ratio equal to 2.0; argon gas, NaK coolant, a NaK pressure drop of 30 psi in both 6-and 8-pass flows, and a heat exchanger cooling effectiveness of 0.95.

Table 8 shows that for fixed cooling effectiveness and fixed $(\dot{m}c_p)_{gas}/(\dot{m}c_p)_{coolant}$, an increase in the number of passes results in decreases in the weight, volume and frontal area of the active core, as well as in the tube length and core axial length. As the number of coolant passes increases, however, the no-flow dimension, the number of tubes and the weight of the return bends also increase.

41

Table 8. Effect of Number of Coolant Passes

Number of coolant passes	6	8	6	8
$(\dot{m}c_p)_{gas}/(\dot{m}c_p)_{coolant}$	0.90	0.90	1.0	1.0
Wt. of wet core (lb)	645	578	1880	1535
Wt. of wet return bends (lb)	190	254	498	568
Wt. of wet core plus return bends (lb)	835	832	2378	2103
Core volume (ft^3)	6.44	5.78	18.6	15.5
Core frontal area (ft^2)	3.24	3.16	4.76	4.52
Tube length (ft)	3.48	2.34	7.43	5.04
No-flow length (ft)	0.93	1.35	0.64	0.90
Axial length (ft)	1.99	1.83	3.91	3.45
No. of tubes	2110	2830	2795	3525

In the heat exchanger configuration in figure 3, the return bends serve the same function as would headers located between successive passes.* The relatively large weight fraction contributed by headers in compact heat exchangers is well known. In the same way, the large contribution of the return bends to the weight of the tube assembly in the 1000 KW system may be noted. In 6-pass coolant flow at a pressure drop of 30 psi as in Table 8, the return bends contribute slightly more than 20 percent of the weight, and in 8-pass flow at a pressure drop of 30 psi the return bends contribute roughly 30 percent of the weight, of the tube assembly. The fact that the weight of the return bends is substantial, and goes up as the number of coolant passes goes up, imposes a limit on the number of passes that can profitably be employed in the

---

* Heat transfer across the return bend surfaces is ignored herein.

heat exchangers of the 1000 KW system.

The upper limit on the profitable number of coolant passes depends on the cooling effectiveness, the gas-to-coolant $(\dot{m}c_p)$-ratio, the allowable coolant pressure drop and the comparative importances of weight and size in the application of interest. If either the cooling effectiveness or gas-to-coolant $(\dot{m}c_p)$-ratio increases, the weight-optimum number of coolant passes increases. Thus, Table 8 shows that at $(\dot{m}c_p)_{gas}/(\dot{m}c_p)_{coolant}$ equal to 0.9, there is no incentive to use more than 6 or 7 coolant passes insofar as the combined weight of the core and return bends is concerned; but when the $(\dot{m}c_p)$-ratio increases to 1.0, there is a 12 percent reduction in weight and a 16 percent reduction in volume as the number of coolant passes increases from 6 to 8; for an $(\dot{m}c_p)$-ratio of 1.0, more than 8 passes might be profitable.

The data in Table 8 for an $(\dot{m}c_p)$-ratio of 0.9 also show that if small volume and short tubes are more important than weight, and if an increase in the number of tubes is tolerable, there is a moderate incentive to increase the number of coolant passes beyond the core-plus-return bend weight-optimum value. It is noteworthy that when the volume decreases, a reduction in weight is obtained through the decrease in shell size.

The optimum number of coolant passes also depends on the allowable coolant pressure drop. It will be seen from later-presented data that when the allowable $\triangle p$ of the coolant decreases, the weight-optimum number of coolant passes may decrease, depending on the

values of cooling effectiveness and gas-to-coolant $(\dot{m}c_p)$-ratio to which the heat exchanger is to be designed.

The foregoing discussion indicates that for high performance cross-counterflow heat exchangers, there exists an optimum number of coolant passes. The existence of such an optimum arises from the fact that the number of passes affects not only the size and weight of the active core, but also the weight of the return bends (or intermediate headers), which may contribute substantially to the total heat exchanger weight. Within limits imposed by fabrication, use of the optimum number of coolant passes is desirable in high performance applications. In the present study, both 6-and 8-pass heat exchangers were computed at every set of operating conditions investigated.

Effect of coolant pressure drop: A lower bound on coolant pressure drop is set by the requirement of reasonably efficient pump operation. Increases in pressure drop beyond the pump-determined lower bound involve increases in pumping power and may give rise to weight increases in order to remain within allowable stress limits. The effects of increases in coolant pressure drop on the heat exchanger characteristics are therefore of interest. Such effects are shown in figure 9.

The values in figure 9 are for heat exchangers of the 1000 KW system defined in Table 1, with the following additional specific-ations: Steel tubes of 3/16 inch o.d., tube i.d.-to-o.d. ratio equal to 0.85, copper fins of .005 inch thickness, 30 fins per

44

inch, fin o.d.-to-i.d. ratio equal to 2.0; argon gas, NaK coolant, a gas-to-coolant $(\dot{m}c_p)$-ratio of 0.90 and a heat exchanger cooling effectiveness of 0.95. Both 6-and 8-pass heat exchangers are presented in figure 9.

Figure 9 shows that as the coolant pressure drop increases from 5 psi toward higher values, the axial length of the core remains nearly constant, signifying that the axial number of banks of tubes changes slowly with increases in coolant pressure drop. The no-flow dimension, however, decreases substantially, and the tube length increases substantially. The total number of tubes decreases strongly. In the pressure drop range from 5 to about 25 psi, the drop in the number of tubes is particularly steep. Beyond a $\triangle p$ of about 25 psi the rate of decrease in the number of tubes is less pronounced, but remains non-negligible even at pressure drops as high as 75 to 100 psi. The fact that the number of tubes responds significantly to the coolant pressure drop is of interest from the viewpoint of the heat exchanger weight.

The effect of coolant pressure drop on the heat exchanger weight may be discussed in terms of the effects of coolant $\triangle p$ on the weight of the wet core (which consists of the tubes, fins and in-tube coolant) and on the weight of the wet return bends; (as noted previously, the return bends contribute a substantial fraction of the total weight of the tube assembly in the heat exchangers of the 1000 KW system).

The weight of the wet core is directly proportional to the core volume. Figure 9 shows that the core volume decreases quite

slowly as the coolant pressure drop increases from 5 to 100 psi; hence the active core weight also decreases very slowly as the coolant Δp increases. The main reason for this is that for the heat exchangers of figure 9, the combined thermal resistance of gas and tube walls comprises about 90 percent of the total thermal resistance in the heat exchanger. Increases in coolant pressure drop by means of increases in coolant velocity reduce the thermal resistance of the coolant and raise the fractional resistance of gas and tube walls from about 0.9 toward 1.0. The range from 0.9 to 1.0 is small from the outset, hence large volume changes could not be expected. In addition, inasmuch as the heat transfer coefficient of the gas remains nearly constant (cf. the near constancy of the core frontal area in figure 9) then, at constant heat load and constant fluid end temperatures, there is little leeway for reduction in the amount of gas and tube wall heat transfer surface, and hence little leeway for reduction in core volume (to which the heat transfer surface is directly proportional). Finally, the coolant pressure drop, which depends on both coolant velocity and tube length, increases more rapidly than the coolant thermal resistance decreases, so that only modest changes in allowable gas-and-wall thermal resistance are achievable before the coolant pressure drop becomes unattractively high. For these reasons the core volume and active core weight are insensitive to coolant pressure drop.

The weight of the return bends, on the other hand, is governed by the total number of tubes and by the bend lengths. For constant

46

tube spacing and essentially constant core axial length as noted above, the lengths of the return bends are also essentially constant. Hence the variation of the return bend weight with increases in coolant pressure drop is governed by the variation in the total number of tubes. Figure 9 shows that, like the total number of tubes, the return bend weight decreases strongly as the coolant pressure drop increases from 5 to about 25 psi, and that for coolant pressure drops beyond about 25 psi the weight of the return bends decreases more slowly.

The net effect of coolant pressure drop on the heat exchanger weight is the sum of the effects on the core and return bend weights. Figure 9 shows that as the coolant pressure drop increases from 5 to about 25 psi, the core-plus-return bend weight decreases substantially, and that for coolant pressure drops greater than about 25 psi the core-plus-return bend weight decreases more slowly. The discussion above indicates that this variation in assembled tube weight is due primarily to the effect of coolant pressure drop on the weight of the return bends.

Figure 9 also shows that at pressure drops below about 25 psi, 6-pass heat exchangers weigh slightly less than 8-pass heat exchangers. The dependence of the weight-optimum number of passes on coolant pressure drop was previously noted during discussion of the effects of the number of coolant passes. The superiority of the 6-pass over the 8-pass arrangement would increase if the cooling effectiveness were lower than the 0.95 value that applies in figure 9, or if the gas-to-coolant (mc_p)-ratio were lower than

0.9. On the other hand, at higher values of cooling effectiveness or gas-to-coolant $(\dot{m}c_p)$-ratio, 8-pass flow would be markedly superior to 6-pass flow, as will be seen from the curves of systematic parametric data presented later in the report. The effects of coolant pressure drop are summarized in Table 9.

Table 9. Effect of Coolant Pressure Drop

Coolant pressure drop (psi)	5	30	100
Wt. of wet core plus return bends (lb)	1079	832	732
Core volume (ft^3)	5.90	5.78	5.62
Core frontal area (ft^2)	3.18	3.16	3.11
Tube length (ft)	1.22	2.34	3.69
No-flow length (ft)	2.61	1.35	0.84
Axial length (ft)	1.85	1.83	1.81
No. of tubes	5580	2830	1735

The values in Table 9 are taken from figure 9 and correspond to the 8-pass heat exchangers of that figure. Table 9 illustrates the previously cited substantial decreases in the total number of tubes, assembled tube weight and core no-flow dimension; the substantial increase in tube length; and the near constancy of the core axial length, frontal area and volume, with increases in the coolant pressure drop. In the present study, heat exchanger data are presented for coolant pressure drops from 5 to 100 psi at every combination of parameters explored.

48

<u>Effect of coolant composition</u>: When high performance liquids
like NaK, lithium and water are employed as coolants, roughly
90 to 97* percent of the thermal resistance is contributed by
the gas and tube walls even when the gas side of the tubes is
extensively finned with such high conductivity fin materials as
copper or aluminum. Inasmuch as the coolant contributes only
about 10 percent or less of the total thermal resistance, it
is of interest to inquire whether there is a large incentive to
use one high performance liquid in preference to another, or
whether it is not preferable simply to use the liquid that is
easiest to handle. This question may be discussed on the basis
of the data in Tables 10 through 12. Table 10 presents pertinent
fluid properties, and Tables 11 and 12 present computed heat
exchanger data for the coolants of interest.

The sources of the data in Table 10 are as follows: for NaK,
Reference 3; for lithium, References 10, 11, 12; for water,
Reference 4 . The values in Table 10 correspond to the average
temperatures at which the heat exchangers discussed in the present
section were computed. Other values of the listed properties were
employed at other temperature levels.

Table 10 shows that the specific heat and thermal conductivity
of lithium are both significantly higher than those of NaK, and
that the density of lithium is roughly 60 percent that of NaK.

----
* The thermal resistance fraction attributable to the gas increases
when the fin material changes from copper to aluminum and also
when the coolant species changes.

Table 10. Coolant Properties*

Power level (KW)	Cooling effectiveness	$\dfrac{(mc_p)_{gas}}{(mc_p)_{coolant}}$	Coolant	c_p $\left(\dfrac{Btu}{lb\ ^oR}\right)$	k $\left(\dfrac{Btu}{hr\ ft^2\ ^oR/ft}\right)$	μ $\left(\dfrac{lb_m}{hr\ ft}\right)$	ρ $\left(\dfrac{lb_m}{ft^3}\right)$
1000	0.95	0.90	NaK	0.210	15.0	0.488	48.5
			Li	1.01	27.2	0.967	30.5
10	0.95	1.0	NaK	0.223	13.8	1.05	52.8
			H_2O	1.10	0.397	0.456	58.9

* Sources of data: NaK, Ref. 3; Li, Ref's 10-12; H_2O, Ref. 4 .

The table shows that NaK is very superior to water as regards thermal conductivity, but that NaK has only one fifth the specific heat of water; the densities of NaK and water are nearly the same at the conditions underlying Table 10. The influences of these properties on heat exchangers involving the listed coolants are reflected in Tables 11-13.

NaK and lithium: The heat exchangers in Table 11 are for the 1000 KW system defined in Table 1, with the following additional specifications: Tubes of 3/16 inch o.d. composed of steel in the NaK heat exchanger and of Cb-1%Zr in the lithium heat exchanger, tube i.d.-to-o.d. ratio equal to 0.85, copper fins of .005 inch thickness, 30 fins per inch, fin o.d.-to-i.d. ratio equal to 2.0; argon gas, NaK and lithium coolants, coolant pressure drop 30 psi in 8-pass cross-counterflow; a cooling effectiveness of 0.95, with $(\dot{m}c_p)_{gas}/(\dot{m}c_p)_{coolant}$ equal to 0.90.

Table 11 shows that for equal temperature and pressure performances, lithium yields a core-plus-return bend weight 28 percent lighter than that yielded by NaK. This result is obtained even though the density of the columbium alloy in the lithium heat exchanger is 536 lb/ft^3 while the density of the steel in the NaK heat exchanger was taken at 500 lb/ft^3.

It is noteworthy that only a portion of the difference in weight between the lithium and NaK heat exchangers is contributed by the active core, where the superior thermal conductivity and specific

51

Table 11. Effect of Coolant Composition (NaK and Lithium)

Coolant	NaK	Lithium
Wt. of wet core (lb)	578	504
Wt. of wet return bends (lb)	254	94
Wt. of wet core plus return bends (lb)	832	598
Core volume (ft^3)	5.78	5.10
Core frontal area (ft^2)	3.16	3.00
Tube length (ft)	2.34	5.00
No flow length (ft)	1.35	0.60
Axial length (ft)	1.83	1.70
No. of tubes	2830	1165

heat of lithium lead to a heat transfer coefficient about twice as large as that of the NaK. If the active core were the only weight-contributing factor, then, by virtue of lithium's superior thermal properties the lithium unit would be about 14 percent lighter than the NaK unit, as shown by Table 11. As has been previously discussed, however, in multipass cross-counterflow heat exchangers, the intermediate headers -- or, in the present configuration, the return bends -- may also contribute significantly to the weight. Table 11 shows that the return bend weight in the lithium heat exchanger is about 0.4 times the return bend weight in the NaK heat exchanger. This is primarily due to the smaller number of return bends in the lithium unit than in the NaK unit. Table 11 shows that the lithium heat exchanger has

only 0.4 times as many tubes, and hence only 0.4 times as many return bends, as the NaK heat exchanger does. The effects of the unequal densities of the tube wall materials and coolants in the two heat exchangers, and the unequal axial lengths, essentially balance each other.

The smaller number of tubes in the lithium heat exchanger is due to the fact that the specific heat of lithium is almost five times the specific heat of NaK at the conditions underlying Table 11. Since for the same gas-to-coolant $(\dot{m}c_p)$-ratio the mass flow of lithium is approximately one fifth the mass flow of NaK, the lithium heat exchanger requires fewer tubes to maintain a reasonable fluid velocity, even though at the temperatures under consideration the density of lithium is only 0.6 times the density of NaK. Thus the high specific heat of lithium, which helps to increase the coolant heat transfer coefficient and to reduce thereby the weight of the active core, also helps to reduce the weight of the return bends. The combined effect of reductions in core and return bend weight leads to a lithium heat exchanger that is 28 percent lighter than the NaK heat exchanger. The fact that the lithium core volume is about 12 percent smaller than the NaK core volume, as shown by Table 11, could also lead to a slightly lighter shell weight in the lithium heat exchanger than in the NaK heat exchanger.

Although the lithium heat exchanger is lighter and has fewer tubes than the NaK heat exchanger does, the relatively unfavorable

53

aspect ratio of the lithium heat exchanger may be noted. The gas face aspect ratio, $\ell_{tube}/\ell_{no\ flow}$, of this heat exchanger is 8.3, which appears undesirable from the viewpoints of gas flow distribution or shape of the approach duct. This problem can be largely mitigated, however, by use of a folded tube construction. The gas face aspect ratio of the NaK heat exchanger is 1.7, which is probably suitable without recourse to tube folding.

The foregoing has shown that lithium heat exchangers are significantly lighter and have fewer tubes than do NaK heat exchangers. If the 360°F freezing point of lithium, the use of Cb-1%Zr to take account of lithium's chemical aggressiveness and the need for a folded tube construction are acceptable, lithium heat exchangers are more attractive than NaK heat exchangers by virtue of substantially smaller weight and smaller number of tubes.

NaK and water: A comparison of NaK and water heat exchangers is presented in Table 12. The heat exchangers in Table 12 are for the 10 KW system defined in Table 1, with the following additional specifications: Steel tubes of 1/8 inch o.d., tube i.d.-to-tube o.d. ratio equal to 0.85, aluminum fins, 30 fins per inch, fin o.d.-to-fin i.d. ratio equal to 2.0, fin thickness .005 inch; argon gas, NaK and water coolants, coolant pressure drop 10 psi in 8-pass cross-counterflow, $(\dot{m}c_p)_{gas}/(\dot{m}c_p)_{coolant}$ equal to 1.0 and a heat exchanger cooling effectiveness equal to 0.95.

Table 12. Effect of Coolant Composition (NaK and Water)

Coolant	NaK	Water
Tube material	Steel	Steel
Wt. of wet core (lb)	46.1	52.3
Wt. of wet return bends (lb)	5.2	2.0
Wt. of wet core plus return bends (lb)	51.3	54.3
Core volume (ft^3)	0.778	0.882
Core frontal area (ft^2)	0.95	1.00
Transverse dimension (ft)*	0.85	2.87
No-flow dimension (ft)	1.11	0.347
Axial length (ft)	0.825	0.884
Number of tubes	295	100

* With folded tubes. The transverse dimension is about $1/8^{th}$ of the tube length.

The heat exchangers in Table 12 show characteristics very similar to those in Table 11. Because of the superior NaK heat transfer coefficient, the active core of the NaK heat exchanger is about 13 percent lighter than that of the water heat exchanger. Because of the higher specific heat of water, the number of tubes and the return bend weight are smaller in the water heat exchanger than in the NaK heat exchanger. The weight of the water return bends is roughly 0.4 times that of the NaK return bends, which is consistent with the comparative numbers and axial lengths of the return bends in the two exchangers. The net effect of the core

and return bend contributions is that the weight of the assembled NaK heat exchanger is only about 5 percent lighter than the assembled water heat exchanger.

Another point of similarity among the heat exchangers of Tables 11 and 12 is the fact that the lithium and water heat exchangers have much longer tubes (or core transverse dimensions) than do the NaK heat exchangers. Thus the high specific heats of lithium and water, which lead to significant reductions in the number of tubes, also lead to substantial increases in the lengths of tubes. Tables 11 and 12 show that just as the tube lengths in the lithium assembly are roughly twice as long as those in the analogous NaK assembly, so are the tube lengths in the water unit nearly 3.5 times as long as those in the comparable NaK unit. These data indicate that if a choice among coolants with widely different values of specific heats is available, the number and length of the tubes can be very significantly influenced by choosing the coolant with an appropriate specific heat.

Also noteworthy in Table 12 is the relatively small weight fraction contributed by the return bends in the heat exchangers of the 10 KW system. In Table 12 the return bends contribute about 10 percent of the assembled NaK heat exchanger weight, and less than 4 percent of the assembled water heat exchanger weight. These percentages are significantly lower than the percentages (20 to 30 percent) contributed by the return bends in the 1000 KW system. These data indicate that the extent to which the return bends affect the heat

exchanger weight depends on the system power level and on the associated pressure and temperature conditions to which the heat exchanger is designed (see Table 1).

Among the significant facts disclosed by Table 12 is that in the 10 KW system of the present study, heat exchangers that use ordinary (non-metallic) coolants can be competitive in weight with heat exchangers that use high performance liquid metals. As previously stated, and as shown by Table 12, the assembled weight of the heat exchanger that uses NaK as coolant is only about 5 percent lighter than the assembled weight of the heat exchanger that uses water as the coolant.

The foregoing has shown that substantial variations in the weight, size and shape of heat exchangers, and large variations in the length and number of tubes, can result from use of various coolants, even when all the coolants are high performance liquids. Through the several physical and thermal properties that affect the magnitude of the heat transfer coefficient and the pressure drop, the coolant affects the weight of the active core. Through its specific heat, the coolant affects the number and length of the tubes and the weight of the return bends. In cross-counterflow heat exchangers the merit of a coolant is determined by its effects on the combined weight of the core and return bends. Because of this fact, heat exchangers that use lithium as coolant are lighter and have longer tubes than do those that employ NaK as coolant; and heat exchangers that employ water as coolant are competitive in weight and have longer tubes than do those that use NaK as coolant.

An additional way in which the coolant composition affects the weight of the heat exchanger is through the tube materials required for coolant containment. This aspect of coolant composition is considered in the following section on the effects of materials.

In the present study, both NaK and lithium were evaluated for the heat exchangers of the 1000 KW system. NaK alone was considered for the heat exchangers of the 500 and 100 KW systems. Both NaK and water were evaluated for the heat exchangers of the 10 KW system.

Effect of materials: If the temperature level is sufficiently low so that aluminum can be used instead of steel or other relatively heavy metals for the tubes and instead of copper for the fins, the weight of the heat exchanger can be reduced significantly. In the 10 KW system of the present study the gas inlet temperature to the heat exchanger is $455^{\circ}F$ ($915^{\circ}R$, Table 1), which is within the operable temperature range of aluminum for the tubes as well as for the fins. In the 100 and 500 KW systems of the present study the gas inlet temperature to the heat exchanger is $733^{\circ}F$ ($1193^{\circ}R$, Table 1) and the highest fin temperature at the hot end of the heat exchanger is about $720^{\circ}F$. Inasmuch as the fins are not structural members and neon is an inert gas, the use of aluminum for the fins appears possible. The effects of using aluminum tubes and fins in the 10 KW system and of aluminum fins in the 100 and 500 KW systems are discussed

58

in the present section.

Tube materials (10 KW system): Reference 3 indicates that at temperatures up to about 430°F the resistance of 2S and 3S aluminum alloys to corrosion by NaK is good in long term applications; and that at temperatures as high as 800 to 1000°F, 2S and 3S aluminum will contain NaK satisfactorily in short term applications. Reference 3 indicates that at temperatures between about 430 and 800°F, the resistance of aluminum to corrosion by NaK has not been adequately studied. Reference 13, which is concerned primarily with liquid metals corrosion at high temperatures, does not appear to treat the subject of NaK containment by aluminum.

In the 10 KW system of the present study, the highest computed tube wall temperature is 436°F, which is close to the 430°F value at which aluminum resists attack by NaK in long term applications (Reference 3). Accordingly brief calculations were made of aluminum heat exchangers with NaK as coolant. Brief calculations were also made of aluminum heat exchangers that use water as coolant. Although the need for fairly elevated pressures to suppress water boiling, and the possibility of corrosion, may in fact exclude the use of aluminum tubes with water in the 10 KW system, the results of calculations on such heat exchangers could be indicative of the advantages of aluminum with non-liquid metal coolants other than water. Table 13 presents a comparison among heat exchangers that use NaK in both steel and aluminum tubes and water in aluminum tubes.

The aluminum tube heat exchangers in Table 13 were computed from the steel tube heat exchangers of Table 12 by multiplying the wall weights of the tubes and return bends of the steel tube heat exchangers by 173/500, and by then adding the weights of the (aluminum) fins and contained coolant that had previously been computed for steel tube heat exchangers. This procedure takes no credit for the reduction in tube wall thermal resistance when the wall material is changed from steel to aluminum. As the tube wall thermal resistance is less than 1 percent of the total thermal resistance in the heat exchangers under discussion, this conservatism affects the results negligibly.

The heat exchangers in Table 13 are for the 10 KW system defined in Table 1, with the following additional specifications: tubes of 1/8 inch o.d., tube i.d.-to-o.d. ratio equal to 0.85, aluminum fins, 30 fins per inch, fin o.d.-to-i.d. ratio equal to 2.0, fin thickness .005 inch; argon gas, NaK and water coolants, coolant pressure drop equal to 10 psi in 8-pass cross-counterflow, $(\dot{m}c_p)_{gas}/(\dot{m}c_p)_{coolant}$ equal to 1.0 and a heat exchanger cooling effectiveness equal to 0.95.

Table 13 shows that if aluminum tubes can be used instead of steel tubes in the heat exchanger of the 10 KW system, the weight of the NaK heat exchanger could be reduced by somewhat more than 35 percent. This overall weight reduction is not as large as the reduction in the tube and return bend wall weights taken by themselves because the fins and the contained liquid also contribute

60

to the total heat exchanger weight and these component weights remain unchanged when aluminum replaces steel in the tube and return bend walls.

Table 13. Effect of Tube Material (10 KW System)

Tube material	Steel	Aluminum	Aluminum
Coolant	NaK	NaK	(H_2O)*
Wt. of wet core (lb)	46.1	30.1	(34.5)
Wt. of wet return bends (lb)	5.2	2.5	(1.0)
Wt. of wet core plus return bends (lb)	51.3	32.6	(35.5)
Core volume (ft^3)	0.778	0.778	(0.882)
Core frontal area (ft^2)	0.95	0.95	(1.00)
Transverse dimension (ft)**	0.85	0.85	(2.87)
No-flow dimension (ft)	1.11	1.11	(0.347)
Axial length (ft)	0.825	0.825	(0.884)
Number of tubes	295	295	(100)

* Because of fairly elevated pressure to suppress water boiling, and because of possible corrosion, aluminum tubes with water coolant may be marginal in the 10 KW system. The data tabulated for the water heat exchanger may, however, be indicative of aluminum heat exchanger weights with other non-liquid metal coolants.

** With folded tubes. The transverse dimension is about 1/8th of the tube length.

(Table 13 also shows that an aluminum heat exchanger with water as coolant is about 10 percent heavier than an aluminum heat exchanger with NaK as coolant. This numerical result may represent a measure of the potential competitiveness of other non-metallic coolants. Coolants with properties less favorable than those of water would lead to heat exchangers that are more than 10 percent heavier than the NaK heat exchanger. It is noteworthy that the merit of any coolant, metallic or non-metallic, will ultimately be determined by its effects on the combined weight of the gas-to-coolant heat exchanger and waste heat radiator, and that a coolant which yields a relatively heavy heat exchanger may also lead to a relatively heavy radiator. The weights of auxiliaries such as pumps and controls, and the ease of handling and containment, also affect the relative merits of coolants.)

In the bulk of the calculations for the 10 KW system, steel tubes were assumed for both NaK and water as coolants. The calculations have indicated that if aluminum tubes can be used, the heat exchanger weights would decrease by about 35 percent. The calculations have also indicated that heat exchangers using non-metallic coolants may be noticeably, but not prohibitively, heavier than those using NaK in the 10 KW system.

Fin materials (100 and 500 KW system): Because 30 fins per inch with a fin o.d.-to-fin i.d. ratio equal to 2.0 represents a substantial amount of fin metal, use of the optimum fin material is desirable. In the 100 and 500 KW systems the highest fin temperature is about 720°F, and since the fins are non-structural members and neon is an inert gas, use of aluminum appears feasible. An alternate possible fin material is copper. A comparison between heat exchangers using aluminum fins and copper fins is presented in Table 14.

The heat exchangers in Table 14 are for the 100 KW system defined in Table 1, with the following additional specifications: Steel tubes of 3/16 inch o.d., tube i.d.-to-tube o.d. ratio equal to 0.85, 30 fins per inch, fin o.d.-to-fin i.d. ratio equal to 2.0, fin thickness .005 inch; neon gas, NaK coolant, coolant pressure drop equal to 30 psi in 8-pass cross-counterflow, $(\dot{m}c_p)_{gas}/(\dot{m}c_p)_{coolant}$ equal to 0.95 and a heat exchanger cooling effectiveness equal to 0.95.

Table 14 shows that the fins contribute a substantial fraction of the total weight of the assembled core-plus-return bends. When aluminum fins are used, the fins weigh somewhat less than 25 percent of the assembled core-plus-bend weight. If copper fins were used, the fin weight would be tripled; the assembled core-plus-return bend weight would increase by somewhat less than 45 percent, and the fin weight would contribute half of the assembled weight. Table 14 shows that, with the exception of

about a 15 percent reduction in the number of tubes, the gains from the use of copper fins do not compensate for the increase in weight that their use incurs. This conclusion, derived from Table 14 for heat exchangers of the 100 KW system, applies equally to heat exchangers of the 500 KW system.

Table 14. Effect of Fin Materials (100 KW System)

Fin material	Aluminum	Copper
Fin weight (lb)	31	95
Wt. wet core plus return bends (lb)	132	190
Core volume (ft^3)	1.63	1.55
Core frontal area (ft^2)	1.12	1.10
Transverse dimension (ft)*	1.16	1.12
No flow length (ft)	0.97	0.98
Axial length (ft)	1.46	1.41
No. of tubes	540	465

* With folded tubes. The transverse dimension is about 1/3rd of the tube length.

In the present study, aluminum fins were assumed for the heat exchangers of the 10, 100 and 500 KW systems. Because of the 1124°F (1584°R, Table 1) inlet gas temperature in the 1000 KW system, copper fins were assumed for the heat exchangers of this

system. For simplicity, copper fins were assumed to be employed on all the tubes. In a design for minimum weight, the use of aluminum fins in the relatively cool portions of the core would lead to heat exchanger weight reductions in the 1000 KW system.

Parametric Data

Table 15 identifies the combinations of parameters explored in systematic calculations of heat exchangers for the four Brayton cycles defined in Table 1. The data presented in figures 4 to 9 and in Tables 2 to 14, which have already been discussed in the foregoing pages, were extracted from the more extensive results of the calculations identified in Table 15. Systematic variations not covered by figures 4 to 9 and Tables 2 to 14 are presented in figures 10 to 24.

Figures 10 through 24 have the following characteristics in common: In each figure the gas-to-coolant $(\dot{m}c_p)$-ratio has the three values 0.90, 0.95 and 1.0; and at each value of the $(\dot{m}c_p)$-ratio, the coolant pressure drop ranges from 5 to 100 psi in both 6- and 8-pass cross-counterflow circuits. Each figure consists of two pages. Of these, the first page presents computed data on the weight of the wet core-plus-wet return bends of the tube assembly, the number of tubes and, in some cases, the core volume. The second page of each figure presents computed values of the tube length -- or the core transverse dimension in the case of the heat exchangers for the 10 KW system, in which folded tubes were assumed --, the core no-flow dimension, the core axial length and, in some cases, the core frontal area. In those cases in which the core volume and frontal area are not explicitly presented, they can be easily computed from the dimensions presented on the second page of the figure.

Table 15. Ranges of Parametric Data

Power level (KW)	Gas	Cool-ant	Cooling effect-iveness	$\dfrac{(\dot{m}c_p)_{gas}}{(\dot{m}c_p)_{cool.}}$	Tube metal	Fin metal	Tube o.d.* (in.)	Fins per inch	Fin (o.d.) (i.d.)	Fin thick-ness (in.)	No. of coolant passes	Cool-ant Δp (psi)
1000	A	NaK	.90	.90	Steel	Cu	3/16	10 to 40	1.8	.005	8	30
								30	1.4 to 2.5			
				.9, .95, 1					2.0		6,8	5 to 100
			.925									
			.95									
			.925							.010		
			.95									
			.925	.90			0.15 to 0.25			.005	8	30
			.925	.9, .95, 1			1/4				6,8	5 to 100
			.95									

* At all tube diameters studied, the tube i.d.-to-tube o.d. ratio was 0.85.

Table 15. Continued

Power level (KW)	Gas	Coolant	Cooling effectiveness	$\dfrac{(\dot{m}c_p)_{gas}}{(\dot{m}c_p)_{cool.}}$	Tube metal	Fin metal	Tube o.d.* (in.)	Fins per inch	Fin $\dfrac{(o.d.)}{(i.d.)}$	Fin thickness (in.)	No. of coolant passes	Coolant $\triangle p$ (psi)
1000	A	Li	.925	.9, .95, 1	Cb-(1 % Zr)	Cu	3/16	30	2.0	.005	6,8	5 to 100
			.95									
500	Ne	NaK	.925		Steel	Al						
			.95									
100			.925									
			.95									
10	A	NaK	.95	.9, .95, 1	Steel	Al	3/16				6,8	5 to 100
				1.0	Steel, Al		1/8				8	10
		H$_2$0		.9, .95, 1	Steel		3/16				6,8	5 to 100
				1.0	Steel, Al		1/8				8	10

* At all tube diameters studied, the tube i.d.-to-tube o.d. ratio was 0.85.

The numbers of tubes presented in figures 10 through 24 are based on the conservative assumption that one complete tubular coolant channel consists of 6 or 8 straight tubes joined in series by means of return bends brazed to them. If long tubes can be bent to eliminate the need for brazed return bends, the actual numbers of tubes would be 1/6th or 1/8th the values presented in figures 10 through 24. (The factors 1/6 and 1/8 apply to 6- and 8-pass coolant circuits, respectively.)

Cartesian, rather than logrithmic, coordinates are used in figures 10 through 24 to accentuate non-linearities that occur, to magnify the separation between often closely spaced curves and to permit placement of more than one group of curves on a page.

Figures 10 through 24 are further described in the following sub-sections.

1000 KW system: Figures 10 through 18 deal with heat exchangers for the 1000 KW system. In figures 10 through 16, the coolant is NaK. In figures 17 and 18 the coolant is lithium.

Within the figures in which NaK is the coolant, parametric variations occur in the cooling effectiveness, fin thickness and tube diameter, as follows: Figures 10 through 12 treat cooling effectivenesses of 0.90, 0.925 and 0.95 for tubes of 3/16 inch o.d. and a fin thickness of .005 inch. Figures 13 and 14 deal with cooling effectivenesses of 0.925 and 0.95 for tubes of 3/16 inch o.d. and a fin thickness of .010 inch. Figures 15 and 16 treat cooling effectivenesses of 0.925 and

0.95 for tubes of 1/4 inch o.d. with a fin thickness of .005
inch. In all parametric figures in which NaK is the coolant,
the tube metal is steel, the fin metal is copper, the fin
o.d.-to-i.d. ratio is 2.0 and there are 30 fins per inch.

In the two figures (17 and 18) in which lithium is the coolant,
the cooling effectiveness takes the values 0.925 and 0.95. The
tube is assumed made of Cb-1%Zr and has a 3/16 inch outside
diameter. The fin is made of copper, has a thickness of .005
inch, an o.d.-to-i.d. ratio of 2.0, and there are 30 fins per
inch.

Note may be taken of the relatively large ratios of tube length-
to-no flow length for the lithium heat exchangers of figures
17 and 18. These aspect ratios can be brought close to unity
by use of folded tubes. Tube folding is further discussed in
connection with the heat exchangers of the 10 KW system.

500 and 100 KW systems: Figures 19 and 20 present heat exchanger
data for the 500 KW system, and figures 21 and 22 present data for
the 100 KW system. At each power level, cooling effectivenesses
of 0.925 and 0.95 are treated. In all these cases, steel tubes
of 3/16 inch o.d., and aluminum fins of .005 inch thickness with
an o.d.-to-i.d. ratio of 2.0 and a freouency of 30 per inch, are
assumed.

The tube lengths and no-flow lengths (and the associated gas face
aspect ratios) presented in figures 19 through 20 are the
unmodified values obtained from straightforward calculations.

Whenever the tube length and no-flow length combine to give an unattractive gas face aspect ratio, tube folding may be considered, as indicated in more detail for the 10 KW system.

10 KW system: Heat exchanger data for the 10 KW system are presented in figures 23 and 24. In figure 23 the coolant is NaK and in figure 24 the coolant is water. In both figures, steel tubes of 3/16 inch o.d., aluminum fins of .005 inch thickness, a fin o.d.-to-i.d. ratio of 2.0 and 30 fins per inch, are assumed.

In the 10 KW system, the original calculations for both NaK and water led to large values of the ratio, $\ell_{tube}/\ell_{no-flow}$, which is the aspect ratio of the gas face of the heat exchanger. In order to provide gas face aspect ratios closer to unity, the tubes were postulated to be folded 8 times. The geometry of a folded tube is suggested in the adjacent sketch. The tube lengths and the no-flow dimensions in figures 23 and 24 correspond to 8-times folded tubes whose developed lengths would be the same as those of the originally computed straight tubes.
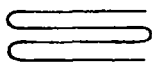
Straight tube

Tube folded 4 times

The quantities principally affected by tube folding are the coolant pressure drop and the total number of tubes (if the tubes cannot be bent, brazed U-bends joining short lengths of straight

tubes become necessary). The calculations for the originally assumed straight tubes showed that in the pressure drop range of interest in the 10 KW system, the return bends of an 8-pass cross-counterflow circuit contribute only about 5 percent of the total coolant pressure drop. The extra pressure drop introduced by the close return bends of an 8-time folded tube with short straight sections, however, would be expected to add considerably more than 5 percent of the total coolant pressure drop.

Figures 23 and 24 show that in the 10 KW system the absolute values of the heat exchanger weight, volume, frontal area and axial length change only slightly even for the twenty fold coolant pressure drop change from 5 to 100 psi; hence these quantities would change quite negligibly for pressure drop increments even as high as 50 percent. As previously indicated, the transverse dimensions and no-flow lengths presented in figures 23 and 24 are for folded tubes of developed length equal to those of the originally computed straight tubes. Figures 23 and 24 indicate only moderate changes in the absolute values of transverse and no flow dimensions for pressure drop increments of the order of 50 percent. Accordingly, with the possible exception of the total number of tubes, the values in figures 23 and 24, based though they are on straight-tube computations, are believed to represent a satisfactory first approximation to the values for folded tube heat exchangers in the 10 KW system.

Uses of parametric data: The parametric data in figures 4

through 24 and in Tables 2 to 14 may be used in a number of ways. Among these are the following:

1. The effects of each parameter may be studied in an effort to obtain insights necessary for sound design. An attempt at such a study is represented by figures 4-9, Tables 2-14 and by the discussion of these figures and tables presented in the foregoing pages.

2. The data may be used for weight trade-off analyses between the gas-to-liquid heat exchanger and the radiator, with possible implications for the pressures, temperatures and efficiencies of other components of the system as well.

3. The data may be used as starting values for heat exchanger detailed design studies.

4. Sample values may be selected as indicative of the magnitudes of heat exchanger weights and dimensions that might be expected at each of the four power levels studied.

For purposes 2 to 4, the values in figures 4 through 24 are believed to represent reasonable starting values of heat exchanger sizes and weights. The effects of geometric thermal, coolant and materials parameters, as discussed under figures 4 to 9 and Tables 2 to 14, may, however, be recalled. That discussion suggests that at any of the four power levels of interest, significant improvements may be made in comparison with the parametric values herein by use of optimum combinations of the entering parameters. Such optimization lies within the scope of detailed design.

In connection with purpose 4, typical values are tabulated herein after the coolant temperatures associated with various cooling effectivenesses and gas-to-coolant $(\dot{m}c_p)$-ratios are discussed in the following section.

Liquid Temperatures And Radiating Potentials

In the gas-to-liquid heat exchanger, the function of the liquid coolant is to extract from the gas the waste heat of the cycle. After leaving the heat exchanger, the function of the liquid is to deliver the waste heat to the walls of the radiator for radiation away to space.

From the viewpoint of heat discard to space, the ideal thermal arrangement would be to have the liquid enter and leave the radiator with temperatures identical to those that the gas would have if the gas itself were the radiator working fluid. If a finite-sized gas-to-liquid heat exchanger is used, however, the liquid temperatures at both entrance to and exit from the radiator are lower than the gas temperatures would be if the gas flowed directly through the radiator.

In order not to nullify the advantages of a liquid working fluid in the radiator, the liquid temperatures at the radiator inlet and outlet must not be too much lower than those that the gas would have if the gas were the radiator working fluid. In order to evaluate the suitability of selected liquid temperatures, the

radiating potentials at those temperatures may be compared with the radiating potentials at the temperatures that would exist if the gas flowed directly through the radiator.

The net radiating potential of a surface at temperature T in an environment of effective temperature T_e is proportional to $(T^4 - T_e^{\,4})$. If the heat transfer coefficient in a liquid-filled radiator is high enough so that the surfaces of the radiator channels are at nearly the same temperatures as the liquid, and if internal fins in a gas-filled radiator bring the surface temperatures of that radiator to nearly the same temperature as those of the gas, then the respective ratios of net radiating potentials at the cold and hot ends of the two radiators are as follows:

$$\left(\begin{array}{l}\text{Ratio of net radi-}\\ \text{ating potentials}\end{array}\right)_{\substack{\text{Radiator}\\ \text{cold end}}} = \left(\frac{T_{\text{liquid}}^4 - T_e^{\,4}}{T_{\text{gas}}^4 - T_e^{\,4}}\right)_{\substack{\text{Radiator}\\ \text{cold end}}}$$

$$\left(\begin{array}{l}\text{Ratio of net radi-}\\ \text{ating potentials}\end{array}\right)_{\substack{\text{Radiator}\\ \text{hot end}}} \simeq \left(\frac{T_{\text{liquid}}^4 - T_e^{\,4}}{T_{\text{gas}}^4 - T_e^{\,4}}\right)_{\substack{\text{Radiator}\\ \text{hot end}}}$$

These two ratios can be used to estimate the suitability of given liquid end temperatures, or equivalently, the suitability of given heat exchanger cooling effectivenesses and gas-to-liquid $(\dot{m}c_p)$-ratios. Liquid temperatures and related ratios of net

74

radiating potentials of liquid and gas radiators are shown in figure 25a, 25b and 25c at various combinations of heat exchanger cooling effectiveness and gas-to-liquid $(\dot{m}c_p)$-ratio.

Figure 25 shows that for the systems under consideration, in which the gas temperatures are fixed (Table 1), the liquid temperature at the cold end of the heat exchanger (and hence at the cold end of the radiator) depends only on the heat exchanger cooling effectiveness and increases as the cooling effectiveness increases. In the cooling effectiveness range 0.90 to 0.95 the variation of the cold-end liquid temperature is essentially linear.

Figure 25 shows that the liquid temperature at the hot end of the heat exchanger (and therefore at the hot end of the radiator) depends on both the heat exchanger cooling effectiveness and the gas-to-liquid $(\dot{m}c_p)$-ratio, and increases as either the effectiveness or $(\dot{m}c_p)$-ratio increases. In the effectiveness range 0.90 to 0.95 the variation of the liquid hot-end temperature is essentially linear with both the cooling effectiveness and $(\dot{m}c_p)$-ratio.

To evaluate the suitability of the liquid temperatures in figure 25, use may be made of the ratios of radiating potentials that are presented in figure 25. Let the condition be arbitrarily imposed that the net radiating potential of the liquid radiator shall not fall below about 70 percent of the net radiating potential at either the hot or cold end of the comparable gas radiator; then figure 25 indicates the following lower bounds on the heat

exchanger cooling effectivenesses and gas-to-coolant $(\dot{m}c_p)$-ratios:

Table 16. Lower Bounds* on $\eta_{cooling}$ and $(\dot{m}c_p)_{gas}/(\dot{m}c_p)_{coolant}$

Power level (KW)	Approximate lower bound on cooling effectiveness	Approximate lower bound on the ratio $(\dot{m}c_p)_{gas}/(\dot{m}c_p)_{coolant}$
10	0.93	0.90
100 and 500	0.91	0.90
1000	0.89	0.90

* In an environment of $425^{O}R$ effective temperature, for (liquid radiating potential) $\geq$ 0.7 x (gas radiating potential).

Table 16 shows that in the systems under consideration, the lower bound on the cooling effectiveness increases as the power level decreases; the lower bound on the gas-to-coolant $(\dot{m}c_p)$-ratio remains essentially constant as the power level changes. These behaviors reflect the influence of the environment temperature on the net radiating potential. The influence of the environment temperature is appreciable when the local radiator temperatures are low, and this is reflected in the behavior of the cooling effectiveness; the influence of the environment temperature decreases as the local radiator temperatures get higher, and this is reflected in the behaviors of both the cooling effectiveness and gas-to-coolant $(\dot{m}c_p)$-ratio. (See Table 1 for the temperature levels of the four systems under consideration.)

It follows from the foregoing discussion that at a given power level, a cold-end liquid temperature is "suitable" if it corresponds to a cooling effectiveness equal to or greater than the value shown in Table 16 for that power level. A hot-end liquid temperature is "suitable" if it corresponds to both a cooling effectiveness and a gas-to-liquid $(\dot{m}c_p)$-ratio equal to or higher than the values shown in Table 16 for the power level under consideration.

Comparison of the cooling effectivenesses and gas-to-coolant $(\dot{m}c_p)$-ratios of Table 15 with the lower bounds shown in Table 16 discloses that all the heat exchangers of the present study meet or exceed the criteria in Table 16. The liquid temperatures and the ratios of radiating potentials that go with the parameter combinations in Table 15 may be read directly from figure 25.

The lower bounds on heat exchanger cooling effectiveness and gas-to-liquid $(\dot{m}c_p)$-ratio in Table 16 permit an estimate of values of these parameters that may be of interest in the systems under consideration. Heat exchanger data at conditions of potential interest may thus be tabulated. Such data are illustrated on page 3 of the report. The illustrative data show that the specific weight and specific volume decrease as the power level increases. The reasons for these decreases are that the gas density and the allowable pressure drop both increase substantially as the power level increases (Table 1).

As previously indicated under "Uses of Parametric Data", the heat exchangers generated in the parametric calculations are capable of

significant improvement by refinement of parameter combinations at each of the power levels studied. The illustrative heat exchangers shown on page 3 of the text represent possible starting configurations that are subject to optimization.

Concluding Remarks

Gas-to-liquid heat exchangers have been discussed in relation to Brayton cycle powerplants for space applications. It has been indicated that for missions in space, a heat exchanger must be highly reliable, as well as light in weight. In order to satisfy the reliability and weight requirements, heat exchangers that employ externally finned tubes have been selected herein.

Computed sizes and weights of externally finned tubular gas-to-liquid heat exchangers have been presented for four Brayton cycle systems capable of generating 10 to 1000 kilowatts of electrical power in space missions. At conditions of very high thermal performance, heat exchanger specific weights between about 1 and 1.5 lb/KW$_e$ have been indicated for cycle power levels in the range 1000 to 100 KW$_e$, and heat exchanger specific weights between about 3.5 and 5.5 lb/KW$_e$ have been indicated for a cycle power level of 10 KW$_e$.

The indicated numerical values have been obtained by postulating tubes of 3/16 and 1/8 inch outside diameters, finned externally with 30 fins per inch of tube length, and arranged so that the fins

of neighboring tubes just touch each other. In order to obtain heat exchanger cooling effectivenesses as high as 0.95 at the gas-to-coolant ($\dot{m}c_p$)-ratios of interest in this study, multipass cross-counterflow liquid circuits have been assumed. In order to provide freedom from thermal stress, disk fins rather than plate fins have been postulated, and the tubes of successive passes have been assumed to be joined to each other by properly shaped U-bends rather than brazed or welded to tube sheets at the junctions of successive passes. In order to maintain a satisfactory gas face aspect ratio, tubes folded in the plane of each tube bank have been considered in the case of the 10 KW system (figure 3b).

The geometric combinations described in the foregoing paragraph may represent significant extensions beyond conventional heat exchanger practice.

The correlations developed and applied in this study for calculating friction and heat transfer in flow across banks of externally finned tubes are based on a large amount of experimental data (figure 26). It is noteworthy, however, that the tubes on which the correlated data were measured were of larger diameter, had considerably fewer fins per inch of tube length, and were spaced significantly farther apart than the postulated tubes of the present study. The assumption that the correlations in figure 26 are applicable to the very compact finned tube geometries of the present report must await experimental verification.

79

APPENDIX A

SYMBOLS

The symbols used herein have the following meanings:

A   area (ft^2)

b   fin height (figure 2) (ft)

$\dot{C}$ $(\dot{m}c_p)_{gas}/(\dot{m}c_p)_{coolant}$ (non-dimensional)

C_{fr} friction coefficient (non-dimensional)

c_p specific heat at constant pressure (Btu/lb^{O}R)

D   diameter (ft)

d   diameter (ft)

F   correction factor for non-pure counterflow (non-dimensional)

f   friction factor (non-dimensional)

G   mass flow per unit flow area ($lb/hrft^2$)

g   gravitational conversion factor $(32.2)(3600)^2 \left(\dfrac{lb_m}{lb_f} \dfrac{ft}{hr^2} \right)$

h   heat transfer coefficient (Btu/hrft^{2O}R)

k   thermal conductivity (Btu/hrft^2(^{O}R/ft))

ℓ length (ft)

$\dot{m}$ mass flow rate (lb/hr)

N   number (of) (non-dimensional)

p   static pressure (lb/ft^2)

Pr   Prandtl number (non-dimensional)

R   thermal resistance (^{O}R/(Btu/hr))

r   tube diagonal spacing parameter (fig. 2) (non-dimensional)

Re   Reynolds number (non-dimensional)

s   tube transverse spacing parameter (fig. 2) (non-dimensional)

T   temperature (^{O}R)

UA   overall thermal conductance (Btu/hr^{O}R)

v   velocity (ft/hr)

x   axial pitch of tubes (fig. 2) (ft)

Greek symbols

Δ change

δ thickness (ft)

η effectiveness (non-dimensional)

μ dynamic viscosity (lb_m/hrft)

ρ density (lb_m/ft^3)

σ spacing between fins (fig. 2) (ft)

Subscripts

av'g   bulk average

b   banks of tubes

c,p   cooling, per pass

c,o   cooling, overall

eff   effective

en   entrance

ex   exit

f   fin; "film" when applied to gas temperature

fr   friction

g	gas, on gas side
gas	gas
i	inside
J	Jameson (Ref. 14)
liq. met.	liquid metal
m	momentum
max	maximum
o	outer
p	coolant passes; per coolant pass
r	rows of tubes
t	tube, tube wall
wall	tube wall

APPENDIX B

CALCULATION PROCEDURE

Orientation

Table 1 of the text defines the following problem:

Given: A gas of specified composition, and values of $(\dot{m}c_p)_g$, $T_{en,g}$ and $p_{en,g}$

Find: The dimensions and weights of heat exchangers that produce prescribed values of ΔT_g and Δp_g.

Solution of this problem involves (a) selection of a basic heat transfer element and visualization of a suitable arrangement of a number of such elements into an overall heat exchanger configuration; (b) selection of a second heat transfer fluid and specification of enough constraints on this fluid to permit detailed solution of the problem under discussion; and (c) organization of pertinent quantitative relations into a calculation sequence suitable for generating parametric solutions to the problem defined.

In the present study the specified gases are argon and neon, and the data stipulated for these gases are listed in Table 1. The selected heat transfer element and the overall heat exchanger configuration are as indicated in figures 2 and 3. The secondary fluids are the liquids, NaK, lithium and water. The calculation

procedure is discussed in the following paragraphs.

An outline of the calculation procedure has previously been
presented on pages 17-19 of the text. An additional, more
detailed description of the calculation sequence is presented
in this appendix. In order to lend concreteness to the more
detailed outline, the elements that are needed for the calcula-
tion are first identified explicitly in sub-sections titled
"Finned tube basic geometric quantities", "Thermal relations",
"Pressure drop relations", "Size and weight relations". The
detailed outline of the calculation sequence follows these
sub-sections.

Elements Of The Calculation

Finned tube basic geometric quantities: Figure 2 presents details
of the finned tube element and of the transverse and axial finned
tube spacings. Every dimension identified in figure 2 is an
independent variable. In order to perform heat exchanger calcula-
tions it is necessary to assign a numerical value to each of these
dimensions. In the following discussion it will be assumed that
such numerical values have been assigned, and that all dimensions
labelled in figure 2 are known numerically. It will be further
assumed that the materials and thermal conductivities of the fins
and tubes are known.

84

For calculations, the following geometric quantities are needed:

$$d_J = \text{Jameson diameter (Ref. 14)}$$

$$d_J \equiv \frac{2}{\pi} \frac{Friction\ surface}{Projected\ perimeter} \tag{1}$$

When the surface exposed by the outer edge of the fin is included in the friction surface, d_J is given by

$$d_J = d_t + \frac{2b(b + \delta_f)}{\sigma + 2b + \delta_f} \tag{2}$$

The friction surface in one tube bank per unit gas flow area is

$$\frac{S_{friction}}{N_b\, A_{flow,g}} = \frac{\pi\left[d_t(\sigma + 2b + \delta_f) + 2b(b + \delta_f)\right]}{4\, d_J(\sigma + \delta_f) - d_t(\sigma + \delta_f) - 2b\,\delta_f} \tag{3}$$

Equation (3) includes the surface of the outer edge of the fin.

The fin heat transfer surface in one tube bank per unit gas flow area is

$$\frac{S_{fin}}{N_b\, A_{flow,g}} = \frac{2\pi b(d_t + b)}{4 d_J(\sigma + \delta_f) - d_t(\sigma + \delta_f) - 2b\,\delta_f} \tag{4}$$

Equation (4) takes no credit for the heat transfer surface contributed by the outer edge of the fin. As a partial compensation

for this conservativism, the portion of the outer tube wall surface covered by the base of the fin is treated herein as though it were exposed to the gas. Thus, the gas side surface of the tubes in one bank per unit gas flow area is taken herein as

$$\frac{S_{tube,g}}{N_\ell \, A_{flow,g}} \cong \frac{\pi \, d_t \, (\sigma + \delta_f)}{\lambda \, d_T \, (\sigma + \delta_f) - d_t \, (\sigma + \delta_f) - 2 \, \ell \, \delta_f} \qquad (5)$$

The tube surface on the coolant side in one tube bank per unit gas flow area is

$$\frac{S_{coolant}}{N_\ell \, A_{flow,g}} = \left(\frac{d_i}{d_t}\right) \frac{S_{tube,g}}{N_\ell \, A_{flow,g}} \qquad (6)$$

The frontal area per unit gas flow area when shell clearance is neglected is

$$\frac{A_{frontal,g}}{A_{flow,g}} = \frac{\lambda \, d_T \, (\sigma + \delta_f)}{\lambda \, d_T \, (\sigma + \delta_f) - d_t \, (\sigma + \delta_f) - 2 \, \ell \, \delta_f} \qquad (7)$$

For calculation of the friction pressure drop the following modified version of a geometric parameter introduced by Jameson (Reference 14) is needed:

$$\binom{Geometric \ function}{in \ friction \ equation} = 2.324 \left(\frac{\ell}{\sigma}\right)^{0.4} \left(\frac{1}{\sqrt{\lambda - 1}} + \frac{1}{\sqrt{\lambda - 1}}\right) \qquad (8)$$

86

Thermal relations: The principal thermal relations required for the calculations are the heat exchanger cooling effectiveness, the gas-to-coolant ($\dot{m}c_p$)-ratio, the overall thermal resistance of the heat exchanger, and the individual thermal resistances of the gas, wall and coolant. These relations are discussed in the present section. The heat transfer coefficients of the gas and coolant are indicated during discussion of the thermal resistances. Subsidiary thermal relations are also indicated during the discussion.

The cooling effectiveness employed herein is the temperature effectiveness

$$\eta_{cooling} \equiv \frac{T_{en,g} - T_{ex,g}}{T_{en,g} - T_{en,coolant}} \equiv \frac{\Delta T_g}{T_{en,g} - T_{en,coolant}} \qquad (9)$$

In the systems of interest in the present study, the gas temperatures are fixed (Table 1). The cooling effectiveness then serves two functions: (1) It determines the coolant entrance temperature according to the re-arranged version of equation (9):

$$T_{en,coolant} = T_{en,g} - \frac{\Delta T_g}{\eta_{cooling}} \qquad (9a)$$

and (2) It contributes to the determination of the required overall thermal conductance (or its reciprocal, the overall thermal resistance) of the heat exchanger, as detailed below. In the present

87

study the cooling effectiveness is an independent variable to which values may be assigned arbitrarily, with the understanding that the heat exchanger will then be sized so as to have that effectiveness, as discussed below.

The ratio $(\dot{m}c_p)_{gas}/(\dot{m}c_p)_{coolant}$ is also an independent variable in the present study. When a value is assigned to this ratio, the heat capacity rate of the coolant, $(\dot{m}c_p)_{coolant}$, and the temperature rise of the coolant are both determined.

$$\left(\dot{m}c_p\right)_{coolant} = \frac{(\dot{m}c_p)_{gas}}{\left[(\dot{m}c_p)_{gas}\Big/(\dot{m}c_p)_{coolant}\right]} \tag{10}$$

$$\Delta T_{coolant} = \left[\frac{(\dot{m}c_p)_{gas}}{(\dot{m}c_p)_{coolant}}\right]\Delta T_g \tag{11}$$

Equations (9a) and (11) together determine the coolant exit temperature from the heat exchanger.

When both a cooling effectiveness and a gas-to-coolant $(\dot{m}c_p)$-ratio are assigned, a definite value of the overall thermal conductance of the heat exchanger is implied. For a multipass cross-counter-flow heat exchanger with both fluids unmixed, as in figure 3 herein, the implied value of the overall conductance can be calculated slightly conservatively (Reference 9) as follows:

Let

N_p = total number of coolant passes;

$\eta_{c,o}$ = heat exchanger overall cooling effectiveness as given by equation (9), the symbol $\eta_{c,o}$ being an abbreviated version of the longer term, "$\eta_{cooling}$";

$\dot{C}$ $\equiv$ $(\dot{m}c_p)_{gas}/(\dot{m}c_p)_{coolant}$;

$\eta_{c,p}$ = cooling effectiveness of each of the N_p passes.

$$\left. \right\} \quad (12)$$

Then, as can be shown to be compatible with the relations discussed in Reference 9,

$$\eta_{c,p} = \frac{1 - \left(\dfrac{1 - \eta_{c,o}}{1 - \dot{C}\,\eta_{c,o}}\right)^{1/N_p}}{1 - \dot{C}\left(\dfrac{1 - \eta_{c,o}}{1 - \dot{C}\,\eta_{c,o}}\right)^{1/N_p}} \quad (13)$$

and the required conductance per pass, $(UA)_p$, can be shown to be given by

$$(UA)_p = \frac{1}{F_p}\left[(\dot{m}c_p)_g \frac{\ln\left(\dfrac{1 - \dot{C}\,\eta_{c,p}}{1 - \eta_{c,p}}\right)}{1 - \dot{C}}\right] \quad (14)$$

in which F_p is a number smaller than unity that corrects for the departure from pure counterflow. F_p is uniquely determined by

the combination $(\dot{C}, \eta_{c,p})$. For coolant passes arranged as in figure 3, the numerical value of F_p is found from the chart in Reference 7 that applies to single-pass pure crossflow with both fluids unmixed.

The overall conductance of the heat exchanger is N_p times the conductance per pass. Thus

$$UA = N_p \left\{ \frac{1}{F_p} \left[(\dot{m}c_p)_g \frac{\ln \left(\frac{1 - \dot{C}\,\eta_{c,p}}{1 - \eta_{c,p}} \right)}{1 - \dot{C}} \right] \right\} \quad (15)$$

Equation (15) is a slightly conservative expression for the required overall conductance of a cross-counterflow heat exchanger of the sort shown in figure 3 when that heat exchanger has N_p passes and a gas-to-coolant $(\dot{m}c_p)$-ratio equal to $\dot{C}$, and is required to have an overall cooling effectiveness $\eta_{c,o}$.

The foregoing equations apply when $\dot{C}$ is either less than or greater than unity.* In either case the numerator and denominator of the bracketed function in equations (14) and (15) have the same algebraic sign and their quotient is positive. Thus, special precautions are not needed with regard to the magnitude of $\dot{C}$ when $\dot{C}$ differs from unity.

For the special case $\dot{C} = 1$, L'Hospital's Rule is applied to equations (13) and (14) to obtain

----
* For non-imaginary values of UA, the term $\dot{C}\,\eta_{c,p}$ must be < 1.

$$\left(\eta_{c,p}\right)_{\dot{C}=1} = \frac{\eta_{c,o}}{\eta_{c,o} + N_p\left(1 - \eta_{c,o}\right)} \qquad (16)$$

$$(UA)_{p,\dot{C}=1} = \frac{1}{F_p}\left[(\dot{m}c_p)_g \; \frac{\eta_{c,p}}{1 - \eta_{c,p}}\right]_{\dot{C}=1} \qquad (17)$$

Then the required overall conductance of the heat exchanger, which is N_p times the conductance per pass, is given by

$$(UA)_{\dot{C}=1} = N_p\left\{\frac{1}{F_p}\left[(\dot{m}c_p)_g \; \frac{\eta_{c,p}}{1 - \eta_{c,p}}\right]_{\dot{C}=1}\right\} \qquad (18)$$

The overall thermal resistance of the heat exchanger is given by

$$Overall \; thermal \; resistance = \frac{1}{UA} \qquad (19)$$

91

in which UA is computed with equation (15) when $\dot{C}$ is not equal to unity, and is computed with equation (18) when $\dot{C}$ is equal to unity.

The thermal resistance of the gas is given by

$$R_{gas} = \frac{1}{(h\,S_{eff})_g} \tag{20}$$

The value of h_g in equation (20) is obtainable from figure 26 herein as soon as a value is assigned to the gas Reynolds number. The value of G required to extract h_g from the Stanton number is obtained as

$$G_{max,g} = \left[Re_{d_T} \Big/ \left(\frac{d_T}{\mu}\,\frac{T_{av'g}}{T_f} \right) \right] \tag{21}$$

The value of the effective surface in equation (20) is computed with the relation

$$\left(S_{eff} \right)_g = N_k\,A_{flow,g} \left[\left(\frac{S_{tube}}{N_k\,A_{flow}} \right)_g + \eta_{fin} \left(\frac{S_{fin}}{N_k\,A_{flow}} \right)_g \right] \tag{22}$$

in which

$$A_{flow,g} = \left(\frac{\dot{m}}{G_{max}} \right)_g \tag{23}$$

Use is made of equations (4) and (5) herein and of the fin effectiveness curves in Reference 8 to determine the bracketed function in equation (22). The number of banks N_b is determined when the gas pressure drop condition is imposed on the heat exchanger, as indicated in the section on "Pressure drop relations".

The thermal resistance of the wall can be expressed in the form

$$R_{wall} = \left[\frac{d_t \ln\left(\frac{d_t}{d_i}\right)}{2\, k_{wall}} \middle/ N_{\ell}\, A_{flow,g} \left(\frac{S_{tube,g}}{N_{\ell}\, A_{flow,g}}\right) \right] \quad (24)$$

The thermal resistance of the coolant is

$$\left. \begin{aligned} R_{coolant} &= \frac{1}{(h\, S)_{coolant}} \\[2em] &= \frac{1}{UA} - \left(R_{gas} + R_{wall}\right) \end{aligned} \right\} \quad (25)$$

which may be solved for the coolant heat transfer coefficient to yield

$$h_{coolant} = \frac{1}{N_{\ell}\, A_{flow,g} \left(\dfrac{S_{coolant}}{N_{\ell}\, A_{flow,g}}\right)\left[\dfrac{1}{UA} - \left(R_{gas} + R_{wall}\right)\right]} \quad (26)$$

93

For convenience, $h_{coolant}$ may be put into non-dimensional form by introducing the Nusselt number which, for the pipe flows under discussion, is equal to the product of $h_{coolant}$ by $d_1/k_{coolant}$. In terms of the Nusselt number, equation (26) takes the form

$$\left(\frac{h\,d_i}{k}\right)_{cool.} = \frac{\left(\dfrac{d_i}{k_{coolant}}\right)}{N_k\,A_{flow,g}\left(\dfrac{S_{coolant}}{N_k\,A_{flow,g}}\right)} \bigg/ \left[\frac{1}{UA} - \left(R_{gas} + R_{wall}\right)\right] \quad (27)$$

Reference 3 indicates that for liquid metals in fully developed turbulent pipe flow,

$$\left(\frac{h\,d_i}{k}\right)_{liq.\,met.} = \propto + .025\left(\frac{\rho\,v\,d_i\,c_p}{k}\right)^{0.8} \quad (28)$$

in which $\propto = 7$ for the case of uniform wall heat flux, and $\propto = 5$ for the case of uniform wall temperature. In a cross-counterflow heat exchanger, neither uniform heat flux nor uniform wall temperature occurs; hence, for the present study $\propto$ was taken equal to 6, and as a conservativism the resulting expression was multiplied by 0.75. Thus, for the liquid metals, the equation for the Nusselt number was taken to be

$$\left(\frac{h\,d_i}{k}\right)_{liq.\,met.} = 0.75\left[6 + .025\left(\frac{\rho\,v\,d_i\,c_p}{k}\right)^{0.8}\right] \quad (29)$$

94

The Nusselt number for ordinary (non-metallic) liquids in fully developed turbulent pipe flow is given in Reference 4. This equation was used with a 10 percent conservativism in the cases in which water was the coolant. Thus, for water, the following equation was used:

$$\left(\frac{h\,d_i}{k}\right)_{water} = .021 \left(\frac{\rho v\,d_i}{\mu}\right)^{0.8} \left(\frac{c_p\,\mu}{k}\right)^{0.4} \tag{30}$$

Equations (29) and (30) show that when the coolant properties and tube inside diameter are specified, the coolant velocity is uniquely determined by the coolant Nusselt number (or heat transfer coefficient). Equation (27) shows that the required value of the coolant Nusselt number depends on earlier computed quantities; hence, the required coolant velocity is also known when the quantities that govern the coolant Nusselt number have been computed.

As indicated above, the calculations require a knowledge of fluid properties. Data are required for both the gas and the coolant. In the present study, coolant properties were based on the data in References 3 and 10-12; properties at the bulk average temperatures of the coolants were employed. Gas properties were based on the computed data presented in Reference 15; properties at the average film temperatures of the gases were used.

<u>Pressure drop relations</u>:   The formula employed herein for the gas static pressure drop was

$$\Delta p_g \;=\; \Delta p_{fr} \;+\; \Delta p_m \tag{31}$$

in which

$$\Delta p_{fr} = C_{fr} \times \left[2.324 \left(\frac{b}{\sigma}\right)^{0.4} \left(\frac{1}{\sqrt{\Delta - 1}} + \frac{1}{\sqrt{r-1}}\right) \right] N_b \; \frac{G_{max}^2}{2g\, \rho_{av'g}} \tag{32}$$

$$\Delta p_m = \frac{G_{max}^2}{g} \left(\frac{1}{\rho_{ex}} - \frac{1}{\rho_{en}}\right) \tag{33}$$

The basis for equation (32) is indicated in Appendix C.   A plot of experimental data relating C_{fr} and Re_{d_J} is presented in figure 26.

When equations (32) and (33) are inserted into equations (31), equation (31) yields the total number of tube banks, N_b.

The formula employed herein for the coolant pressure drop was

$$\Delta p_{coolant} \;=\; 4 f \left(\frac{\ell}{d_i}\right)_{eff} \left(\frac{\rho v^2}{2g}\right) \tag{34}$$

$$f = \frac{.046}{\left(\rho v d_i / \mu\right)^{0.2}} \tag{35}$$

$$\left(\frac{\ell}{d_i}\right)_{eff} = N_p \left(\frac{\ell_{tube,p}}{d_i}\right) + 50\left(N_p - 1\right) \tag{36}$$

In equation (36), the term $50(N_p - 1)$ allows an effective ℓ/d of 50 for each return bend, as recommended in Reference 4 for 180° bends of medium radii. The coolant velocity v in equations (34) and (35) is the value determined from the required coolant Nusselt number, as discussed under "Thermal relations".

Size and weight relations: The core dimensions desired are the axial length, the no-flow length and the transverse length. In order to compute these dimensions it is necessary to calculate the number, distribution and lengths of the tubes. The relations required for determining the core dimensions are indicated in the present section. The weights desired are the weights of the tubes, fins and return bends, and the weight of the liquid contained in the tubes and return bends. These relations are also indicated in the present section.

When the total number of tube banks in the gas flow direction is N_b, the axial length of the heat exchanger is

$$\ell_{axial} = \left(N_b - 1\right)x + D_o \tag{37}$$

formula for the no-flow length per bank is

$$\ell_{no\text{-}flow\ per\ bank} = \left(N_n - 1\right) \Delta d_J + D_o \qquad (42)$$

The no-flow dimension of the <u>core</u>, when allowance is made for a fin-to-shell clearance of $D_o/4$ at both the top and bottom rows of tubes, and when account is taken of the staggered arrangement of successive banks, is given by

$$\ell_{no\text{-}flow,\ core} = \left(N_n - 1\right) \Delta d_J + 2 D_o \qquad (43)$$

The no-flow lengths in equations (42) and (43) differ by D_o. If there are many rows per bank, this difference is negligible in parametric studies. If there are very few rows per bank, however, the difference is not negligible.

The active length of a tube in any one pass is

$$\ell_{tube,p} = \left(\frac{A_{frontal,g}}{\ell_{no\text{-}flow\ per\ bank}}\right) \qquad (44)$$

Equation (44) applies both to straight tubes and to tubes folded in the plane of a bank. In equation (44), $A_{frontal,g}$ has the value determined by joint use of equations (7) and (23).

The transverse dimension of the core is equal to $\ell_{tube,p}$ if

the tubes are straight.

$$\left(\ell_{transverse} \right)_{\substack{straight \\ tubes}} = \ell_{tube, p} \tag{45}$$

If the tubes are folded in the plane of a bank, however, the core transverse dimension is given approximately by the expression

$$\left(\ell_{transverse} \right)_{\substack{folded \\ tubes}} \cong \frac{\ell_{tube, p}}{\left(\substack{No. \ of \ straight \ legs \\ of \ folded \ tube} \right)} \tag{46}$$

An exact determination of the transverse dimension is obtained when the U-bends of the folded tubes are calculated precisely.

The total number of active tube-feet is given by

$$Total \ active \ tube\text{-}feet = \left(\ell_{tube, p} \right)\left(No. \ of \ tubes \ per \ pass \right) N_p \tag{47}$$

Equation (47) applies both to straight tubes and to tubes folded in the plane of a bank. Equation (47) does not include the lengths of the return bends that join the tubes of successive passes.

Equations (37) through (47) represent the relations needed for determining pertinent core dimensions and tube data. The following relations are employed for computing the weights of the heat exchanger components.

The weight of the tube walls in the active core is

$$Wt.\ tube\ walls = \rho_t \left\{ \frac{d_t \left[1 - \left(\frac{d_i}{d_t}\right)^2 \right]}{4} \left[N_\ell A_{flow,g} \left(\frac{S_{tube,g}}{N_\ell A_{flow,g}} \right) \right] \right\} \quad (48)$$

The weight of the fins, with an additional 10 percent allowance for the weight of braze material, is

$$Wt.\ (fins + braze) = \rho_f \left\{ 1.1 \left(\frac{\delta_f}{2}\right) \left[N_\ell A_{flow,g} \left(\frac{S_{fin}}{N_\ell A_{flow,g}} \right) \right] \right\} \quad (49)$$

The weight of coolant contained within the tubes of the active core is

$$\left(\begin{matrix} Wt.\ in-tube \\ coolant \end{matrix} \right) = \rho_{coolant} \left\{ \frac{d_i}{4} \left[N_\ell A_{flow,g} \left(\frac{S_i}{N_\ell A_{flow,g}} \right) \right] \right\} \quad (50)$$

in which the term $d_i/4$ is the ratio of the total coolant volume to the total surface swept by the coolant within the tubes of the active core.

When it is observed that each tube effectively gets displaced a distance equal to $(N_p - 1)$ times the axial dimension of one pass in progressing through the multipass circuit, and when allowance is made for a semi-circular shape of return bend, it is possible to derive the following expression for the total tube-feet

contributed by all the return bends

$$\left(\sum \ell\right)_{return\ bends} = \frac{\pi}{2} \frac{N_p - 1}{N_p} \left[\frac{x}{A d_J} N_\ell^2 \ell_{no-flow}\right] \quad (51)$$

The weight of the walls of the return bends is then given by

$$Wt.\ return\ bends = \rho_t \left\{\frac{\pi}{4}\left(d_t^2 - d_i^2\right)\left(\sum \ell\right)_{return\ bends}\right\} \quad (52)$$

The weight of the coolant contained in the return bends is given by

$$\binom{Wt.\ of\ coolant}{in\ return\ bends} = \rho_{coolant}\left\{\frac{\pi}{4} d_i^2 \left(\sum \ell\right)_{return\ bends}\right\} \quad (53)$$

An allowance may be made, also, for a thickness $\delta_{coolant}$ in entrance and exit plenums each of width $N_b x/N_p$. The combined weight of the two coolant thicknesses is

$$\binom{Wt.\ of\ coolant\ layers}{in\ entr.-exit\ plenums} = \rho_{cool.}\left\{2\delta_{cool.} \frac{N_\ell x}{N_p} \ell_{no-flow}\right\} \quad (54)$$

Equations (48) through (54) were employed for computing the weights of the wet core-plus-return bends reported herein. In computing the weights, the densities employed for the several tube and fin materials are shown in the following table; also shown are the

thermal conductivities employed.

Table 17. Employed Densities And Thermal Conductivities of Solids

Material	Density (lb_m/ft^3)	Thermal conductivity $[Btu/hrft^2(^{\circ}R/ft)]$
Steel	500	10
Cb-1%Zr	536	20
Aluminum	173	110
Copper	555	200

Densities and thermal conductivities employed for the coolants
were based on data in References 3,4 and 10-12, and were treated
as functions of temperature. The thickness of the coolant layers
in the entrance and exit plenums was taken to be 1 inch.

Outline of Calculation Sequence

An outline of the calculation procedure has previously been
presented on pages 17-19 of the text. A more detailed calculation
sequence is presented in the following paragraphs. The sequence
employs the gas Reynolds number as the key independent variable;
employs the gas pressure drop to determine the gross amounts of
surface contained in the gas and coolant channels, as well as the
tube wall area across which heat flows by conduction; employs

the prescribed overall thermal performance to determine a required coolant velocity; and uses the coolant velocity to resolve the gross surfaces into discrete tubes arranged in a well defined pattern that implies definite core dimensions and weight, and coolant pressure drop. Details of the calculation sequence are as follows:

Preliminary steps:

1. Local geometric dimensions are assigned to the finned tube configuration, and the parameters defined by equations (1)-(8) are computed.

2. A cooling effectiveness, $\eta_{c,o}$, a gas-to-coolant $(\dot{m}c_p)$-ratio, $\dot{C}$, and a number of coolant passes, N_p, are assigned, and the associated overall thermal resistance, 1/UA, is computed. In computing 1/UA, use is made of equations (12)-(15) when $\dot{C}$ differs from unity and of equations (12) and (16)-(18) when $\dot{C}$ equals unity. The gas and coolant temperatures that determine pertinent fluid properties, and the properties themselves, are also evaluated, making use of the prescribed gas temperatures and of equations (9a) and (11).

Main calculation sequence:

3. The gas Reynolds number is used as the key independent variable. Its definition herein is

$$Re_{d_T} \equiv \left(\frac{G_{max} \, d_T}{\mu_{film}} \, \frac{T_{av'g}}{T_{film}} \right)_g \qquad (55)$$

The range of interest of the gas Reynolds number is first found by performing exploratory calculations. These calculations involve a sufficient number of steps in the main calculation sequence detailed below to determine the coolant pressure drop and establish that the pressure drop is in the range of interest. When the coolant is a high performance liquid, the range of suitable gas Reynolds numbers is very narrow and substantial effort may be entailed in locating the proper Reynolds number range.

When the range of interest of the gas Reynolds number has been located, a set of Re_{d_J} values is arbitrarily assigned in this range. Very small increments may be involved within the set of assigned values.

4. For each assigned Re_{d_J}, the gas quantities $G_{max,g}$, $A_{flow,g}$ and $A_{frontal,g}$ are found with equations (21), (23) and (7). The assigned Re_{d_J}, in conjunction with figure 26 herein, also determines a value of C_{fr} for use in the pressure drop equation.

5. The prescribed gas pressure drop (Table 1) is then substituted for Δp_g in equation (31) and this equation is solved for N_b, use being made of equations (32) and (33) and of the quantities determined in step 4.

6. With N_b and $A_{flow,g}$ both known, their product $N_b A_{flow,g}$ is formed.

7. The thermal resistance of the gas, R_{gas}, is then found as follows: The assigned Re_{d_J}, in conjunction with figure 26 herein, determines a value of the heat convection parameter $(h/c_p G_{max})Pr^{2/3}$.

106

For known gas properties and previously determined $G_{max,g}$ (Step 4), the gas heat transfer coefficient, h_g, is computed from the heat convection parameter. The fin effectiveness is then determined in accordance with Reference 8. The effective gas surface is then computed with equation (22), use being made of the value $N_b A_{flow,g}$ determined in Step 6 and of the specific surfaces detailed in equations (4) and (5).

8. The wall thermal resistance, R_{wall}, is then computed with equation (24), use being made of the specific surface detailed in equation (5).

9. The required thermal resistance of the coolant, the required coolant heat transfer coefficient and the required coolant Nusselt number are then computed with equations (25)-(27), employing the specific surface detailed in equation (6).

10. The required coolant velocity is then computed with either equation (29) or (30), employing the Nusselt number that was found in Step 9.

11. With the coolant velocity known, the tube and core parameters detailed in equations (38), (39), (41) and (42) are used (in conjunction with the value of $A_{frontal,g}$ found in Step 4) to compute the tube length per pass, $\ell_{tube,p}$ by means of equation (44).

12. With $\ell_{tube,p}$ known, equations (34) through (36) are used to find the coolant pressure drop. (Note that equation (36) applies only to tubes that are straight (unfolded) in any one pass. If

the tubes are folded in the plane of a bank, an additional term must be introduced into equation (36) to account for the U-bends of the folded tube.)

13. The remaining heat exchanger quantities of interest are then calculated straightforwardly with equations (37), (40), (43), (45)---or equation (46) if tubes folded in the plane of a bank are used and proper allowance is made for the U-bend pressure drops, as noted in Step 12 ----, and equations (47) through (54).

14. When the component weights detailed in equations (48) - (50) and (52) - (54) have been computed, their sum yields the weight of the wet core-plus-return bends.

15. The core volume is found as $(A_{frontal,g})$ x (ℓ_{axial}), which involves terms previously computed.

APPENDIX C

GAS FRICTION AND HEAT TRANSFER CORRELATIONS

In Reference 14, Jameson reports and correlates his extensive data on friction and heat transfer in flow across banks of externally finned tubes. Jameson's parameters correlate both his friction data and his heat transfer data with spreads of less than ± 10 percent relative to the arithmetic average of the experimental values at most Reynolds numbers. Such close correlations are exceptionally good.

For studies of the type performed herein on the effects of geometric parameters, reliable heat transfer and friction correlations are necessary. Hence it was investigated whether Jameson's parameters correlate five sets of data available in References 9 and 16 in addition to his own data. Inasmuch as it was thought convenient to use a single definition of Reynolds number for friction and heat transfer, rather than to use two different definitions as Jameson does, the available data were re-worked to a single Reynolds number basis, as discussed in the following paragraphs.

Jameson points out that the heat transfer coefficient is apparently affected only by the characteristic dimension, d_J, of a single bank of tubes, and not by the spacing between successive banks. He points out that the pressure drop, however, is affected not only

by the local geometry of one tube bank but also by tube bank
spacing in the gas flow direction. He therefore employs another
characteristic diameter, D_J, to correlate pressure drop. In any
one flow, the Reynolds number for heat transfer, Re_{d_J}, differs
in magnitude from the Reynolds number for friction, Re_{D_J}.

By use of Jameson's definitions of d_J and D_J it is readily shown
that Jameson's friction factor correlation is expressible as a
simple function of his tube bank spacing parameter and his
Reynolds number for heat transfer, as follows:

$$
\left.
\begin{aligned}
4f_J &\equiv \frac{\Delta p_{fr}}{N_\ell \left(G_{max}^2 / 2g\rho\right)} \\
&= \frac{2.324 \left(\dfrac{\ell}{\sigma}\right)^{0.4} \left(\dfrac{1}{\sqrt{\lambda-1}} + \dfrac{1}{\sqrt{\lambda-1}}\right)}{Re_{d_J}^{0.25}}
\end{aligned}
\right\} \quad (56)
$$

For convenience, a friction coefficient that depends only on Re_{d_J}
can be defined as

$$
\left.
\begin{aligned}
C_{fr} &\equiv \frac{4f_J}{2.324 \left(\dfrac{\ell}{\sigma}\right)^{0.4} \left(\dfrac{1}{\sqrt{\lambda-1}} + \dfrac{1}{\sqrt{\lambda-1}}\right)} \\
&= \frac{1}{Re_{d_J}^{0.25}}
\end{aligned}
\right\} \quad (57)
$$

C_{fr} should correlate against the heat transfer Reynolds number Re_{d_J}. The friction equation in terms of C_{fr} would be

$$\Delta p_{fr} = C_{fr} \times \left[2.324 \left(\frac{b}{\sigma} \right)^{0.4} \left(\frac{1}{\sqrt{\lambda - 1}} + \frac{1}{\sqrt{\hbar - 1}} \right) \right] N_b \frac{G_{max}^2}{2g\,\rho_{avg}} \quad (58)$$

in which C_{fr} depends only on Re_{d_J} and the bracketed geometric expression allows for the effects of bank spacing.

Equation (58) is identical with equation (56), which is Jameson's equation. The sole gains from using C_{fr} are that both heat transfer and friction data can then be plotted against a single Reynolds number, Re_{d_J}, and that the effects of tube spacing are seen to be multiplicative with the Reynolds number function, C_{fr}, that applies to a single bank.

In order to obtain curves of C_{fr} and $(h/C_p G_{max})Pr^{2/3}$ versus Re_{d_J}, as well as to investigate the applicability of Jameson's parameters to the new data in References 9 and 16, all the available data were re-worked. The data that were processed consisted of the ten original sets of Jameson data as reported in Reference 9, the four additional sets of data presented in Reference 9, and the data of Reference 16. Analysis showed that in order to obtain C_{fr} from the friction factors reported in References 9 and 16, it was necessary to multiply those friction factors by the term

$$\frac{S_{friction}}{N_b\, A_{flow, g}} \Bigg/ 2.324 \left(\frac{b}{\sigma} \right)^{0.4} \left(\frac{1}{\sqrt{\lambda - 1}} + \frac{1}{\sqrt{\hbar - 1}} \right)$$

in which the quantity $S_{friction}/N_b A_{flow,g}$ is as given in equation (3) herein. A fair amount of basic re-work of the data in Reference (16) was also performed.

In order to allow for gas property variation with temperature, properties at the film temperature were used in Re_{d_J} as defined in equation (55) herein, and in the Prandtl number. In keeping with the finding in Reference (16) that the bulk density is more appropriate than the film density in pressure drop across banks of tubes, the bulk density is stipulated in equations (58) and (32) herein.

Correlations of C_{fr} and of $(h/C_p G_{max})Pr_{film}^{2/3}$ versus $(Re_{d_J}, film)$ are presented in figure 26. The spreads in the friction and heat transfer correlations are about $\pm$ 25 percent and about $\pm$ 15 percent, respectively, relative to the arithmetic average values in the data bands. The working curves employed for calculations herein are also shown in figure 26.

REFERENCES

1. Lieblein, S., Special Requirements on Power Generation Systems for Electric Propulsion, NASA SP-22, December 1962.

2. Glassman, A. J., Summary of Brayton Cycle Analytical Studies for Space-Power System Applications, NASA TN D-2487, September 1964.

3. Jackson, C. B., Editor-in-Chief, Liquid Metals Handbook, Sodium-Nak Supplement, TID 5227, sponsored by the Atomic Energy Commission and Department of the Navy, available from U. S. Gov't Printing Office, Washington, D.C., July 1, 1955

4. McAdams, W. H., Heat Transmission, McGraw-Hill Book Co., N. Y., 1954.

5. Coombs, M. G. and Norman, L., Application of the Brayton Cycle to Nuclear Electric Space Power Systems, Garrett Corp., AiResearch Manufacturing Division Report prepared for presentation at the AIAA Third Biennial Aerospace Power Systems Conference, September 1-4, 1964.

6. Fraas, A. P., Design Precepts for High-Temperature Heat Exchangers, Nuclear Science and Engineering, Vol. 8, No. 1, July 1960.

7. Bowman, R. A., Mueller, A. C. and Nagle, W. M., Mean Temperature Difference in Design, Trans. ASME, May 1940, p. 283ff.

8. Gardner, K. A., Efficiency of Extended Surface, Trans. ASME, Nov. 1945.

9. Kays, W. M. and London, A. L., Compact Heat Exchangers, McGraw-Hill Book Co., Inc., New York, 1958 (reprinted from the 1955 edition published by the National Press, Palo Alto, California).

10. Lyon, R. N., Editor, Liquid Metals Handbook, Second Edition, NAVEXOS P-733 (Rev.), U. S. Gov't Printing Office, Washington, D.C., June 1952.

11. Weatherford, W. D., Jr., Tyler, J. C., Ku, P. M., Properties of Inorganic Energy-Conversion and Heat-Transfer Fluids for Space Applications, WADD Technical Report 61-96, November 1961.

12. Hodgman, C. D., Handbook of Chemistry and Physics, Forty First Edition, Chemical Rubber Publishing Co., Cleveland, Ohio, 1959.

13. NASA-AEC Liquid Metals Corrosion Meeting, Volume I, NASA SP-41, Office of Technical Services, Dept. of Commerce, Washington, D.C. 20230, Oct. 2-3, 1963.

14. Jameson, S. L., Tube Spacing in Finned-Tube Banks, Trans. ASME, Nov. 1945, p. 633ff.

15. Svehla, R. A., Estimated Viscosities and Thermal Conductivities of Gases at High Temperatures, NASA TR R-132, 1962.

16. Ragsdale, R. G., Heat Transfer and Friction Measurements with Variable Properties for Airflow Normal to Finned and Unfinned Tube Banks, NASA Memo 10-9-58E, December 1958.
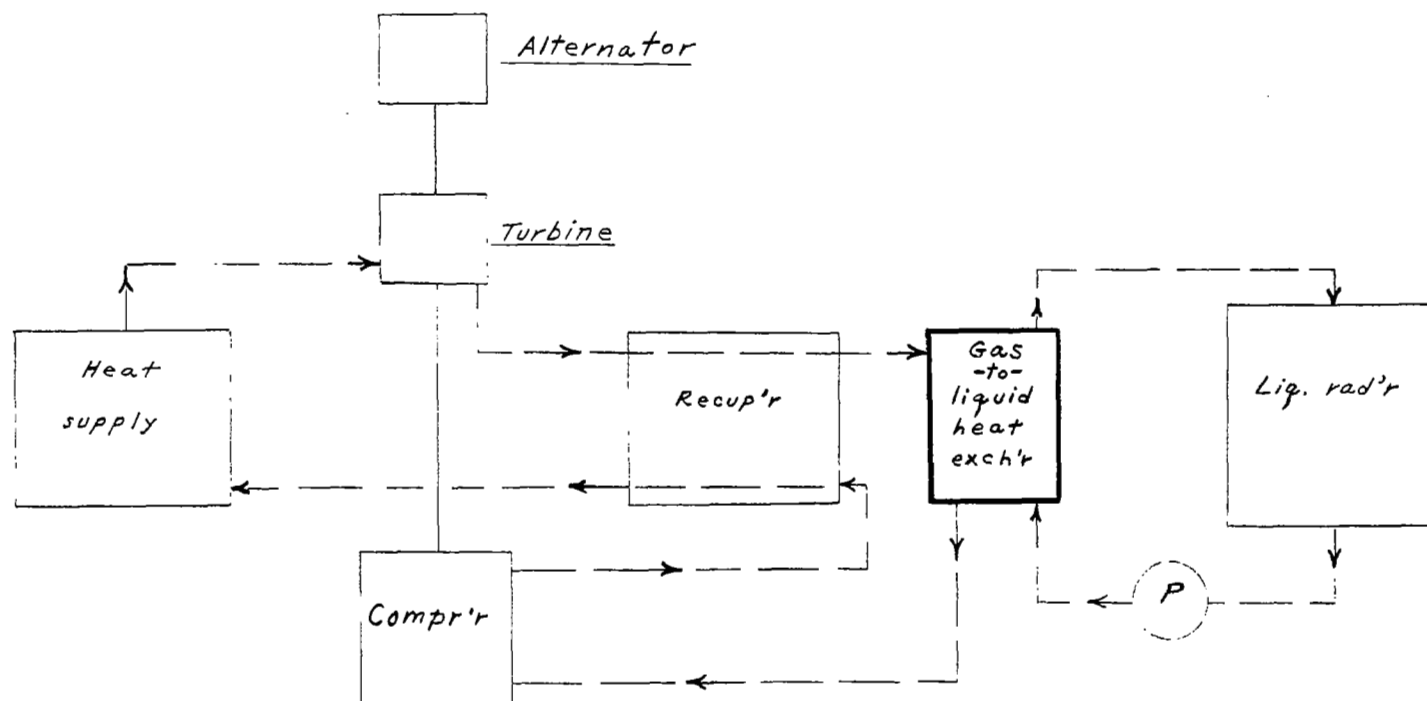
Figure 1.

HEAT EXCHANGER ELEMENT
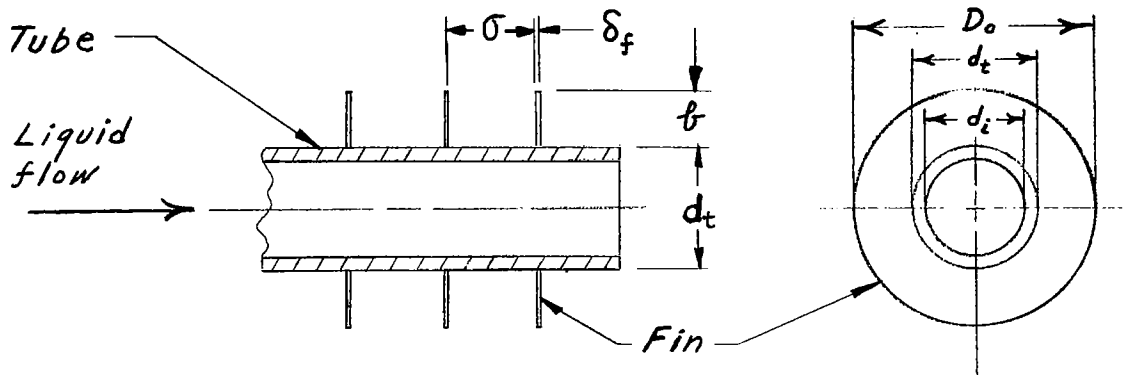
Tube with circular external fins
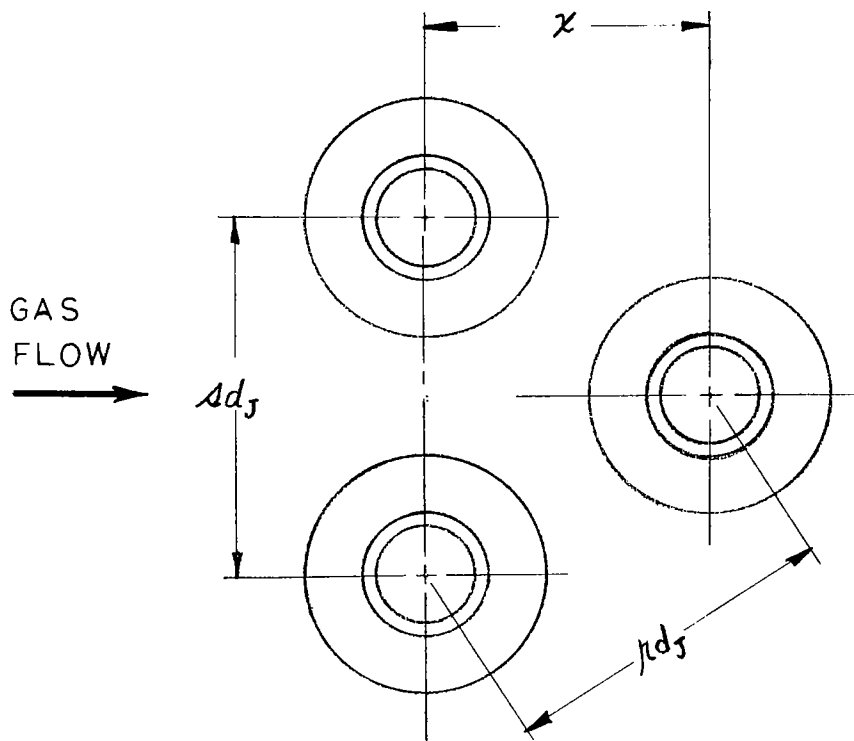
Circularly finned tubes in staggered array

Figure 2.

MULTIPASS CROSS—COUNTERFLOW HEAT EXCHANGER
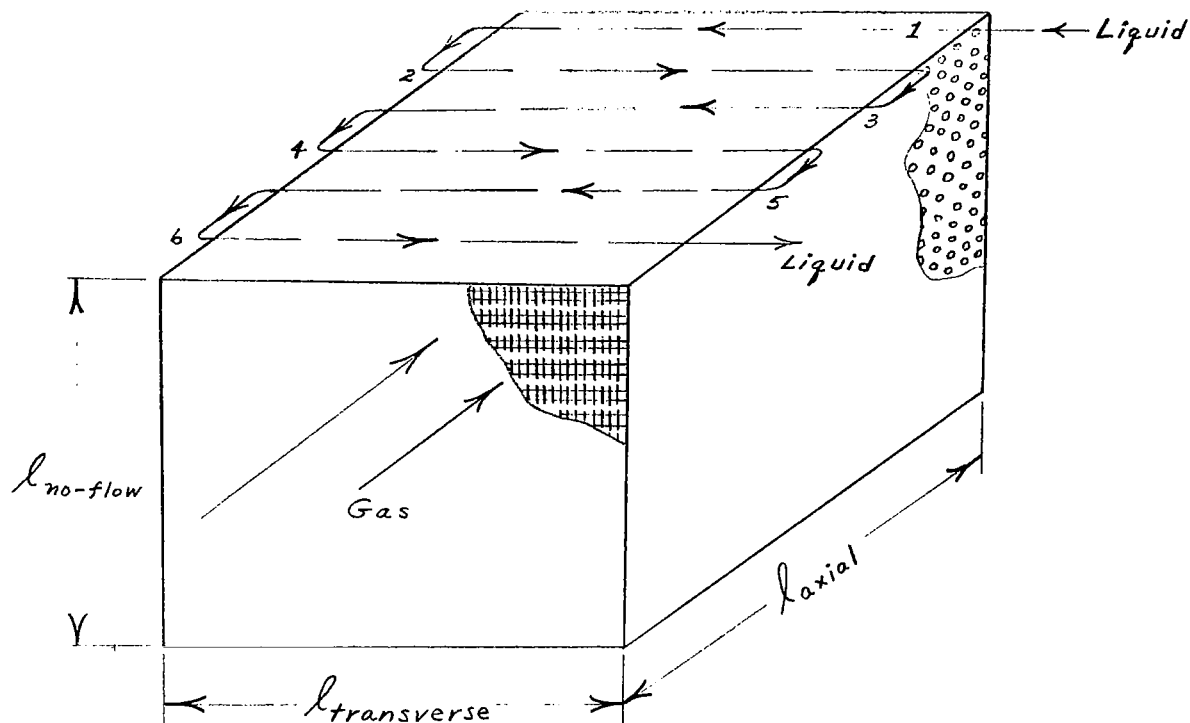
a. Fluid flow paths & core dimensions
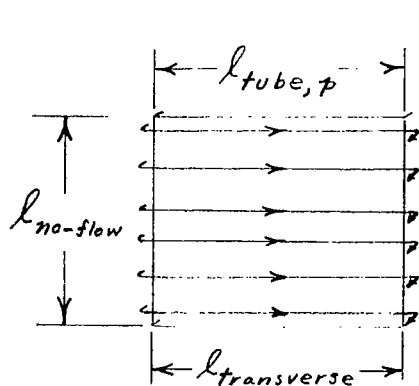
Straight tubes
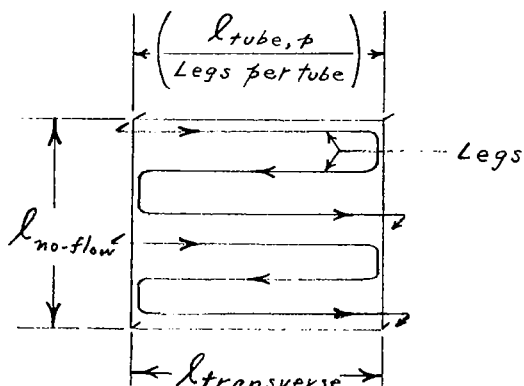
Tubes folded in plane of tube-bank

b. Tube nomenclature

Figure 3.

Figure 4.

EFFECT OF NUMBER OF FINS PER INCH

1000 KW, argon gas, NaK coolant, $\eta_{cooling}$ = 0.90, $(\dot{m}c_p)_{gas}/(\dot{m}c_p)_{coolant}$ = 0.90, 8 coolant passes, $\Delta p_{coolant}$ = 30 psi; steel tubes, 3/16" tube o.d., tube(i.d./o.d.) = 0.85, copper fins, fin thickness = .005 inch, fin (o.d./i.d.) = 1.8.
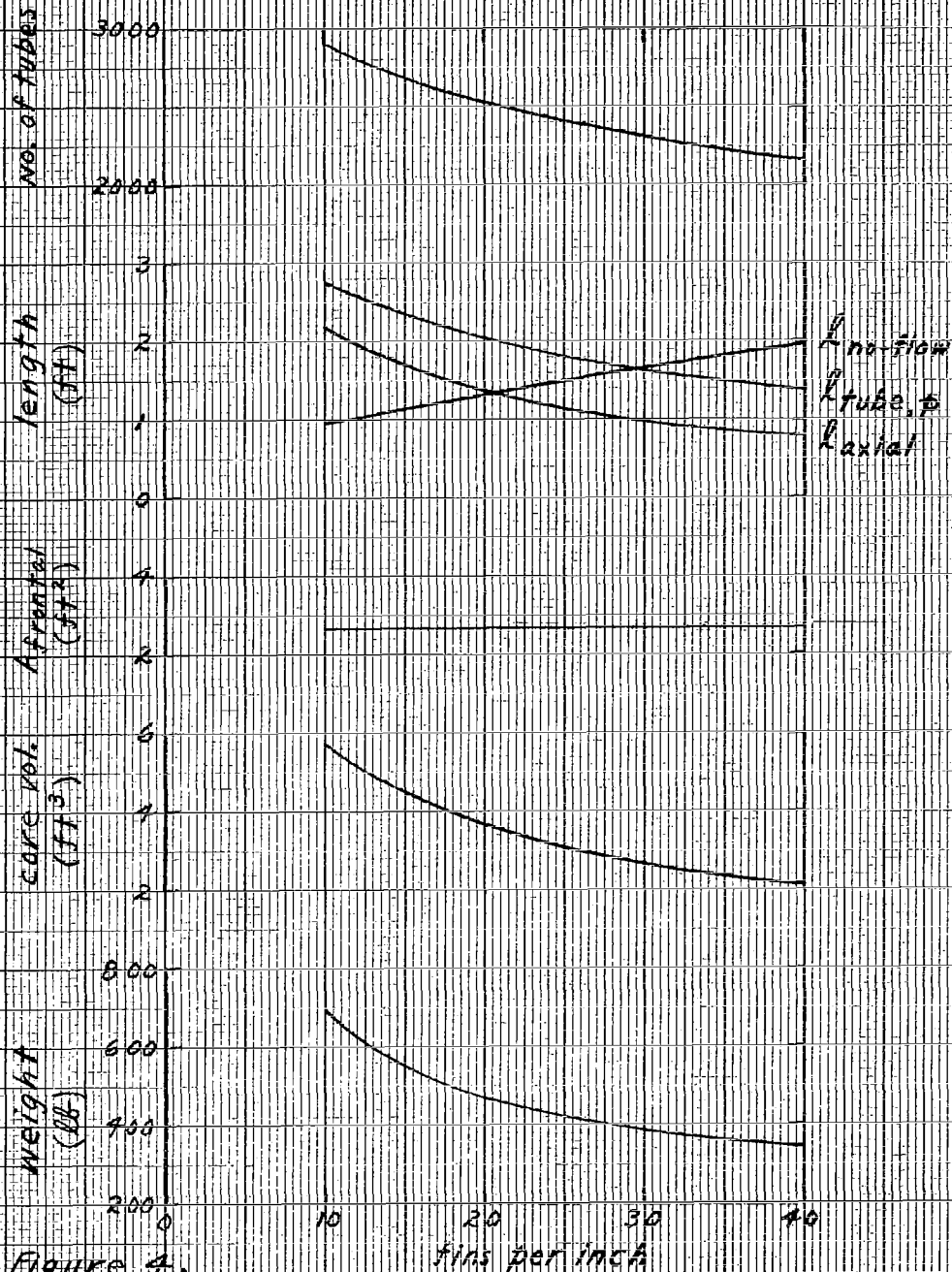
Figure 5.

EFFECT OF FIN (o.d./i.d.)

1000 KW, argon gas, NaK coolant, $\eta_{cooling}$ = 0.90, $(\dot{m}c_p)_{gas}/(\dot{m}c_p)_{coolant}$ = 0.90, 8 coolant passes, $\Delta p_{coolant}$ = 30 psi, steel tubes, 3/16" tube o.d., tube (i.d./o.d.) = 0.65, copper fins, fin thickness = .005 inch, 30 fins per inch.
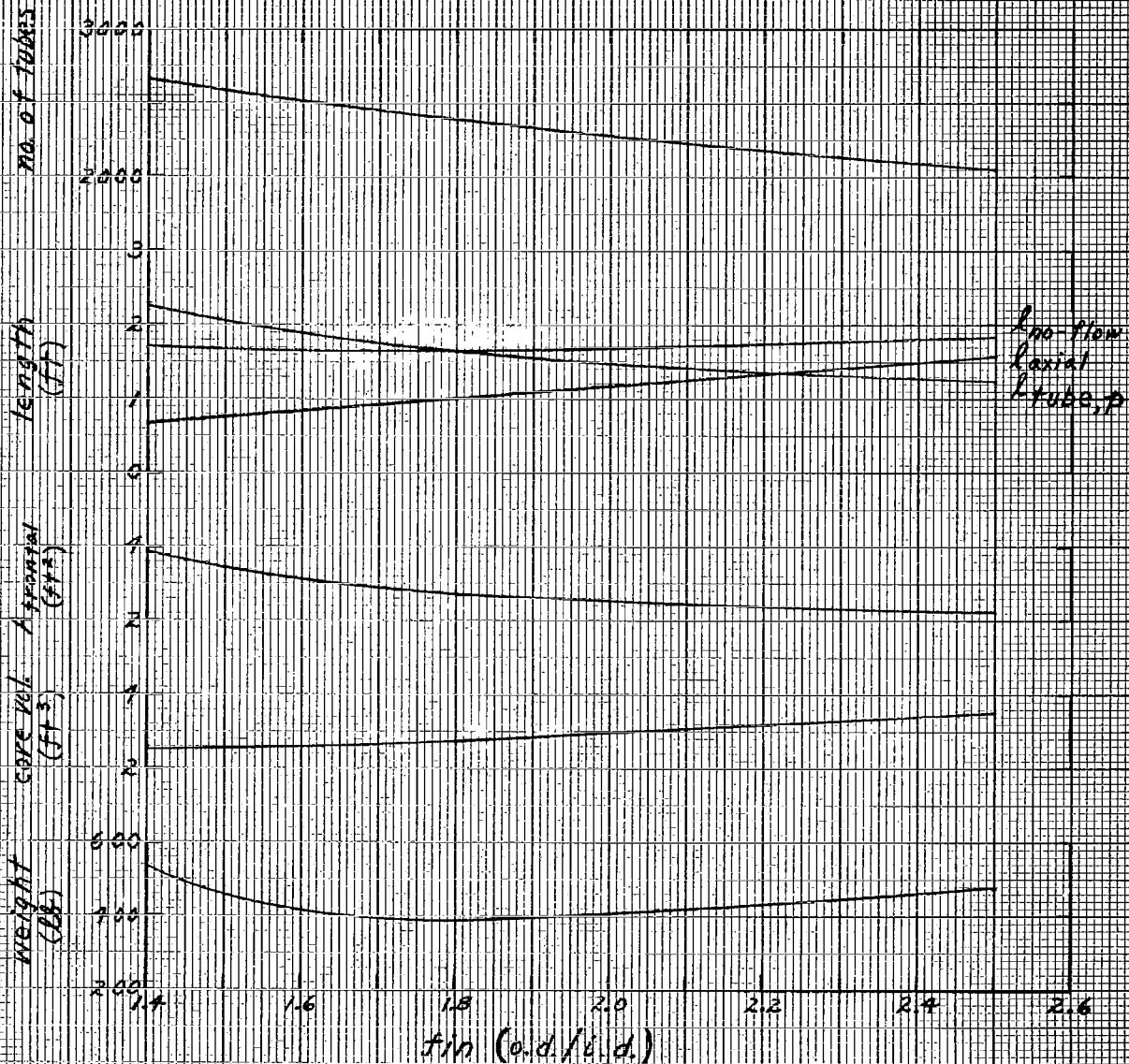
EFFECT OF TUBE DIAMETER

1000 KW, argon gas, NaK coolant, $\eta_{cooling} = 0.925$, $(\dot{m}c_p)_{gas}/(\dot{m}c_p)_{coolant} = 0.90$, 8 coolant passes, $\Delta p_{coolant} = 30$ psi, steel tubes, 3/16" tube o.d., tube (i.d./o.d.) = 0.85, copper fins, fin thickness = .005 inch, fin (o.d./i.d.) = 2.0, 30 fins/inch.
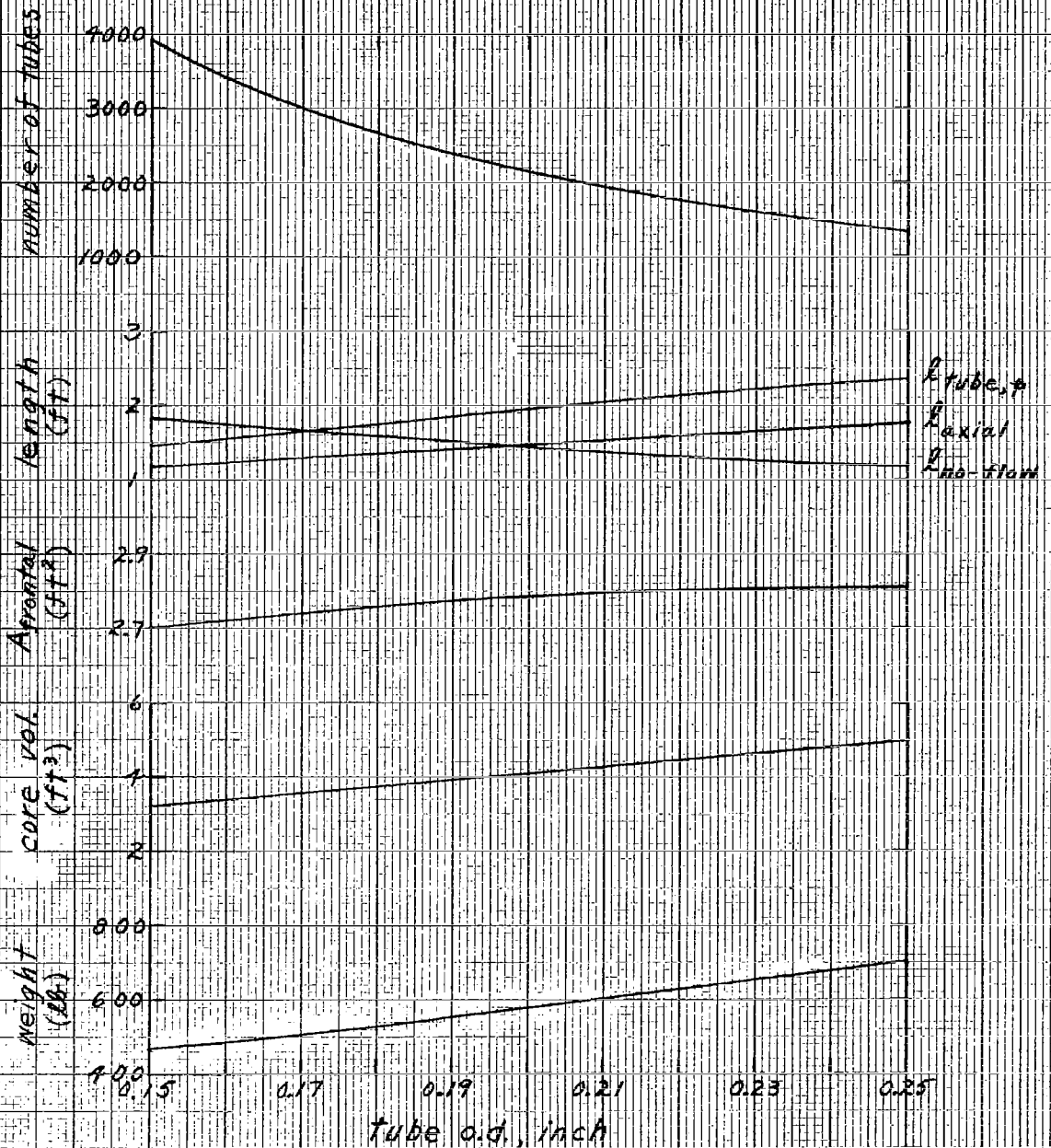
Figure 6.

EFFECT OF COOLING EFFECTIVENESS

1000 KW, argon gas, NaK coolant, $\eta_{cooling}$ variable, $(mc_p)_{gas}/(mc_p)_{coolant} = 0.90$, 8 coolant passes, $\Delta p_{coolant} = 30$ psi, steel tubes, 3/16" tube o.d., tube (i.d./o.d.) = 0.85, copper fins, fin thickness = .005 inch, fin (o.d./i.d.) = 2.0, 30 fins/inch.

Figure 7. cooling effectiveness
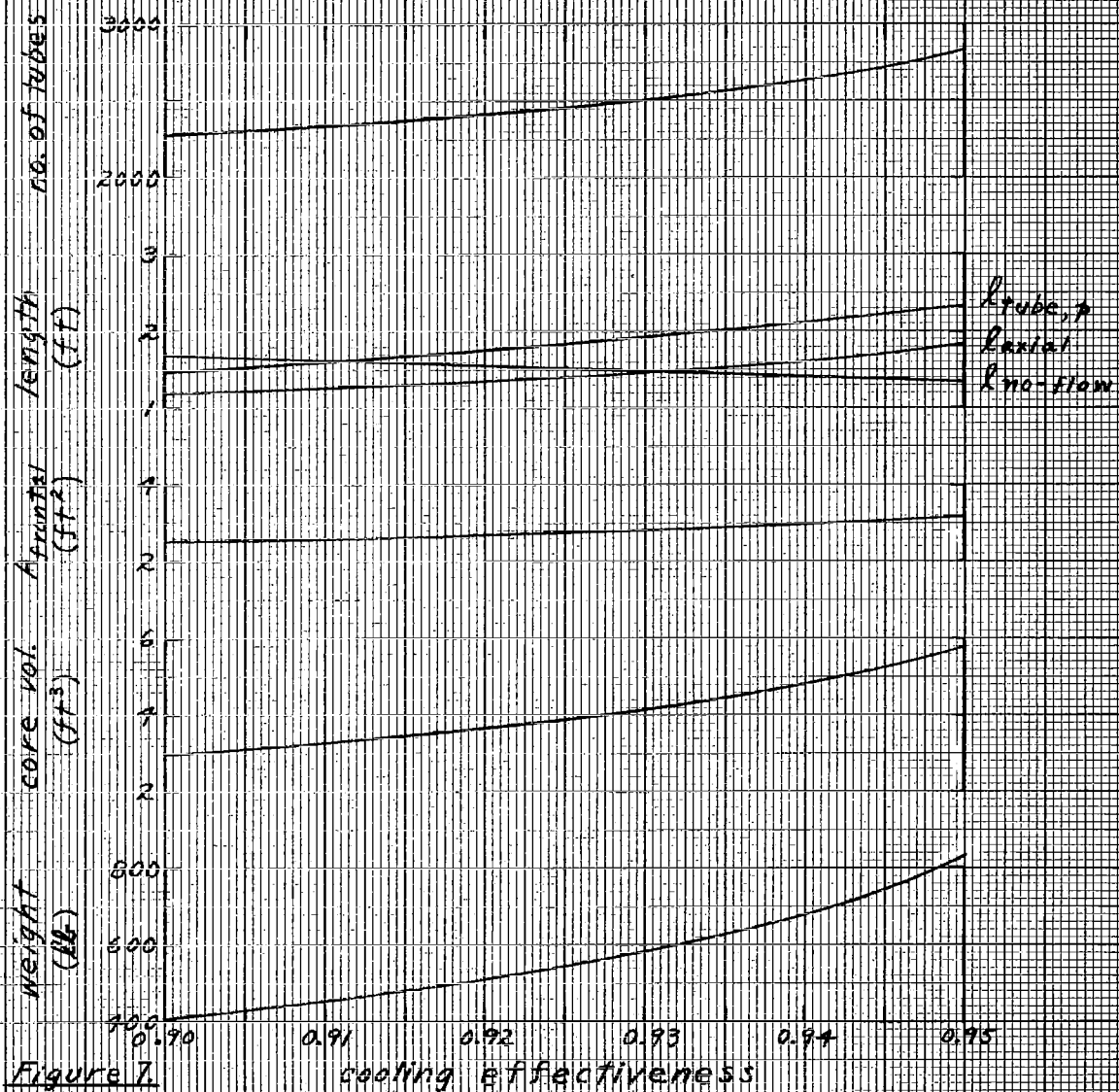
Figure 8.

EFFECT OF $(\dot{m}c_p)_{gas}/(\dot{m}c_p)_{coolant}$

1000 KW, argon gas, NaK coolant, $\eta_{cooling} = 0.90$, $(\dot{m}c_p)_{gas}/(\dot{m}c_p)_{coolant}$ variable, 8 coolant passes, $\Delta p_{coolant} = 30$ psi, steel tubes, 3/16" tube o.d., tube (i.d./o.d.) = 0.85, copper fins, fin thickness = .005 inch, fin (o.d./i.d.) = 2.0, 30 fins/inch.
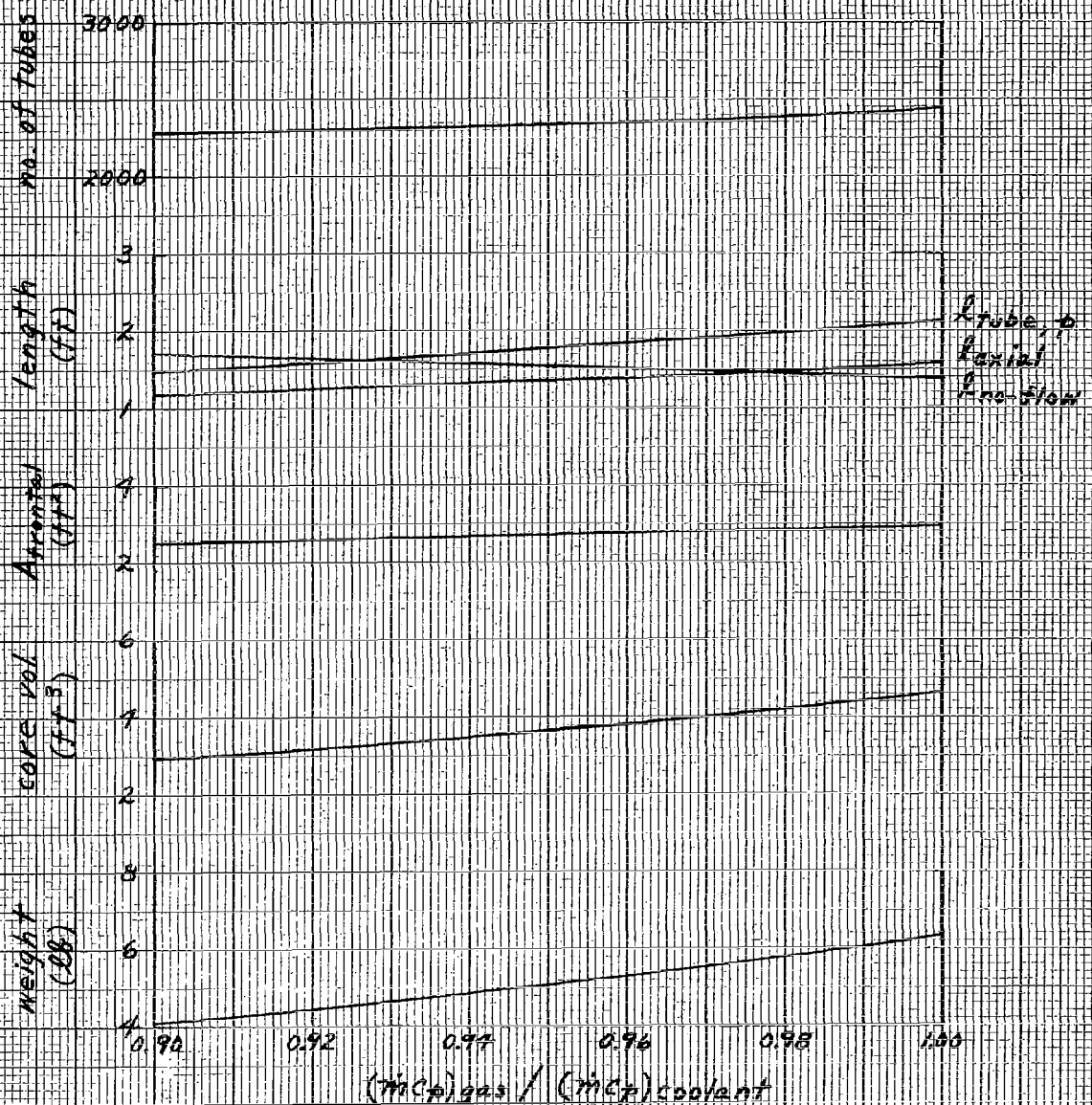
Figure 9.

EFFECT OF COOLANT PRESSURE DROP

1000 KW, argon gas, NaK coolant, $\eta_{cooling} = 0.95$, $(mc_p)_{gas}/(mc_p)_{coolant} = 0.90$, 6 and 8 coolant passes, $\Delta p_{coolant}$ variable; steel tubes, 3/16" tube o.d., tube (i.d./o.d.) = 0.85, copper fins, fin thickness = .005 inch, fin (o.d./i.d.) = 2.0, 30 fins/inch.
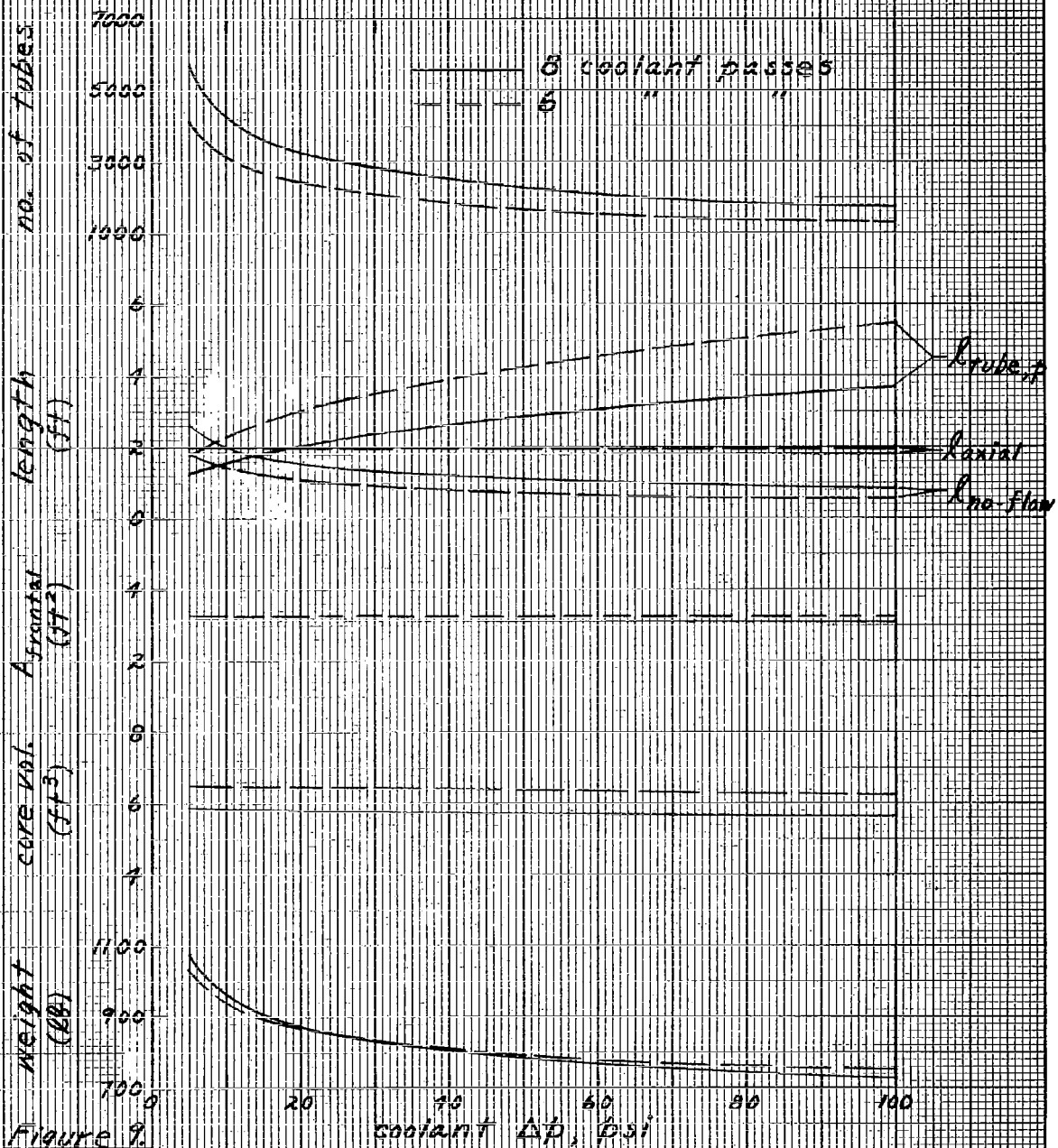
HEAT EXCHANGER PARAMETRIC DATA

1000 KW argon gas, NaK coolant, $\eta_{cooling} = 0.90$.
Steel tubes, 3/16" tube o.d., tube (i.d./o.d.) = 0.85;
copper fins, fin thickness = .005 inch, 30 fins/inch,
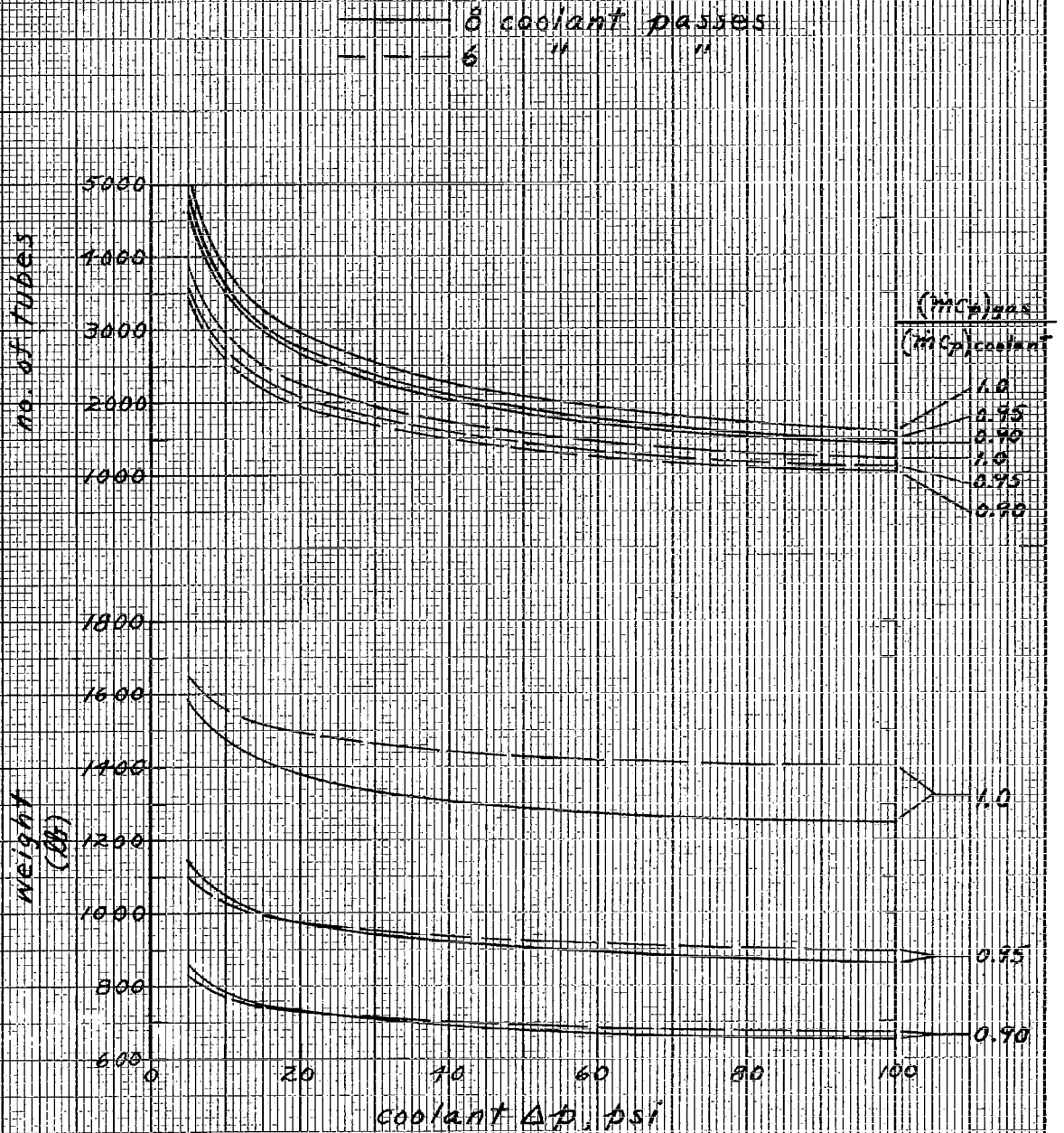fin (o.d./i.d.) = 2.0.
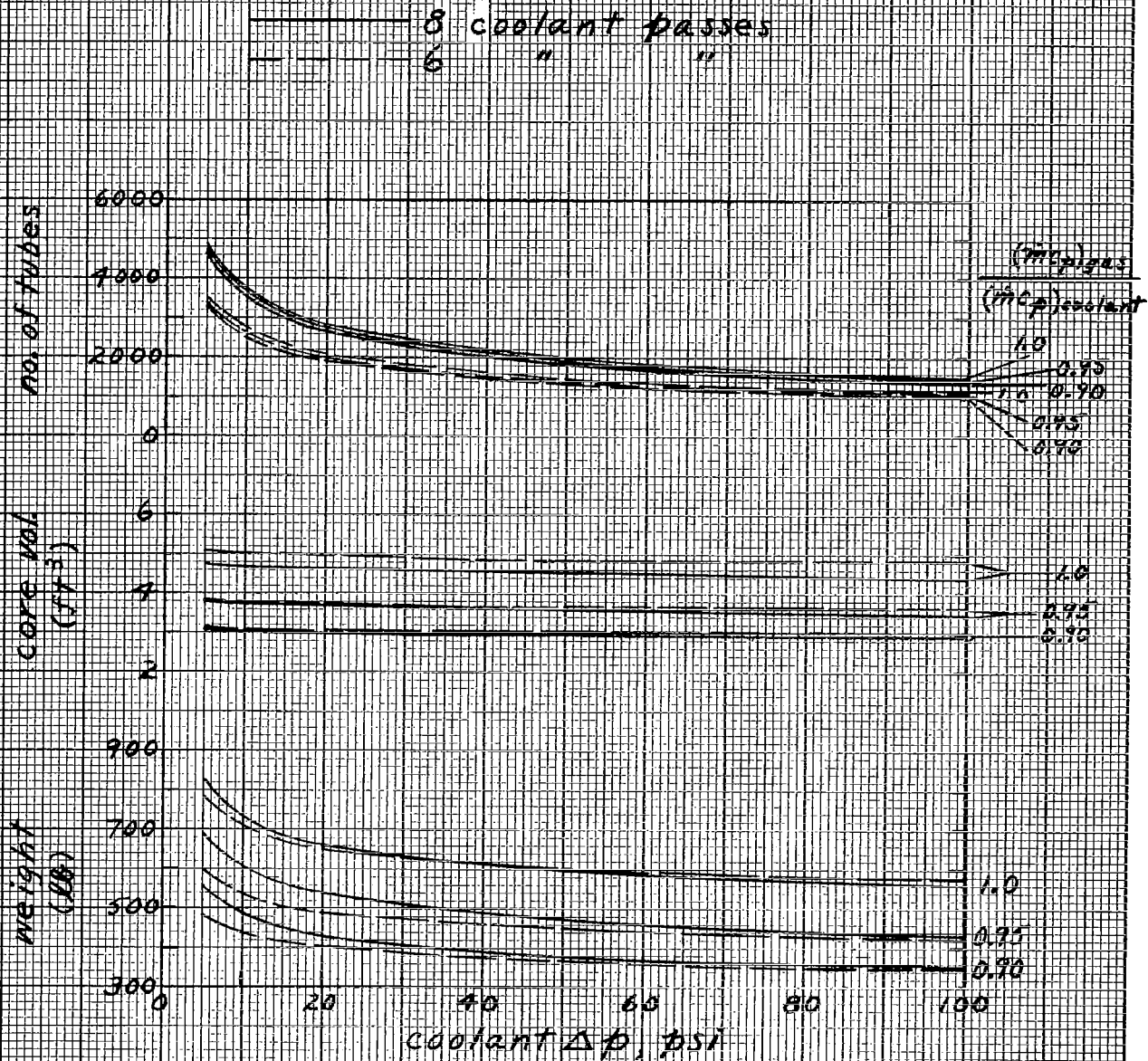
Figure 10.
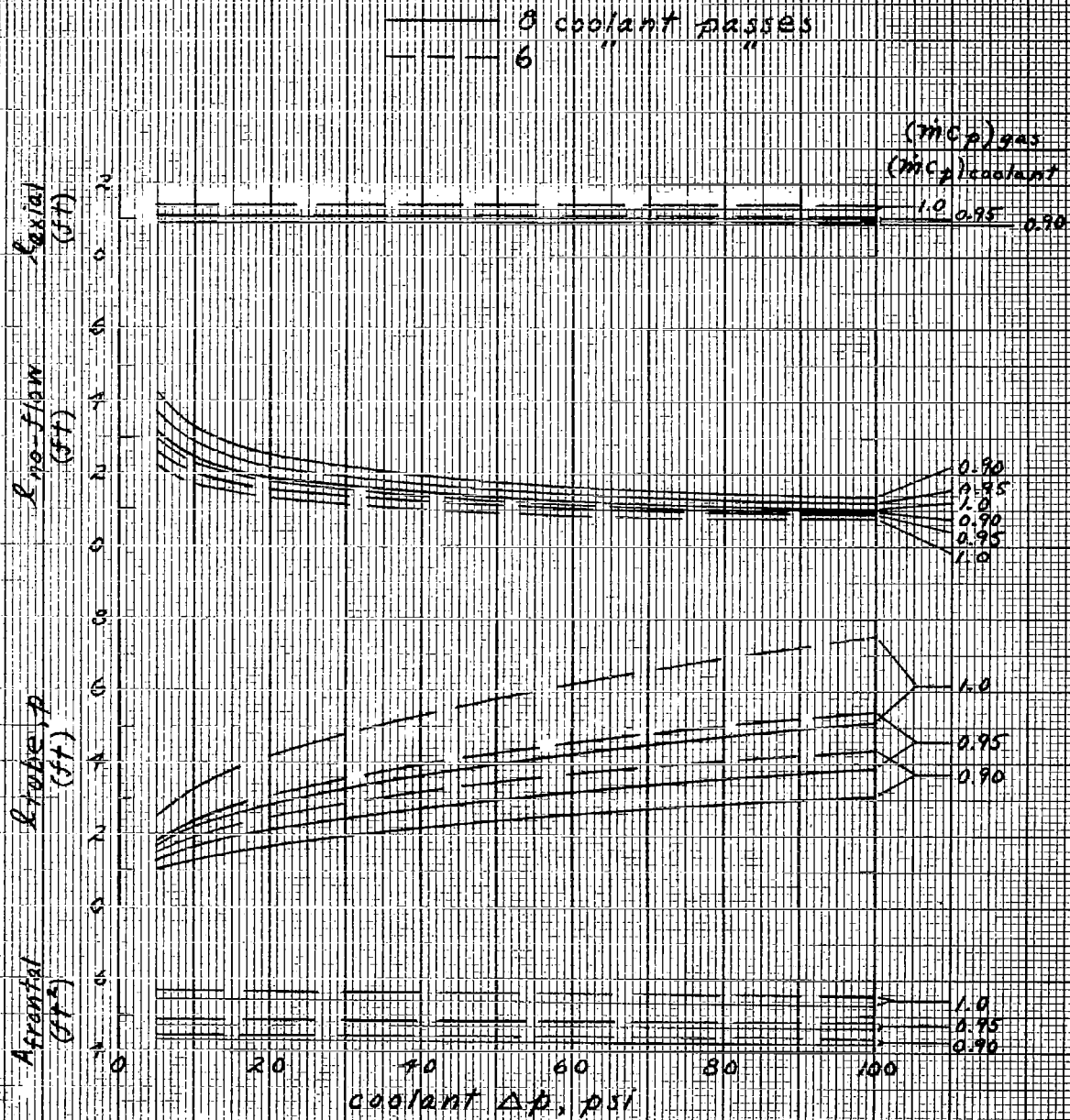
HEAT EXCHANGER PARAMETRIC DATA

(Figure 10 cont'd)
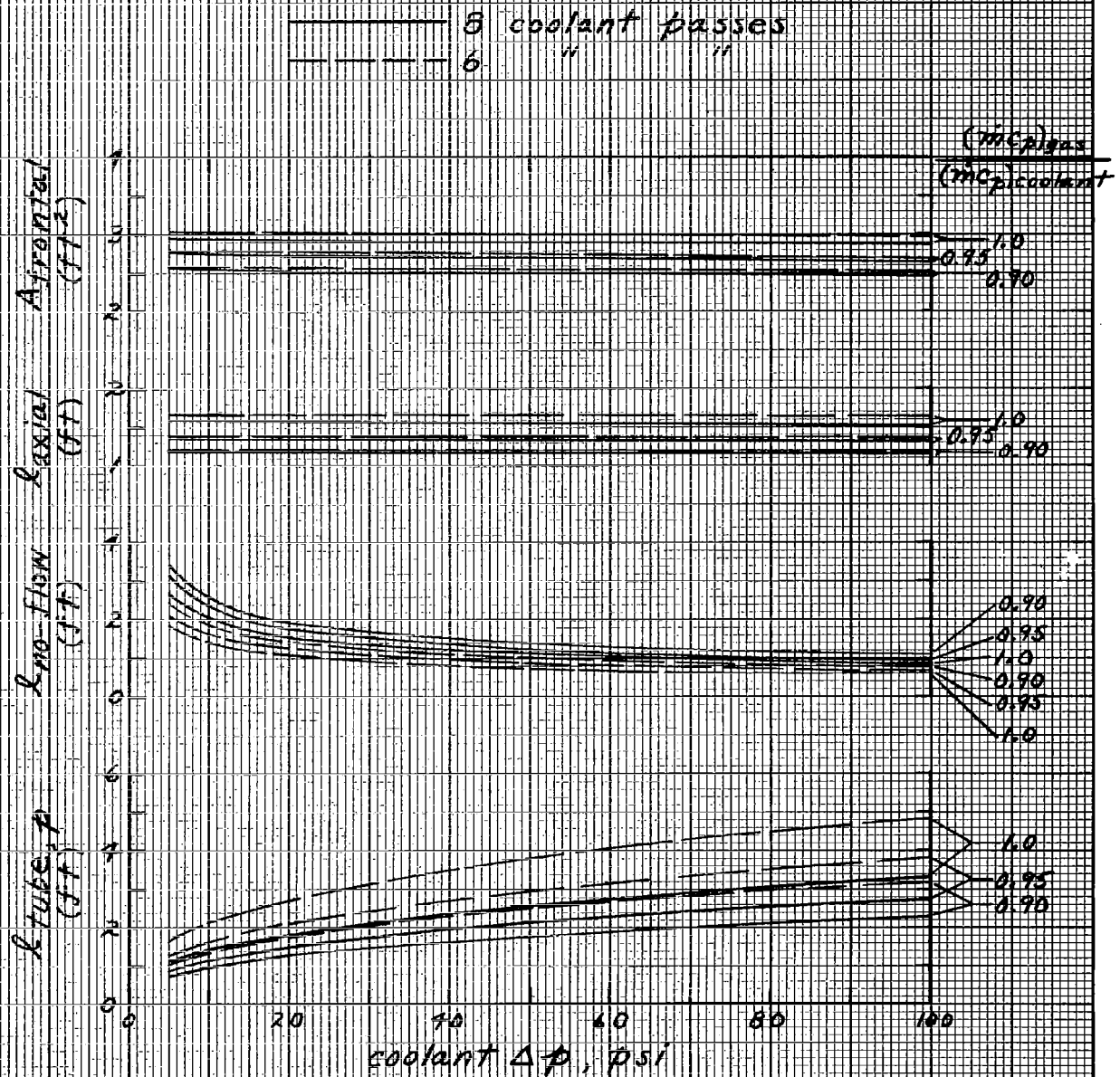
Figure 10 (cont'd).

HEAT EXCHANGER PARAMETRIC DATA

1000 KW, argon gas, NaK coolant, $\eta_{cooling} = 0.925$,
steel tubes, 3/16" tube o.d., tube (i.d./o.d.) = 0.85,
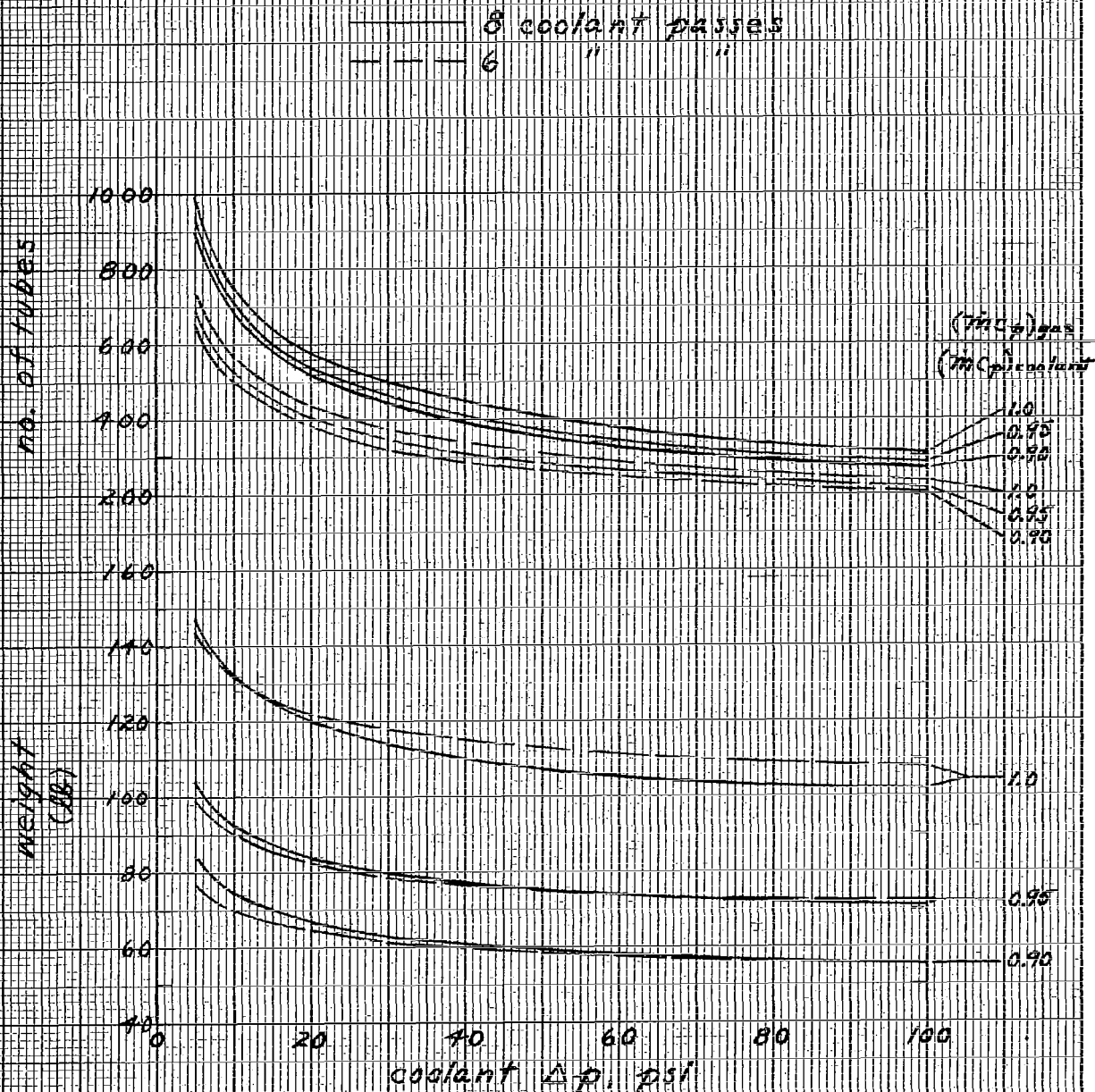copper fins, fin thickness = .005 inch, 30 fins/inch,
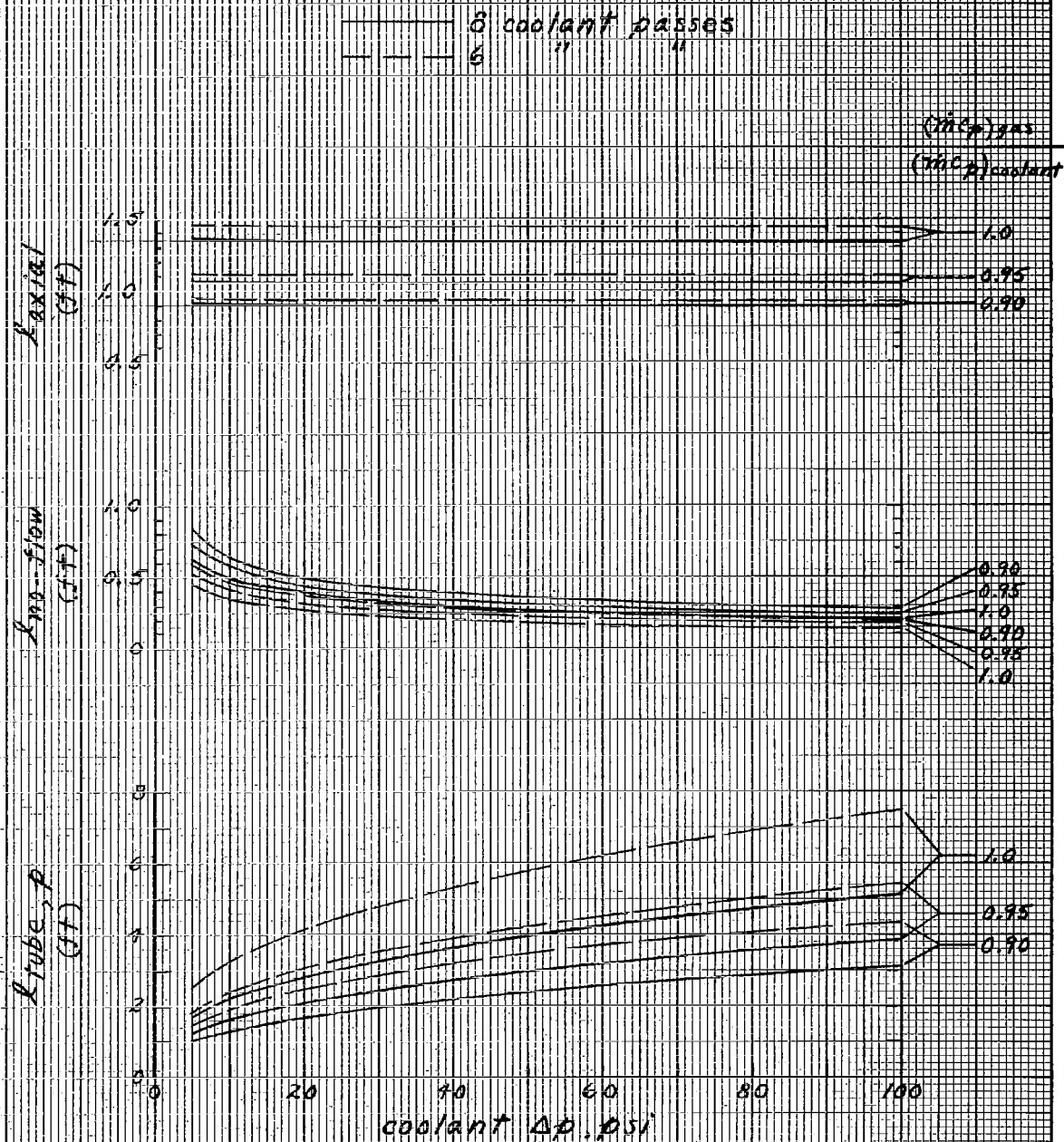fin (o.d./i.d.) = 2.0.
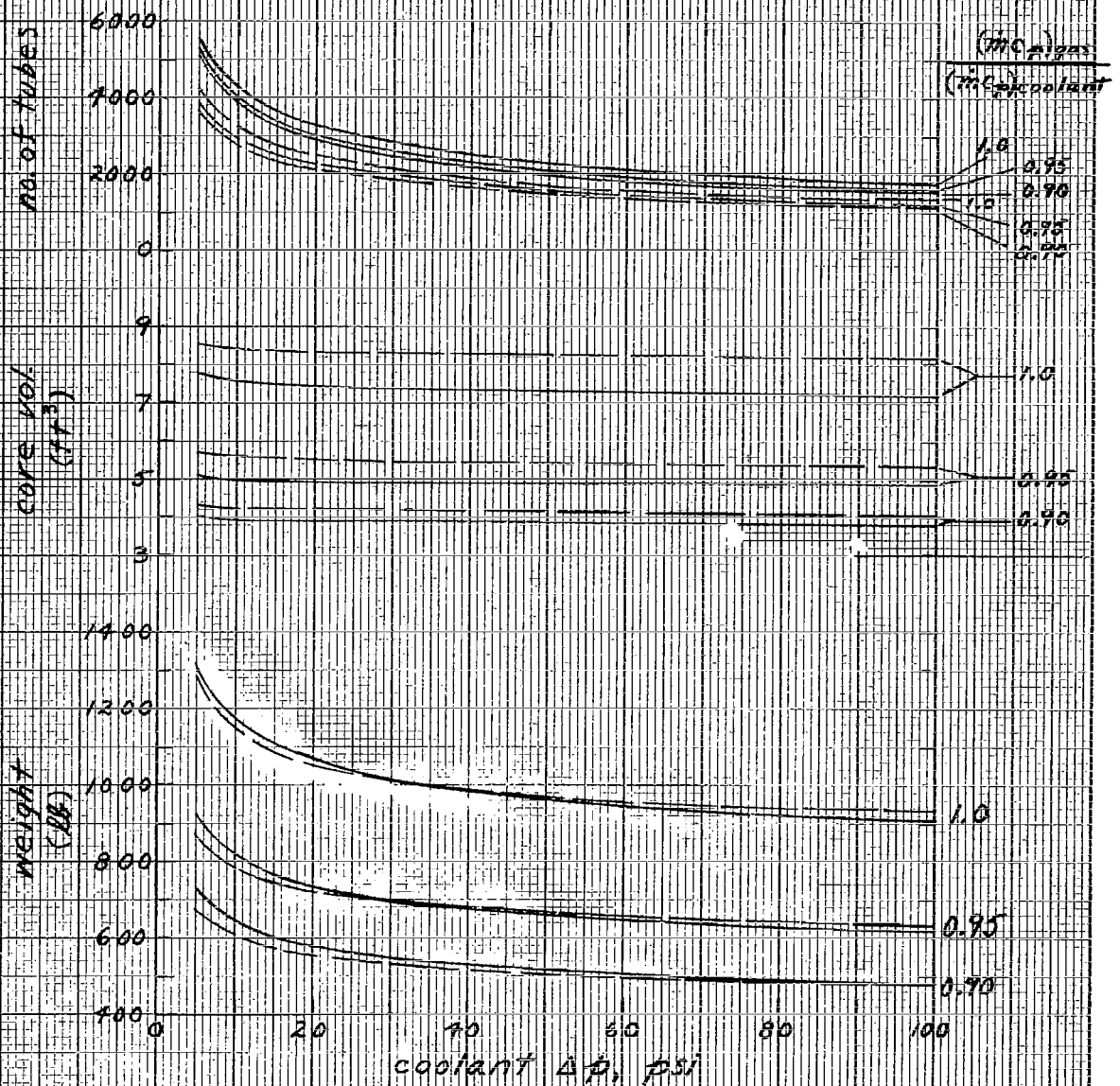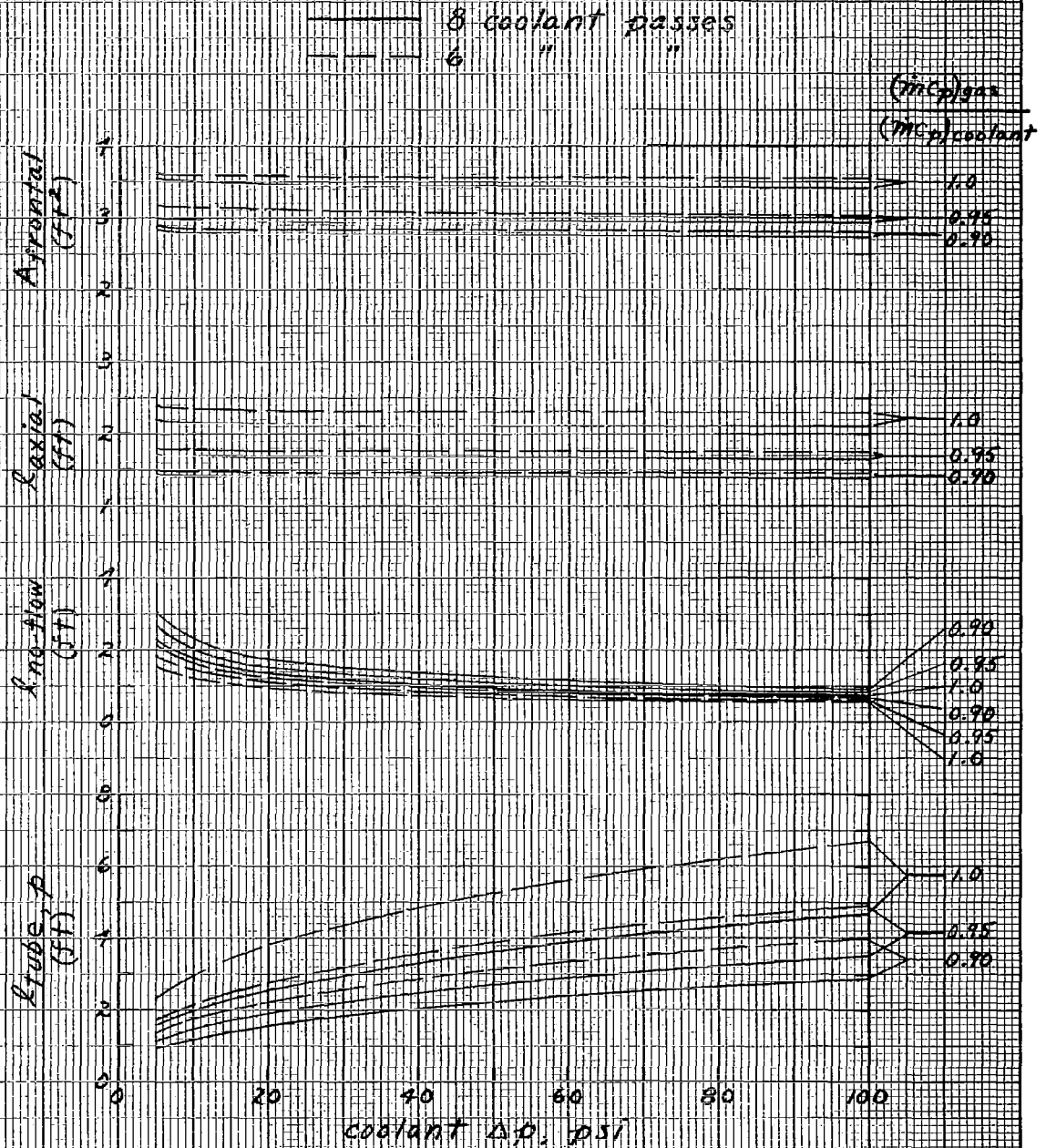
Figure 11.

Figure 11 (cont'd)

HEAT EXCHANGER PARAMETRIC DATA

1000 KW, argon gas, NaK coolant, $\eta_{cooling} = 0.750$
Steel tubes, 3/16" tube o.d., tube (i.d./o.d.) = 0.85;
copper fins, fin thickness = .005 inch, 30 fins/inch,
fin (o.d./i.d.) = 2.0

Figure 12
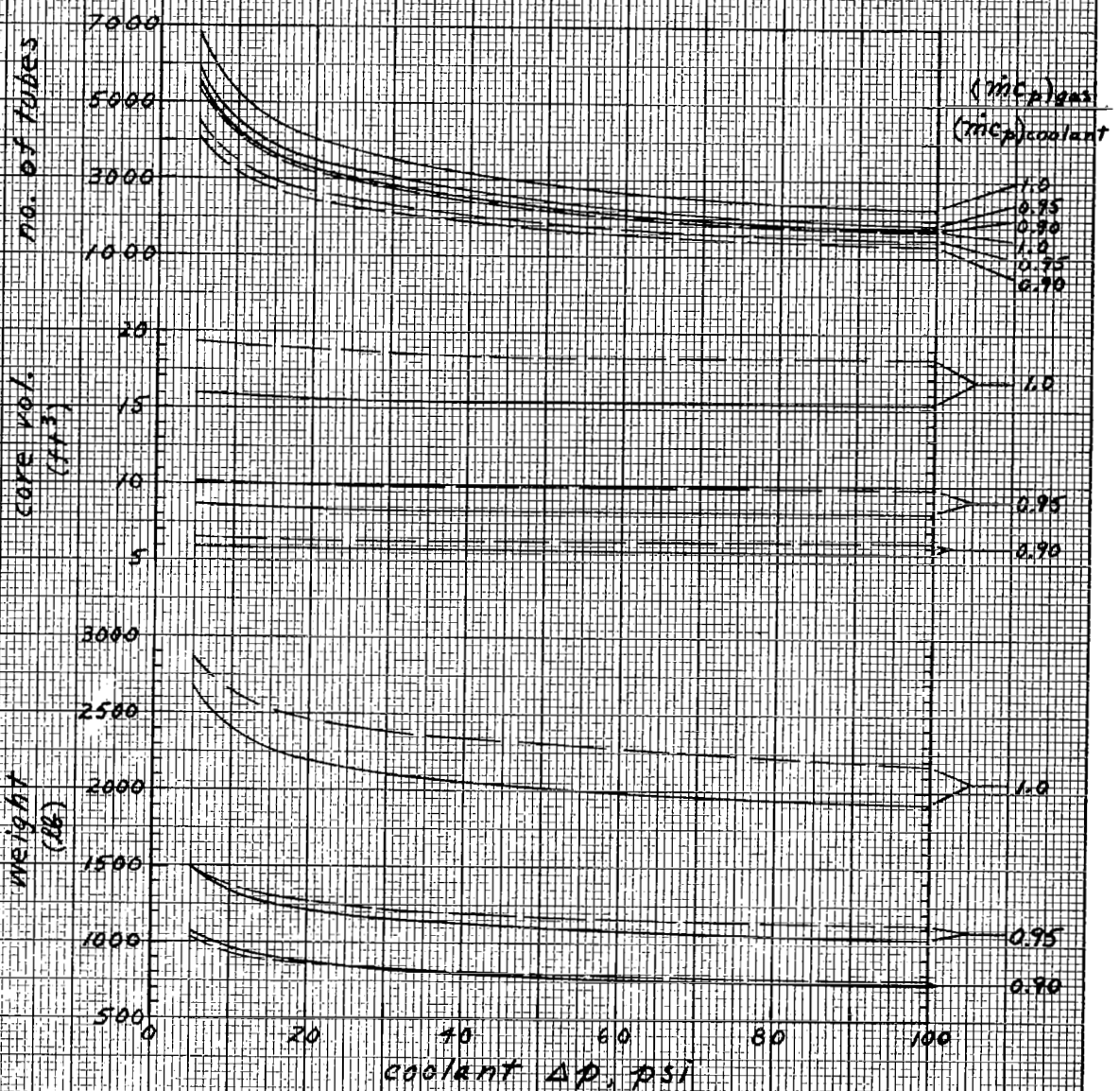
HEAT EXCHANGER PARAMETRIC DATA
(Figure 12 cont'd)

Figure 12 (cont'd)

Figure 13

Figure 19 (cont'd)

HEAT EXCHANGER PARAMETRIC DATA

100 KW, neon gas, NaK coolant, $\eta_{cooling} = 0.725$
Steel tubes, 3/16" tube o.d., tube (i.d./o.d.) = 0.85,
aluminum fins, fin thickness = .005 inch, 30 fins/inch,
Fin (o.d./i.d.) = 2.0

Figure 21

146

HEAT EXCHANGER PARAMETRIC DATA
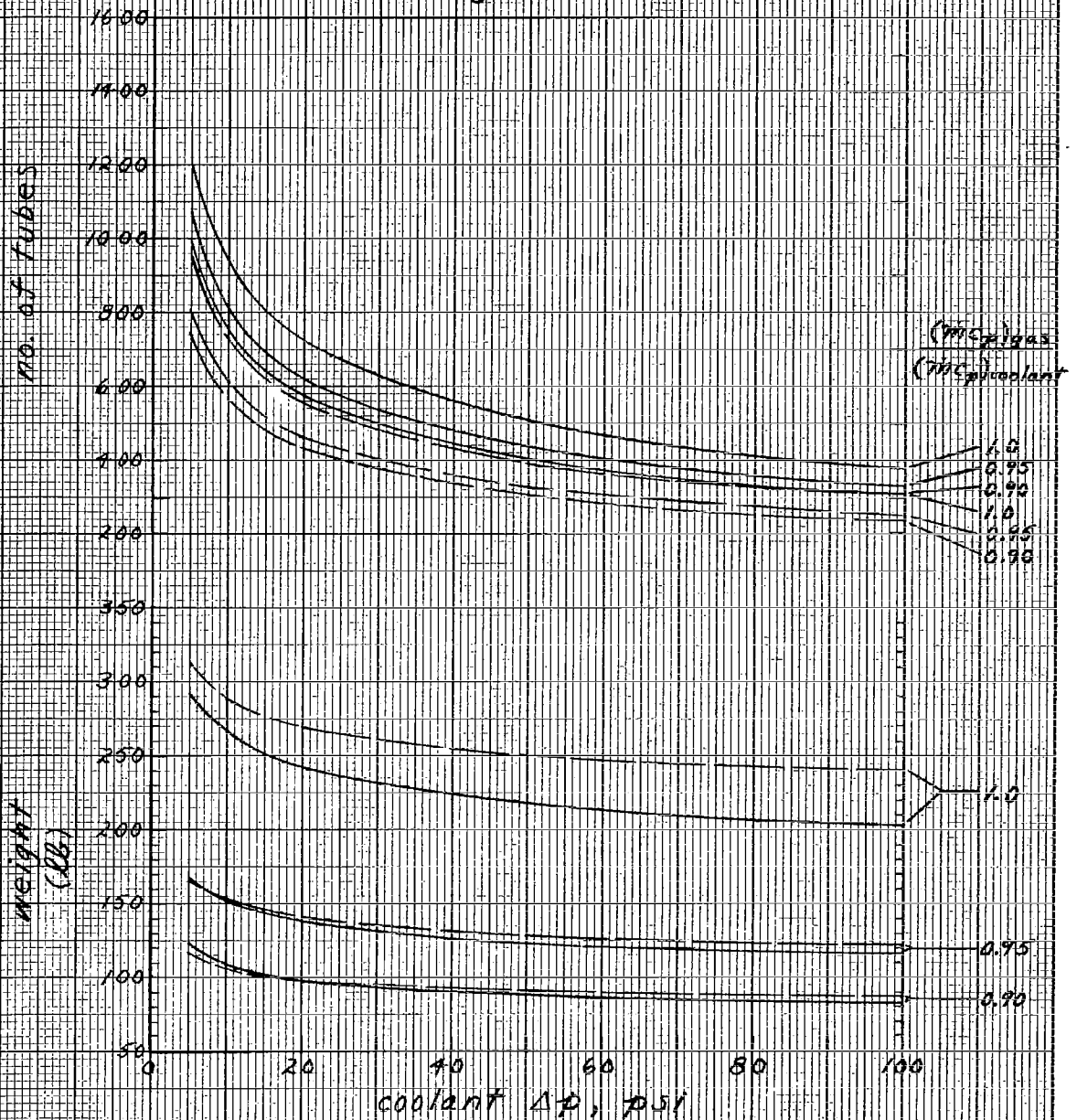
(Figure 21 cont'd)

Figure 21 (cont'd)

Figure 22

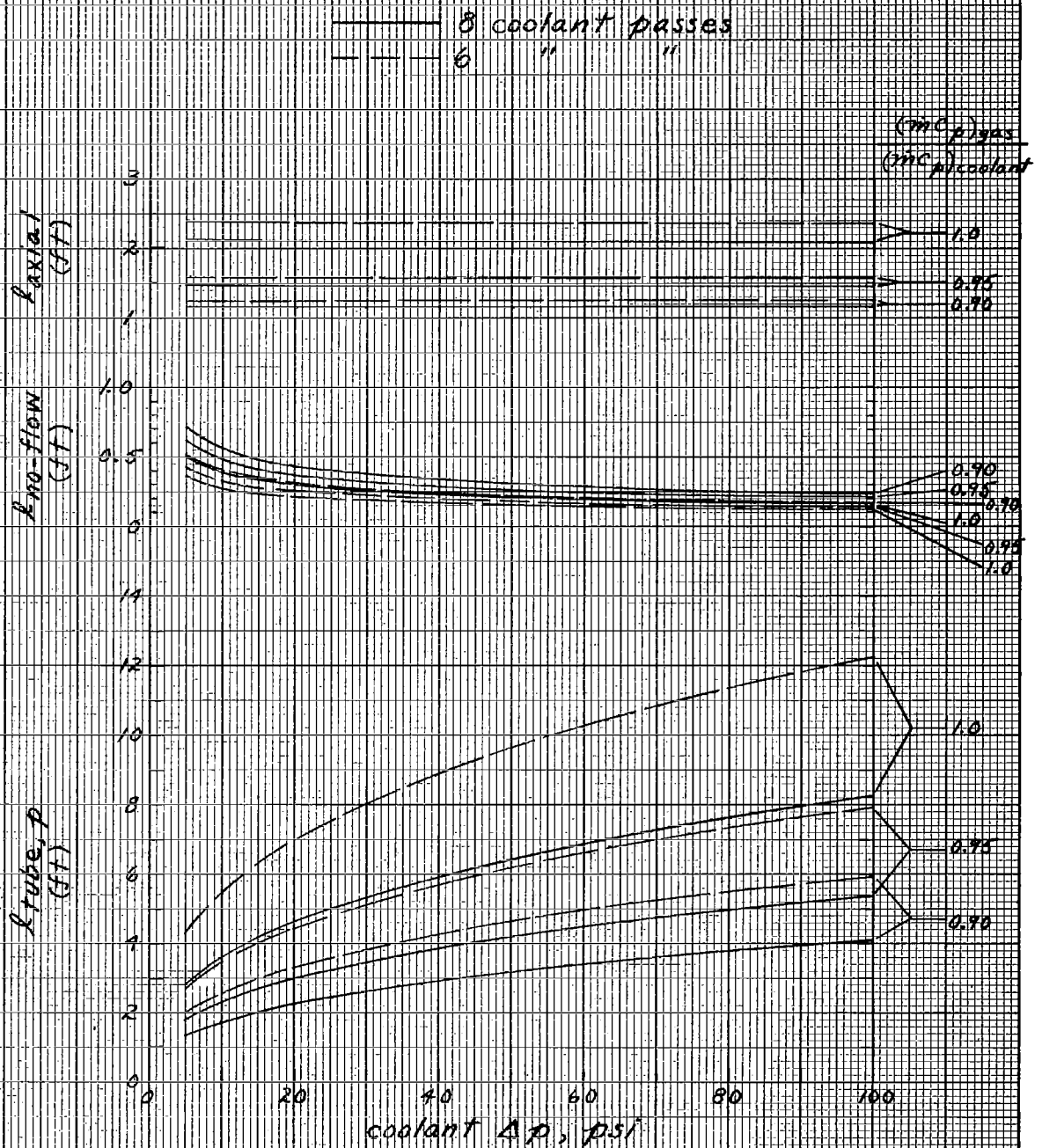HEAT EXCHANGER PARAMETRIC DATA

(Figure 22 cont'd)

Figure 22 (cont'd)

149

Figure 23

HEAT EXCHANGER PARAMETRIC DATA

10 KW, argon gas, NaK coolant, $\eta_{cooling}$ = 0.95
steel tubes, 3/16" tube o.d., tube (i.d./o.d.)=0.83
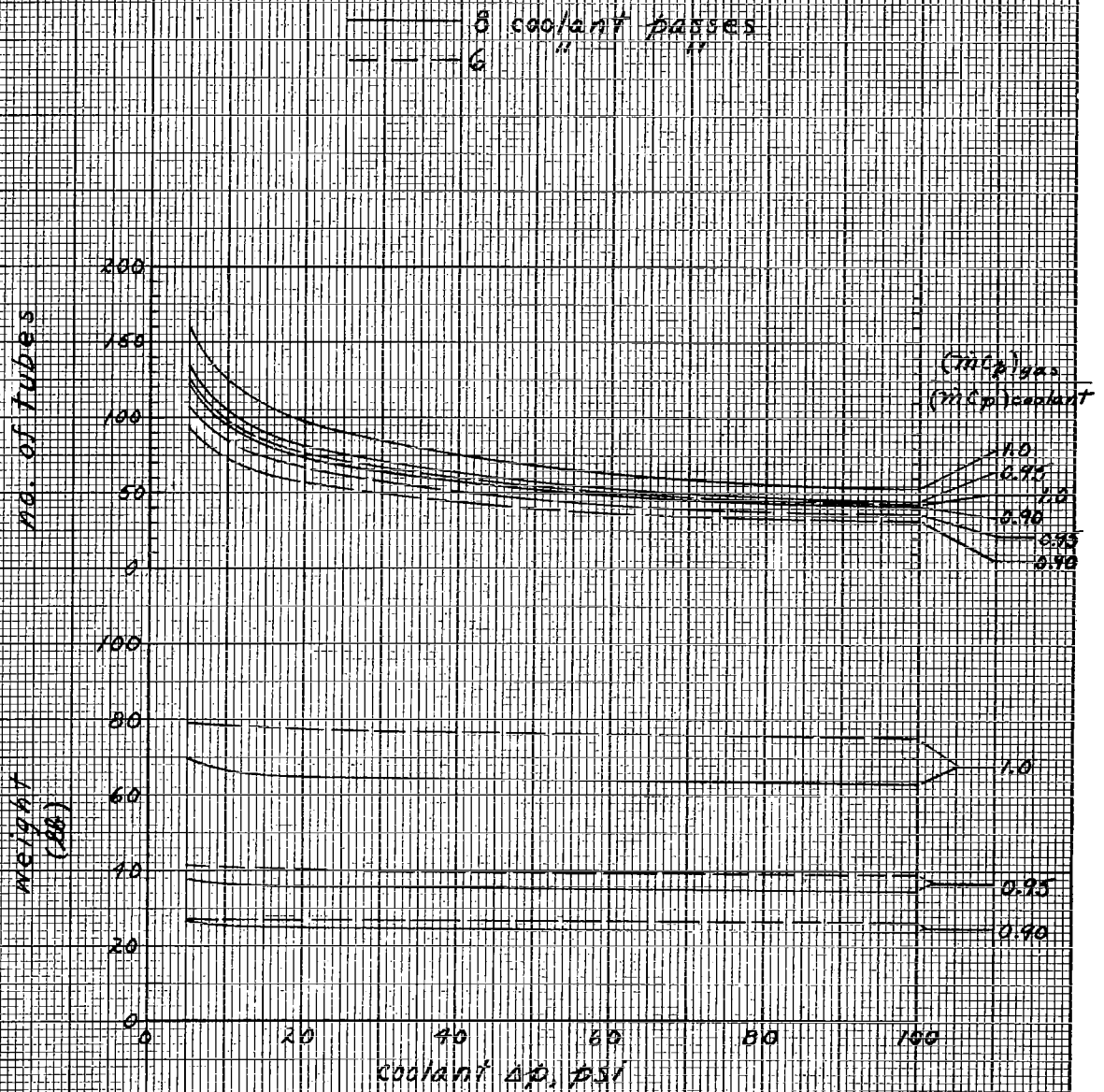aluminum fins, fin thickness = .005 inch, 30 fins/inch
fin (o.d./i.d.)= 2.0

Figure 23 (cont'd)

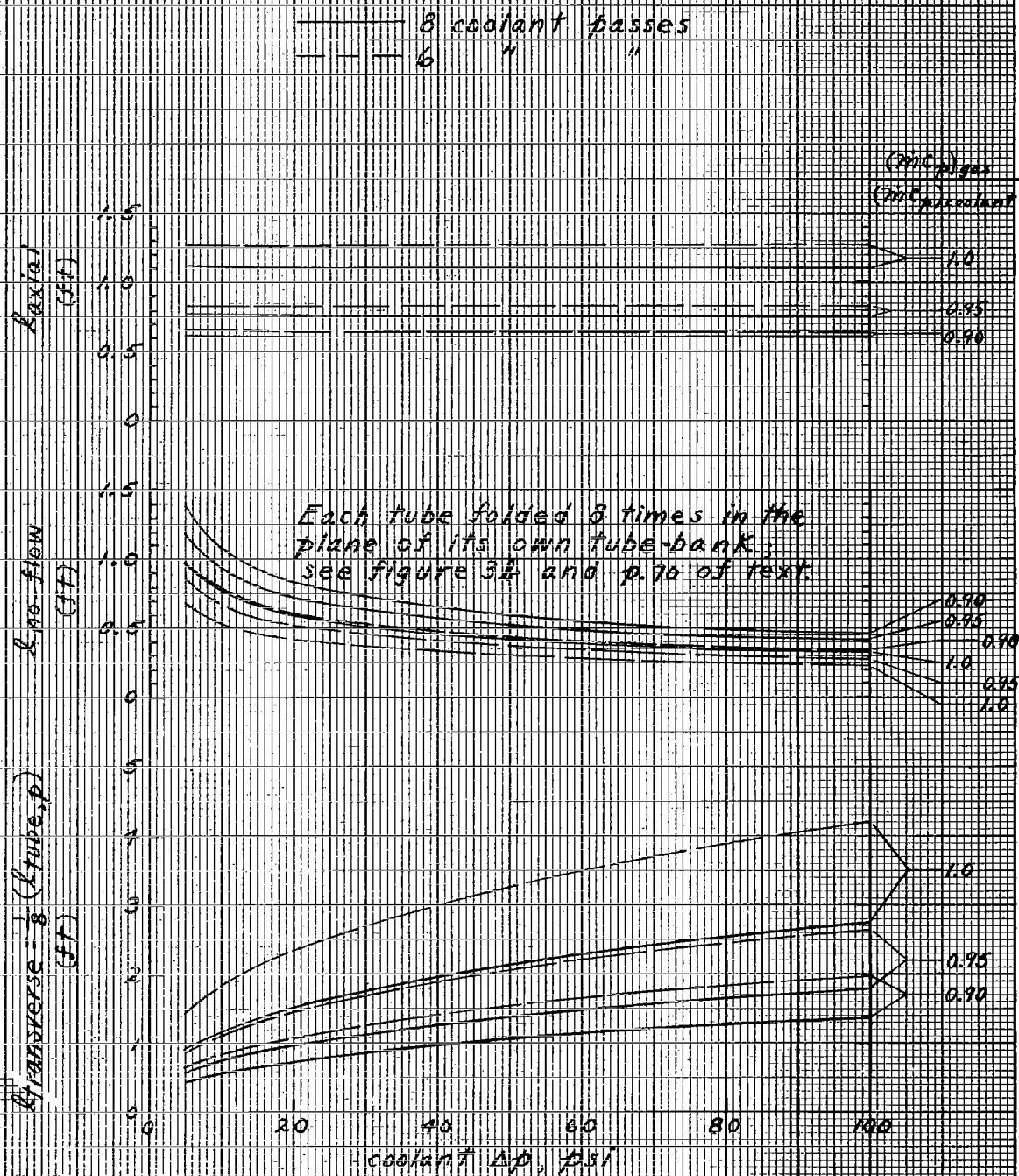HEAT EXCHANGER PARAMETRIC DATA

(Figure 23 cont'd)

8 coolant passes
6 " "

$\frac{(mc_p)_{gas}}{(mc_p)_{coolant}}$

Each tube folded 8 times in the plane of its own tube-bank, see figure 34 and p. 70 of text.

coolant Δp, psi

151

Figure 24

HEAT EXCHANGER PARAMETRIC DATA

(Figure 24 cont'd)

8 coolant passes
6 " "

$\dfrac{(mc_p)_{gas}}{(mc_p)_{coolant}}$

Each tube folded 8 times in the plane of its own tube-bank; see figure 3A and p. 70 of text.

Figure 24 (cont'd)   coolant Δp, psi

153
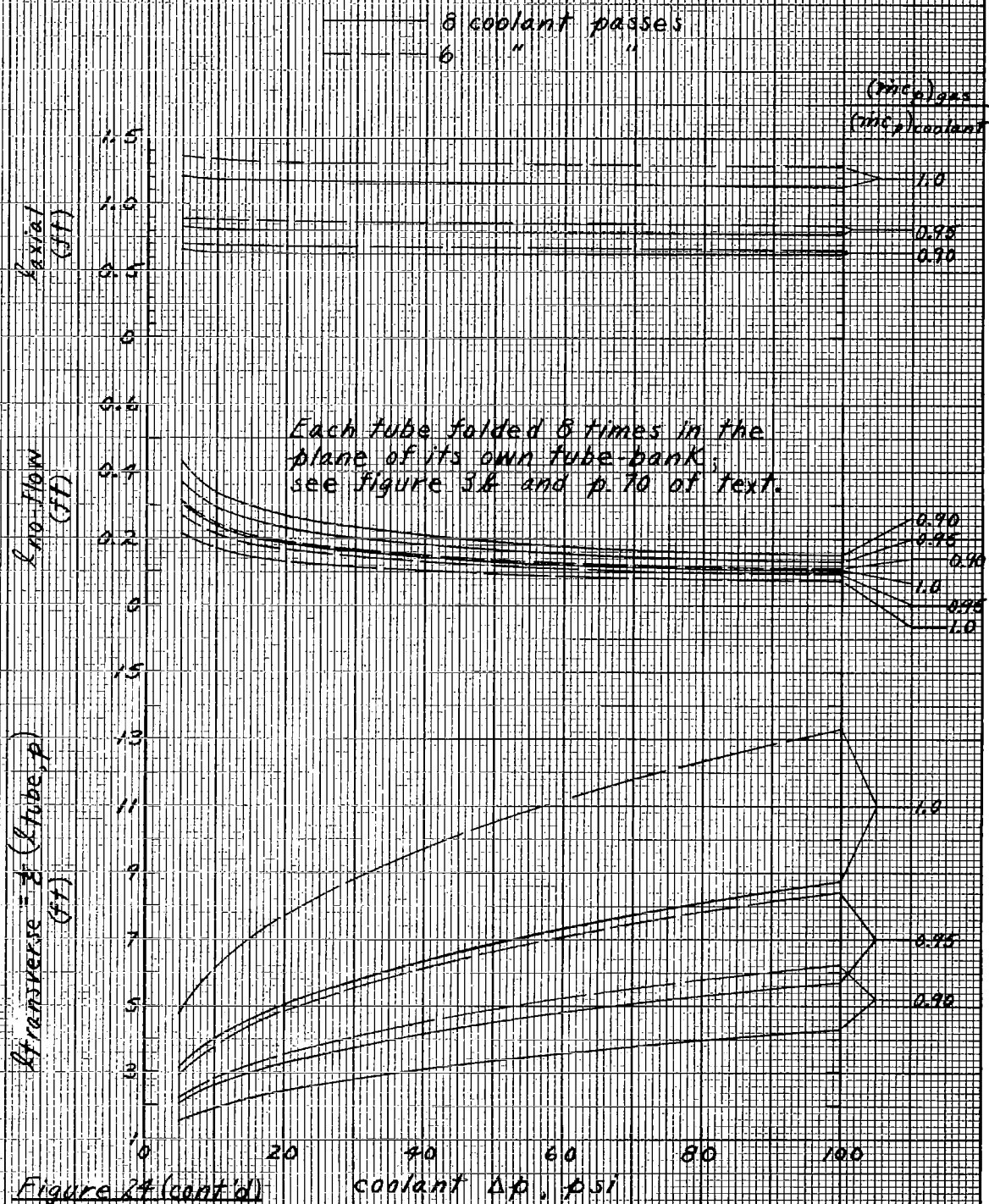
LIQUID TEMPERATURES AND RELATIVE RADIATING POTENTIALS

1000 KW SYSTEM

gas

1600

Hot end of ht. exch'r $\bar{C} = \dfrac{(mc_p)_{gas}}{(mc_p)_{liquid}}$

1550   1.0   1.0

.95

1500   .1   1.0

liquid   .90

1450   .8   .95

.90

gas   .7

980   all values
of $\bar{C}$

Cold end of ht. exch'r   .6   cold end of rad'r
960   hot end of rad'r

.5   .90   .91   .92   .93   .94   .95

940   all values
of $\bar{C}$ $\eta_{cooling}$

liquid

920

900
.90   .91   .92   .93   .94   .95

$\eta_{cooling}$

Temperature, °R

$(T_{liq}^4 - T_e^4)/(T_{gas}^4 - T_e^4)$

$\bar{C}$
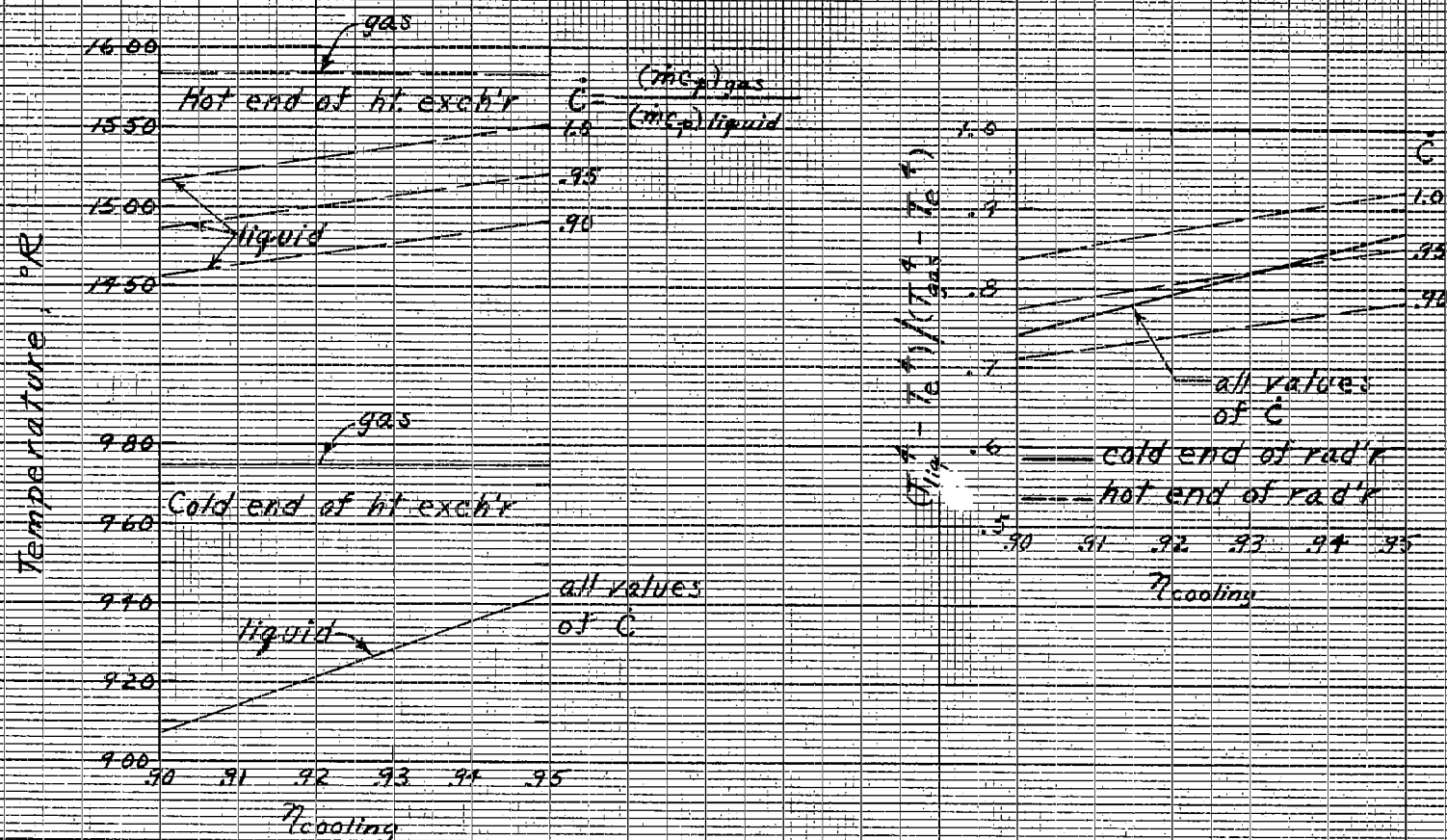
Figure 25a.

LIQUID TEMPERATURES AND RELATIVE RADIATING POTENTIALS

500 & 100 KW SYSTEMS

Temperature °R

$$C = \frac{(\dot{m}c_p)_{gas}}{(\dot{m}c_p)_{liquid}}$$

1200 — gas
Hot end of ht exch'r — 1.0
1150 — 0.95
— 0.90
1100 — liquid

1050

700 — gas
680 Cold end of ht exch'r
660 all values of C
640 liquid
620
.90 .91 .92 .93 .94 .95
η cooling

$(T^4 - T_0{}^4)/(T_{gas}{}^4 - T_0{}^4)$

cold end of rad'r
hot end of rad'r — C
1.0
0.95
0.90
all values of C

1.0
.9
.8
.7
.6
.5
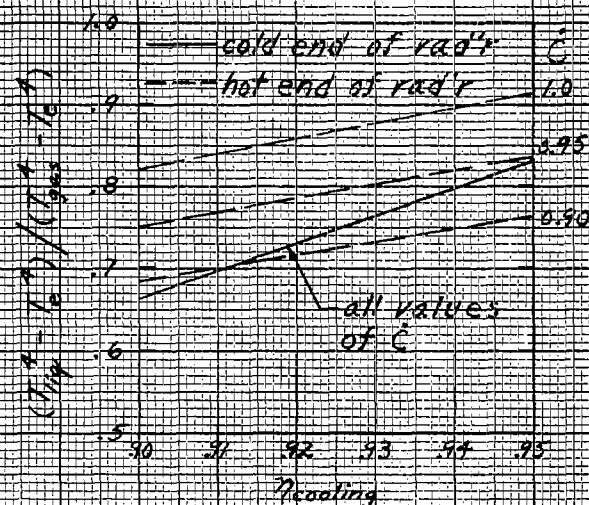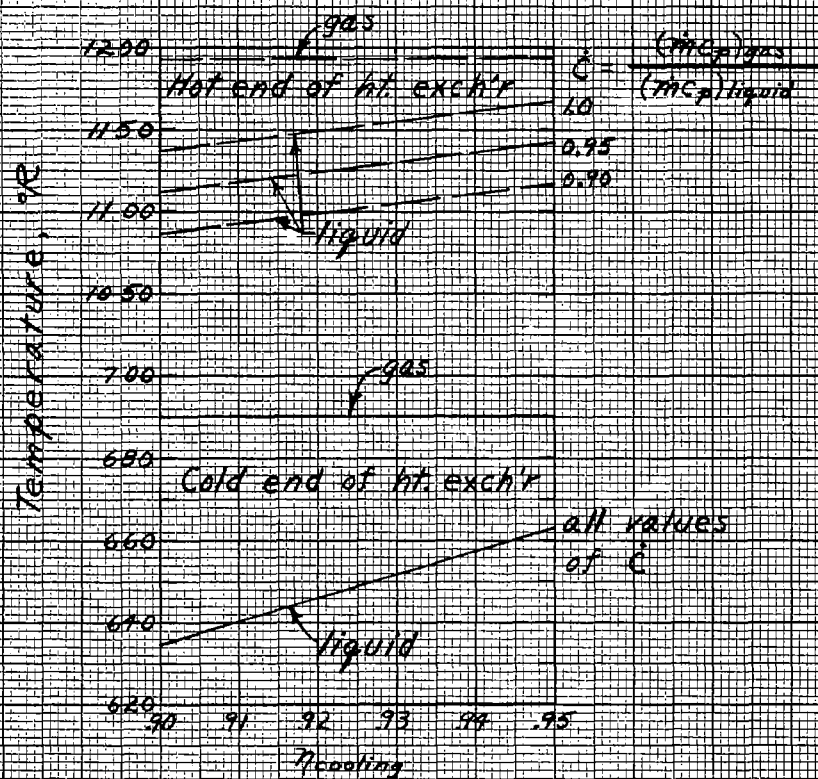.90 .91 .92 .93 .94 .95
η cooling

Figure 25 R.

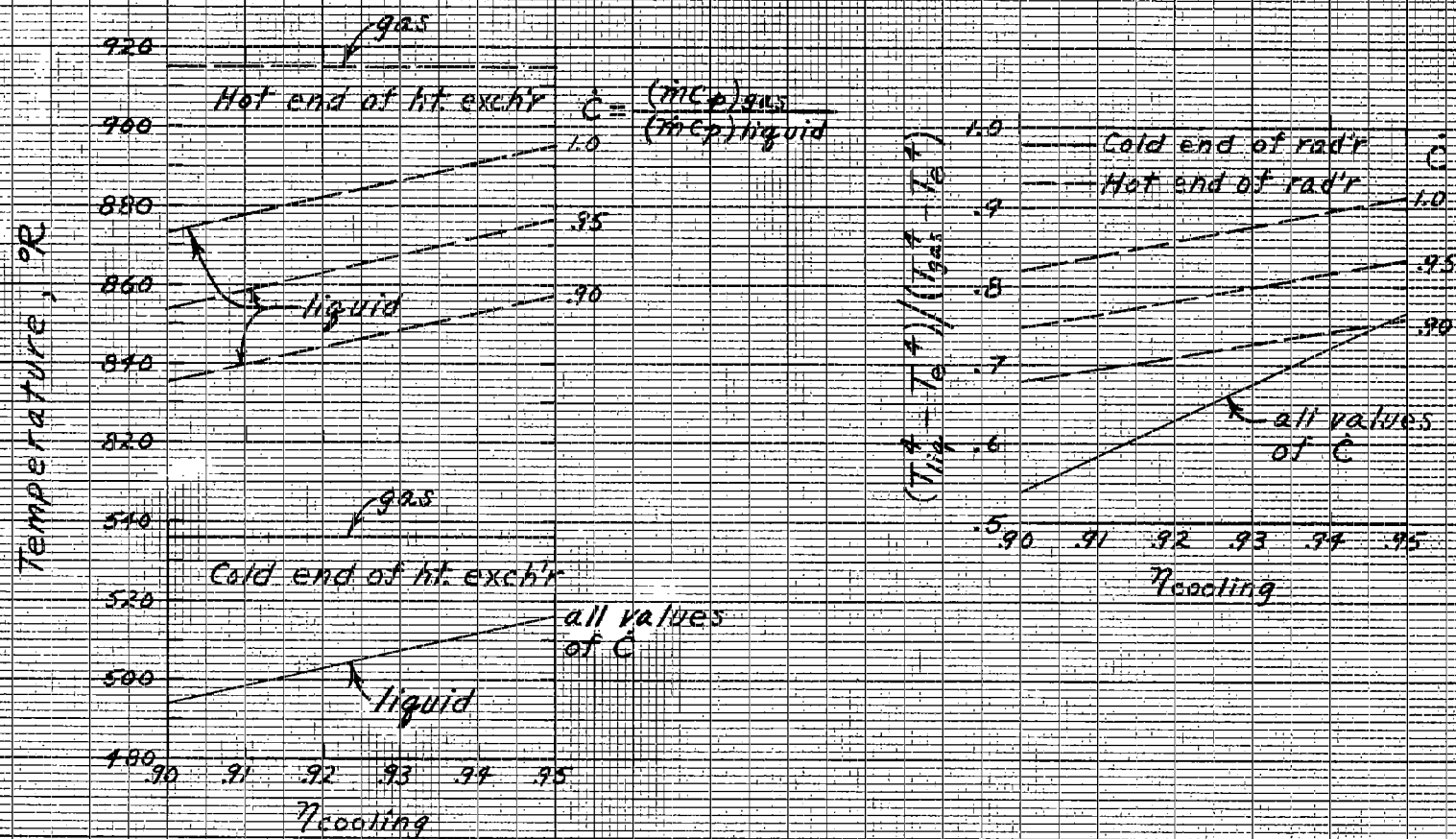LIQUID TEMPERATURES AND RELATIVE RADIATING POTENTIALS

10 KW SYSTEM

Figure 25c.

FRICTION AND HEAT TRANSFER CORRELATIONS
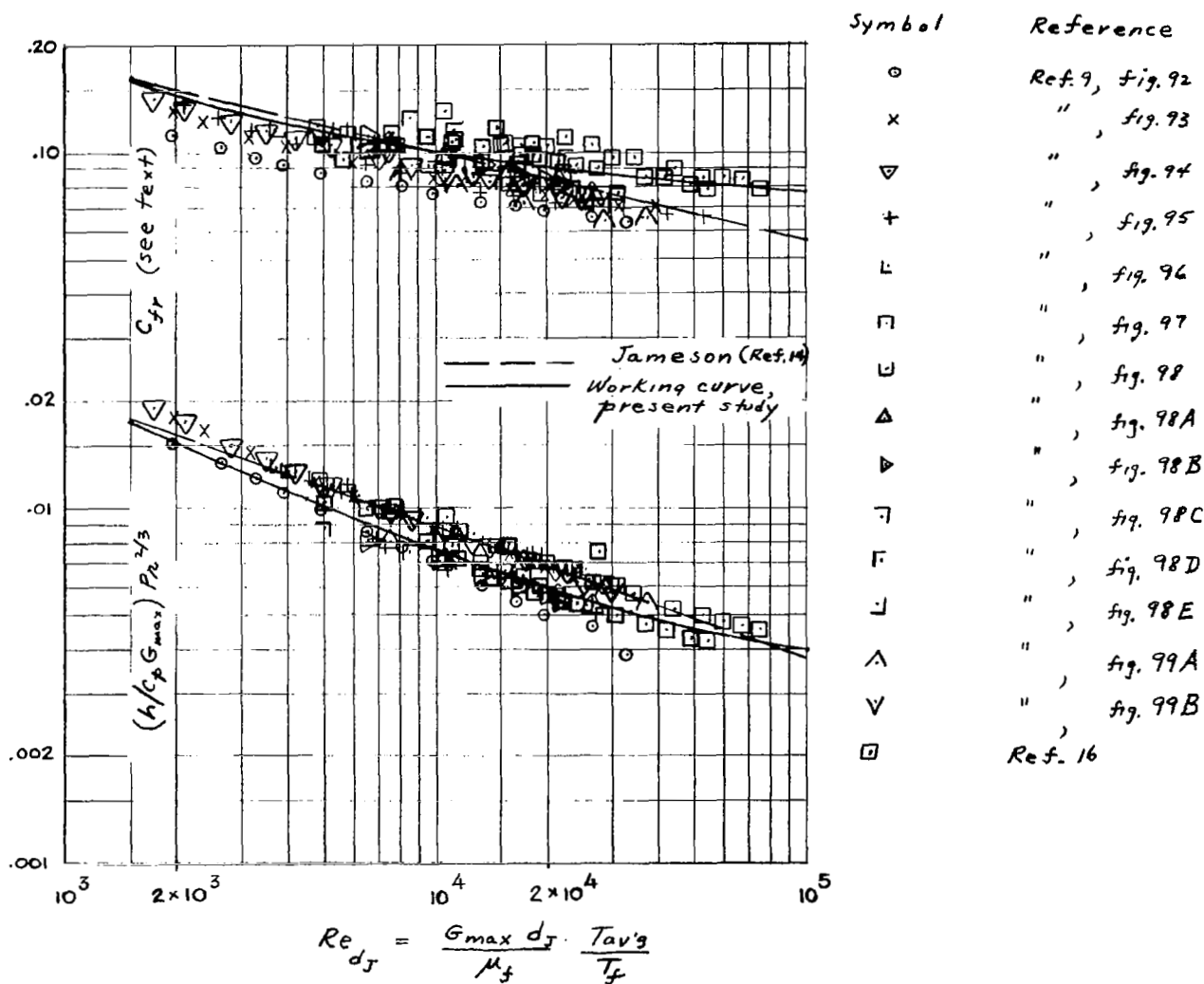## FOR FLOW ACROSS BANKS OF EXTERNALLY FINNED TUBES

Symbol	Reference
⊙	Ref.9, fig.92
×	" , fig.93
▽	" , fig.94
+	" , fig.95
⌐	" , fig.96
⊓	" , fig.97
⊔	" , fig.98
△	" , fig.98A
▷	" , fig.98B
⌐	" , fig.98C
⌐	" , fig.98D
⌐	" , fig.98E
∧	" , fig.99A
∨	" , fig.99B
⊡	Ref. 16

Jameson (Ref.14)
Working curve, present study

$$Re_{d_J} = \frac{G_{max}\, d_J}{\mu_f} \cdot \frac{T_{av'g}}{T_f}$$

Figure 26.